Award Number: **W81XWH-11-1-0241**

TITLE: **Determining Changes in Neural Circuits in Tuberous Sclerosis**

PRINCIPAL INVESTIGATOR: **Mark Zervas, Ph.D.**

CONTRACTING ORGANIZATION: **Brown University**
Providence, RI 02912-9079

REPORT DATE: **May 2013**

TYPE OF REPORT: **Final**

PREPARED FOR: **U.S. Army Medical Research and Materiel Command**
Fort Detrick, Maryland 21702-5012

DISTRIBUTION STATEMENT: **Approved for Public Release;**
Distribution Unlimited

The views, opinions and/or findings contained in this report are those of the author(s) and should not be construed as an official Department of the Army position, policy or decision unless so designated by other documentation.

REPORT DOCUMENTATION PAGE

Form Approved
OMB No. 0704-0188

Public reporting burden for this collection of information is estimated to average 1 hour per response, including the time for reviewing instructions, searching existing data sources, gathering and maintaining the data needed, and completing and reviewing this collection of information. Send comments regarding this burden estimate or any other aspect of this collection of information, including suggestions for reducing this burden to Department of Defense, Washington Headquarters Services, Directorate for Information Operations and Reports (0704-0188), 1215 Jefferson Davis Highway, Suite 1204, Arlington, VA 22202-4302. Respondents should be aware that notwithstanding any other provision of law, no person shall be subject to any penalty for failing to comply with a collection of information if it does not display a currently valid OMB control number. **PLEASE DO NOT RETURN YOUR FORM TO THE ABOVE ADDRESS.**

1. REPORT DATE	2. REPORT TYPE	3. DATES COVERED
May 2013	Final	15 April 2011 - 14 April 2013

4. TITLE AND SUBTITLE
Determining Changes in Neural Circuits in Tuberous Sclerosis

5a. CONTRACT NUMBER
W81XWH-11-1-0241

5b. GRANT NUMBER
W81XWH-11-1-0241

5c. PROGRAM ELEMENT NUMBER

6. AUTHOR(S)
Mark Zervas

E-Mail: mark_zervas@brown.edu

5d. PROJECT NUMBER

5e. TASK NUMBER

5f. WORK UNIT NUMBER

7. PERFORMING ORGANIZATION NAME(S) AND ADDRESS(ES)
Brown University

Providence RI 02912-9079

8. PERFORMING ORGANIZATION REPORT NUMBER

9. SPONSORING / MONITORING AGENCY NAME(S) AND ADDRESS(ES)
U.S. Army Medical Research and Materiel Command
Fort Detrick, Maryland 21702-5012

10. SPONSOR/MONITOR'S ACRONYM(S)

11. SPONSOR/MONITOR'S REPORT NUMBER(S)

12. DISTRIBUTION / AVAILABILITY STATEMENT
Approved for Public Release; Distribution Unlimited

13. SUPPLEMENTARY NOTES

14. ABSTRACT. The purpose of our research proposal is to unravel how neural circuits and neuronal physiology of the thalamus contribute to brain dysfunction in Tuberous Sclerosis. Using a novel genetic circuit mapping approach along with temporal gene deletion we were able to ascertain the temporal role of *Tsc1* in establishing thalamocortical circuitry and to determine how *Tsc1* loss during embryonic development impacts thalamocortical circuit function. Specifically, we show that deletion of *Tsc1* during a discrete time window results in ectopic parvalbumin-expressing thalamic neurons and their axons that exit the thalamus and do not properly innervate the somatosensory cerebral cortex, which is a direct target of thalamocortical circuits. The aberrant thalamus to cortex circuit was accompanied by a secondary patterning defect in the somatosensory cortex, which demonstrates a cell non-autonomous component accompanies the primary genetic lesion. These alterations cause excessive repetitive grooming and robust seizures that were present in all eleven conditional mutant mice. We also show that thalamic neurons have enlarged soma and concomitant alterations in intrinsic membrane properties (membrane capacitance and input resistance) and have disrupted firing properties in both the burst and tonic firing modes. Finally, we report that global neural networks in somatosensory cortex are altered as determined by recording by local field potentials. The major findings during the entire research period are that we identified a critical developmental window during which *Tsc1* deletion in the embryonic thalamus causes deficits in thalamocortical neural circuit architecture, altered electrophysiological properties of neurons, and behavioral abnormalities. Thus, *Tsc1* deletion in the thalamus mimicked salient features of human Tuberous Sclerosis including mosaicism, autism and epilepsy. This research progress deepened our understanding of Tuberous Sclerosis by linking temporal gene function, mTOR function, physiology, neural circuitry, and behavior.

15. SUBJECT TERMS
Temporal gene deletion and genetic circuit mapping, Genetic neuroanatomy, Mouse model of Tuberous Sclerosis, Spatially and temporally controlled mosaicism

16. SECURITY CLASSIFICATION OF:			17. LIMITATION OF ABSTRACT	18. NUMBER OF PAGES	19a. NAME OF RESPONSIBLE PERSON
					USAMRMC
a. REPORT	b. ABSTRACT	c. THIS PAGE			19b. TELEPHONE NUMBER *(include area code)*
U	U	U	UU	65	

Table of Contents

INTRODUCTION

The stated purpose of our research proposal was to unravel how neural circuits and neuronal physiology of the thalamus contribute to brain dysfunction in Tuberous Sclerosis. Using a novel genetic circuit mapping approach along with temporal gene deletion we were able to complete our proposed research. We ascertained the temporal role of *Tsc1* in establishing thalamocortical circuitry and determined how *Tsc1* loss during embryonic development impacted thalamocortical circuit function. Specifically, we showed that deletion of *Tsc1* during a discrete time window results in ectopic parvalbumin-expressing thalamic neurons. We also showed that parvalbumin expressing thalamic neurons have enlarged soma and concomitant alterations in intrinsic membrane properties (membrane capacitance and input resistance) and have disrupted firing properties in both the burst and tonic firing modes. We also proposed to assess thalamus to cortex circuitry and showed that thalamic axons exit the thalamus but do not properly innervate the somatosensory cerebral cortex, which is a direct target of thalamocortical circuits The aberrant thalamus to cortex circuit was accompanied by a secondary patterning defect in the somatosensory cortex, which demonstrates a cell non-autonomous component accompanies the primary genetic lesion. Finally, we report that global neural networks in somatosensory cortex were altered as determined by recording by local field potentials. Thus, the major findings during the entire research period are that we identified a critical developmental window during which *Tsc1* deletion in the embryonic thalamus causes deficits in thalamocortical neural circuit architecture, altered electrophysiological properties of neurons, and behavioral abnormalities. Thus, *Tsc1* deletion in the thalamus mimicked salient features of human Tuberous Sclerosis including mosaicism, autism and epilepsy. This research progress deepened our understanding of Tuberous Sclerosis by linking temporal gene function, mTOR function, physiology, neural circuitry, and behavior.

BODY

The information extracted from our proposed research “Determining Changes in Neural Circuits in Tuberous Sclerosis” has advanced our understanding of brain dysfunction in human Tuberous Sclerosis (TS). TS is a genetic mosaic disorder in which the inheritance of a mutant allele of one copy of the *Tsc1* gene may subsequently be paired with a second somatic mutation that renders cohorts of cells with the complete loss of function of *Tsc1.* Notably, this situation results in a mosaic tapestry of mutant and otherwise genetically unaffected cells. The loss of function of *Tsc1* in the brain causes intellectual disability, seizures, sleep disorders, and autism. We took advantage of our *CreER/loxP* based approach, that allows for temporal and spatial control of gene deletion, to begin to unravel how *Tsc1* mutant neurons in the thalamus affected thalamocortical circuit formation and neural function. We chose the thalamus because it integrates sensory information and modulates the cerebral cortex and is absolutely critical for proper brain function. Notably, the thalamus is an epicenter that synchronizes information processing and generates rhythmic activity. Not surprisingly, the thalamus is a focal point of research related to aberrant electrical activity in the brain underpinning epilepsy and seizures, both of which are prominent in TS. More directly, in recent study, patients with TS have been shown to have structural changes in the thalamus that is tightly linked to poor performance on cognitive tasks (Ridler et al., 2001). In addition, the thalamus has been linked to the autism component in human TS (Asano et al., 2001). The information presented above indicates that the thalamus is poised to play an important role in brain dysfunction in TS.

We took advantage of sophisticated genetic approaches in mice (Joyner and Zervas 2006, Brown et al., 2009; Ellisor et al., 2009; Ellisor et al., 2010) and have advanced the foundation technology in a novel system that allows for the deletion of *Tsc1* with fine temporal and spatial

control while also genetically marking mutant neurons and their axons (See for example, Ellisor et al., 2009; Hagan et al., 2012). During this funding period, we linked genetic mutations directly to neural circuits (Normand et al., 2013, Appendix 1). It is important to note that the mutant thalamic circuits that we analyze were in the context of *Tsc1* loss in the thalamus while surrounding brain regions are genetically and phenotypically normal (Figure 1 and Normand et al., 2013 (See Appendix 1 for experimental details).

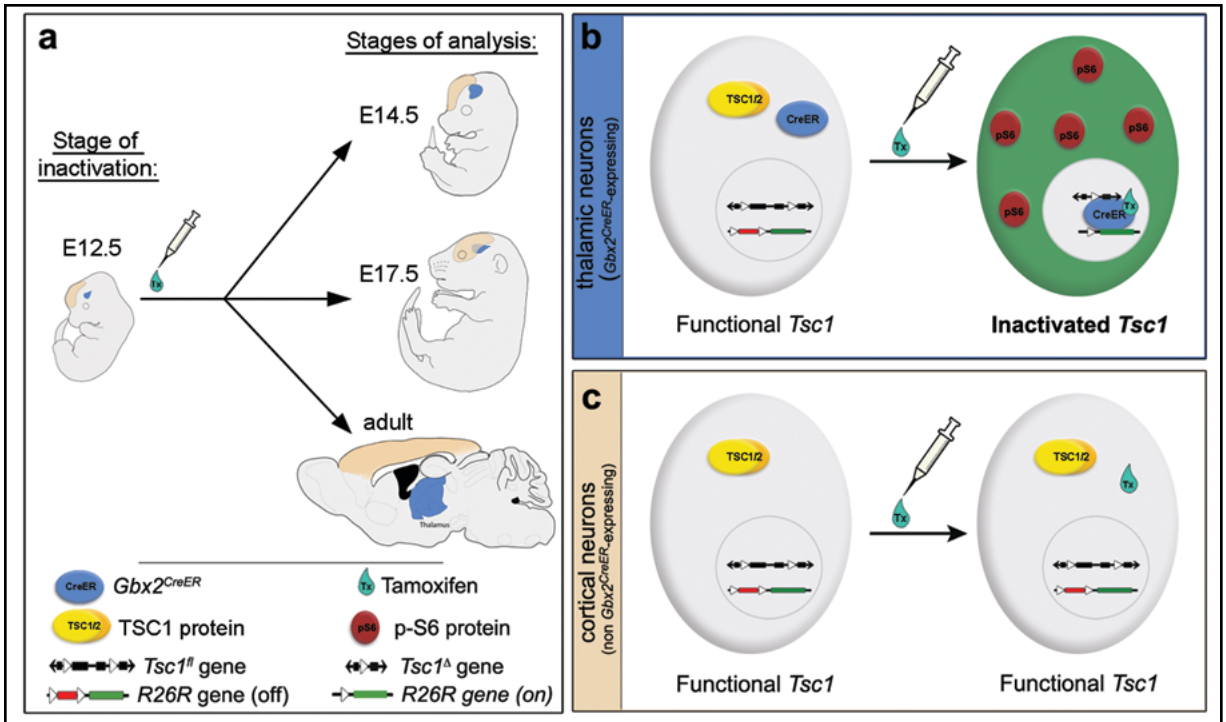

Figure 1. Conditional *Tsc1* inactivation strategy. (**a**) Experimental design is shown. To induce CreER-based recombination of the *Tsc1fl* allele in the thalamus (blue) but not in surrounding brain regions such as the cerebral cortex (tan), tamoxifen is administered to pregnant females harboring E12.5 stage *Gbx2*^{CreER};*Tsc1*^{fl} embryos (left). Pups can then analyzed at developmental stages or at adulthood (right) for cellular and behavioral phenotypes. This proposal analyzed changes in the adult thal. (b, left cell) A *Gbx2*^{CreER}-expressing neuron in the thalamus possesses the *Tsc1*^{fl} allele and the quiescent *R26R* reporter allele. This cell produces TSC1/2 protein (yellow) as well as CreER protein that is sequestered in the cytoplasm (blue). (b, right cell). Upon tamoxifen exposure, tamoxifen (aqua) binds to CreER, releasing it from hsp90 binding (not shown) and allowing it to translocate the nucleus. Once in the nucleus, CreER mediates recombination of *loxP* sites (white triangles), leading to conversion of the *Tsc1*^{fl} allele into the *Tsc1*$^{\Delta}$ deleted allele and conversion of the quiescent *R26R* allele into the activated form. Activated *R26R* produces ß-gal protein, which indelibly labels recombined cells (green). (c, left cell) A non-*Gbx2*^{CreER}-expressing cell, such as one in the cerebral cortex, possesses the *Tsc1*^{fl} and *R26R* allele and produces functional TSC1/2 protein, but do not express CreER protein. (c, right cell) Upon tamoxifen exposure, tamoxifen enters the cell, but has no CreER to bind. Thus, the *Tsc1*^{fl} allele remains functional and TSC1/2 protein continues to be produced by the cell. Additionally, the *R26R* allele remains quiescent, so the cell produces no ß-gal. From Normand et al., 2013, Appendix 1.

The first task we proposed in our Statement of Work was to ascertain the developmental profile of thalamocortical circuitry in *Tsc1* conditional mutant mice. Specifically, we proposed to assess axonal projections of *Tsc1*-deficient neurons located in the thalamus as they innervate their target sites in cortex. We completed this aim using distinct genetic reporter alleles (*R26*^{lacZ} or *R26*^{tdTomato}) (Soriano 1999; Madisen et al., 2010; Hagan et al., 2012; Normand et al., 2013) to monitor mutant thalamic neurons. With this approach, the *Gbx2* lineage in the thalamus was

marked concomitant with conditional gene deletion of *Tsc1* using *Gbx2*^{CreER};*R26*^{lacZ};*Tsc1*$^{fl/fl}$ mice or *Gbx2*^{CreER};*R26*^{tdTomato};*Tsc1*$^{fl/fl}$ mice as shown in Figures 1 and 2. These allelic combinations allowed us to convert the *Tsc1*$^{fl/fl}$ alleles to *Tsc1*$^{\Delta E12/\Delta E12}$ (deleted alleles with the ΔE12 indicating the stage of deletion) and to visualize mutant thalamic axons. We linked the *Tsc1* gene deletion with mutant axons using the *R26*^{tdTomato} reporter that encodes a red fluorescent protein that fills axons (Madisen et al., 2010, Hagan et al., 2012, Normand et al., 2013, Normand et al., 2013a, Appendices 1 and 2). We deleted *Tsc1* at E12.5 and analyzed the adult thalamocortical axons that originate in the thalamus (Figure 2). In control animals, thalamocortical axons were

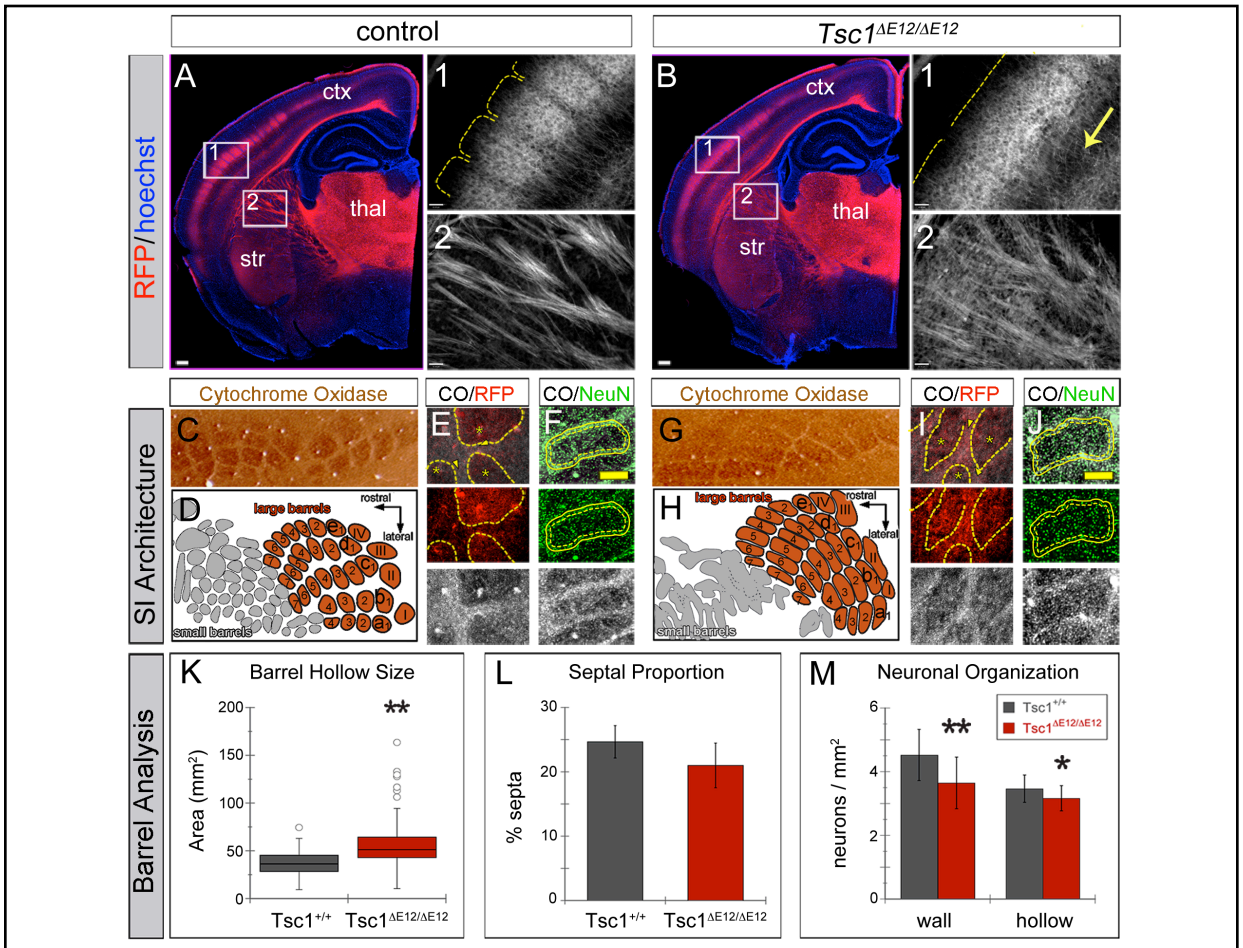

Figure 2. *Tsc1*$^{\Delta E12/\Delta E12}$ mutants have abnormal thalamic circuits. (A and B) RFP+ TCAs (red) delineated individual vibrissa barrels in *Tsc1*$^{+/+}$ neocortex, but were diffuse in *Tsc1*$^{\Delta E12/\Delta E12}$ mutants (region 1). Mutants had excess axonal processes in deep cortical layers (arrow) and RFP+ TCA fascicles that were less defined in the internal capsule (region 2). (C-J) Cortical vibrissa barrels stained with cytochrome oxidase (CO). (C and D) Controls had well-defined CO+ barrels (brown) separated by CO negative septa. (E and I) *Tsc1*$^{+/+}$ RFP+ TCAs (red) targeted the CO+ barrel hollows (black, asterisks) but were less restricted in *Tsc1*$^{\Delta E12/\Delta E12}$ mice. (F and J) Barrel neurons (NeuN+, green) clustered around the perimeter of CO+ barrel hollows (black). Dashed line represents extent of CO+ barrel hollow. Solid line represents 15μm outer perimeter ("wall") used for quantification in (M). (G and H) *Tsc1*$^{\Delta E12/\Delta E12}$ cortex had misshapen barrels (brown) and small vibrissa barrels were nearly indistinguishable (gray). (K) Average CO+ barrel size was larger in *Tsc1*$^{\Delta E12/\Delta E12}$ mutants. (L) The septa proportion showed no difference. (M) *Tsc1*$^{\Delta E12/\Delta E12}$ mice had lower neuron density in the barrel wall and hollow versus *Tsc1*$^{+/+}$ animals. Scale bars: 240μm in (A,B); 61μm in (A1,A2,B1,B2); 130μm in (F,J). thal, thalamus; str, striatum; ctx, neocortex. *p<0.05, **p<0.005. Data are represented as mean ± s.d. From Normand et al., 2013, Appendix 1.

tdTomato+ and could be observed exiting the thalamus (Figure 2A). In contrast, the deletion of *Tsc1* resulted in axons that traversed toward their cortical target and disrupted their projection pattern (Figure 2B). The thalamic relay neurons in the ventrobasal nucleus are typically innervated by parvalbumin (PV) expressing projections from the thalamic reticular nucleus, but the relay neurons themselves (tdTomato+) do not express PV (Figure 3C-D'). However, $Tsc1^{\Delta E12/\Delta E12}$ caused substantial ectopic accumulation of PV in the relay neurons and their axonal projections (Figure 3E-F'). To definitively identify the source of the aberrant projections, we immunolabeled sections with antibodies that showed that tdTomato+ axons were PV+ and therefore from the relay neurons and not TRN neurons passively swept into the internal capsule (Compare Figures 3C,C' and 3E,E'). Thus, aberrant parvalbumin expressing thalamocortical axons do not appropriately innervate somatosensory cortex.

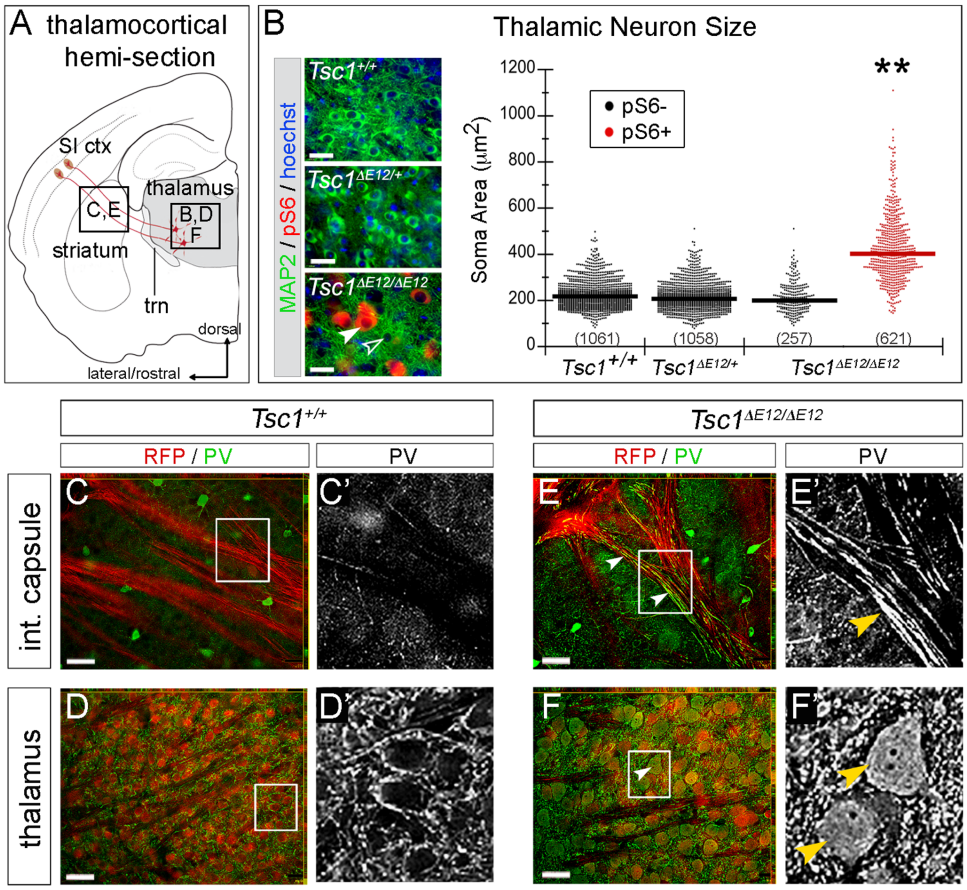

Figure 3. Cellular phenotypes caused by *Tsc1* deletion in thalamus at E12.5 (A) Thalamocortical regions of interest. (B) Sections were immunolabeled for MAP2 (green), pS6 (red), and counterstained with hoechst (blue). Thalamic neurons of $Tsc1^{+/+}$ and $Tsc1^{\Delta E12/+}$ mice were pS6-. Recombination produced a mosaic thalamus of unaffected (pS6-, open arrowhead) and affected (pS6+, filled arrowhead) neurons. Soma area is plotted by genotype and pS6 status. Numbers of neurons are listed and geometric means indicated by horizontal lines. (C-F') Analysis of PV (green) and RFP (red) revealed PV+ fibers in the internal capsule of $Tsc1^{\Delta E12/\Delta E12}$ mice (E and E' arrowheads), but not in controls (C and C'). Soma of $Tsc1^{\Delta E12/\Delta E12}$ RFP+ neurons were also PV+ (F and F' arrowheads, which was not seen in controls (D and D')). n=3 animals per genotype. Scale bars: (B) 32μm (C-F) 48μm. **p<0.005. From Normand et al., 2013, Appendix 1.

An additional part of this task was to evaluate the cerebral cortex in response to thalamic $Tsc1^{\Delta E12/\Delta E12}$ which we accomplished using cytochrome oxidase and NeuN staining and

quantification (Figure 2C-M). Control thalamocortical axons innervated layer 4 whisker barrels in somatosensory cortex, with synapses located in discrete clusters corresponding to individual whiskers, similar to descriptions from studies using non-genetic labeling methods (Figure 2A,E). In contrast, *Tsc1*$^{\Delta E12/\Delta E12}$ mice had a noticeably more diffuse pattern of whisker barrel cortical innervation (Figure 2B,I). Within the internal capsule of the *Tsc1*$^{\Delta E12\Delta/E12}$ brains, thalamocortical axon fascicles also appeared more diffuse and disorganized compared to controls (Figure 2A2 versus 2B2). Because previous TS mouse models have described decreased cortical myelination we assayed for myelination (MBP) in the *Tsc1*$^{\Delta E12/\Delta E12}$ thalamus. Control mice had clear MBP labeling throughout the brain, including within the thalamus and the internal capsule and MBP labeling was not different in *Tsc1*$^{\Delta E12/\Delta E12}$ mutant brains (See Appendix 1). During this funding period, we analyzed the identity of the cerebral cortex in response to the thalamic mutant projections. We completed this task and demonstrated that somatosensory cortex was abnormally patterned as evident by cytochrome oxidase staining, which delineates the thalamocortical target structures in somatosensory cortex (Figure 2C-J). We quantified alterations in the cyctoarchitectural arrangement in this (Figure 2K-M), which demonstrated a cell non-autonomous affect on the genetically unaffected cortex.

In this report we now show for the first time, the mosaic deletion of *Tsc1* in the thalamus and link it to specific structural abnormalities and behavioral alterations. Therefore, one of the product/deliverables that was described in our initial Statement of Work that has been provided through this grant period is a complex allelic line of mice (*Gbx2*$^{CreER/+}$*;R26*$^{tdTomato/+}$*;Tsc1*$^{fl/fl}$) that is available to the TS and Neuroscience community and can be used to evaluate pharmacological approaches to diminish the affects of *Tsc1* loss of function and rescue of the proper establishment of this neural circuit. We have produced a top tier publication regarding this work and an additional manuscript related to this project. The first is a direct application of conditional gene deletion and circuit mapping to show a sensitive time period whereby *Tsc1* deletion causes neural circuit changes and behavioral abnormalities (Normand et al., 2013, Appendix 1). The second describes the use of conditional gene deletion and marking and tracking neural circuits (Normand et al., 2013a, Appendix 2). We also received an award to use these mice and the concept of circuit mapping to ascertain how mTOR inhibitors can rescue neural circuits disrupted by *Tsc1* deletion (See Reportable Outcomes, below).

The second task in our Statement of Work was to determine how *Tsc1* loss during embryonic development impacts thalamocortical circuit function and whether this impacts the cerebral cortex (target site). First, we validated by $pS6_{240}$ labeling in thalamic neurons, which is a high fidelity readout of mTOR signaling (Figure 3A,B). Our genetic approach resulted in a mosaic tapestry of 70% mutant (enlarged $pS66_{240}$+) and 30% unaffected (normal size, $pS6_{240}$-) neurons (Figure 3B and Normand et al., 2013, Appendix 1). Thus we are recapitulating a salient cellular feature of TS in our novel mouse model. We proposed to use a combination of GIFM, gene inactivation, and electrophysiology to delineate whether specific cohorts of *Tsc1*-deficient neurons in the thalamus affected the physiology of the developing neural circuits. This was further warranted by the ectopic expression of parvalbumin in mutant thalamic neurons (described above, Figure 3C-F‘).

For the first part of this task, we used thalamocortical slices (Agmon and Connors 1991; Normand et al., 2013, See Appendix 1 for additional details) obtained from postnatal day (P)20-23 mice (Figure 4). *Gbx2*^{CreER}*;Tsc1*$^{+/+}$ and *Gbx2*^{CreER}*;Tsc1*$^{\Delta E12/\Delta E12}$ slices were obtained and we performed whole cell patch clamp recordings and measured resting properties including input resistance, capacitance, and resting membrane potential (Figure 4A, Normand et al.,

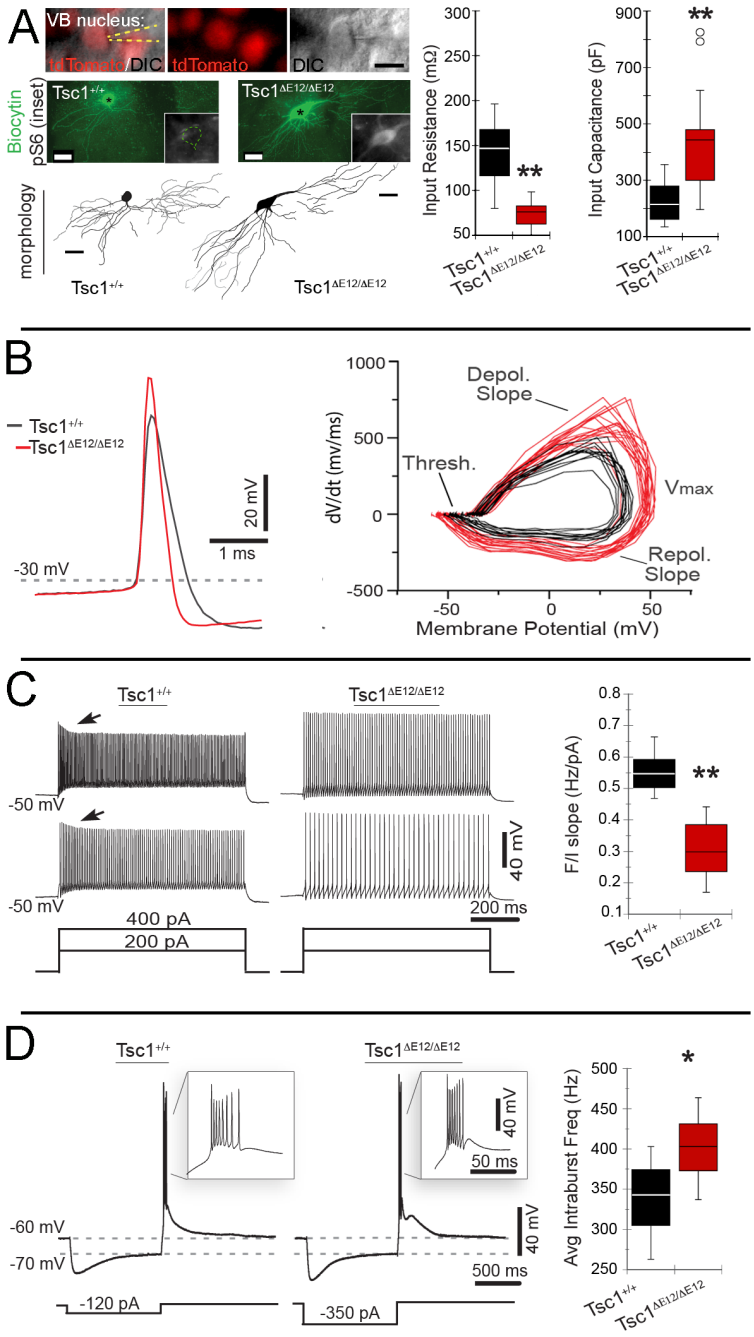

Figure 4. *Tsc1*$^{\Delta E12/\Delta E12}$ thalamic neurons have altered electrophysiological properties. (A) DIC/ fluorescence shows electrode (yellow dashed lines) targeted to a RFP+ (red) VB neuron. Neurons were filled with biocytin (green) and immunostained for pS6 (white, insets). Morphology was reconstructed as shown below each filled neuron. *Tsc1*$^{\Delta E12/\Delta E12}$ neurons had significantly lower membrane input resistance and higher input capacitance. (B) Representative traces from E12.5 control and mutant shows *Tsc1*$^{\Delta E12/\Delta E12}$ action potentials were faster and larger. *Tsc1*$^{\Delta E12/\Delta E12}$ action potential dynamics (right) had significantly different depolarization rates, maximum amplitude, and repolarization rate. controls (black). (C) Representative tonic voltage response of a Tsc1$^{+/+}$ and *Tsc1*$^{\Delta E12/\Delta E12}$ neuron to current injections (400 pA, top and 200 pA, bottom); The linear slopes of the F/I curves are quantified. (D) Representative voltage response of a *Tsc1*$^{+/+}$ and a Tsc1$^{\Delta E12/\Delta E12}$ thalamic neuron to hyperpolarizing current step. Insets show rebound bursts. Mean intraburst firing frequencies are quantified. Box plots represent minimum, first quartile (Q1), median, Q3, and maximum. Outliers (open circles) were >Q3+1.5*IQR or <Q1-1.5*IQR. Scale bars: (A) 20 μm (DIC), 30 μm (biocytin/ morphology). *p<0.05, **p<0.005.

2013, Appendix 1). We then determined action potential dynamics (Figure 4B), frequency-current curves (tonic firing mode) and average intraburst frequency (burst mode) (Figure 4B-D). Each of these physiological properties was altered in response to *Tsc1* deletion. Thus, we met the first part of this goal by analyzing thalamic neurons in which both copies of *Tsc1* were deleted. This experiment was very informative because we linked temporal gene deletion to altered neuronal activity *in vivo*.

The second part of this task was to determine how the structure and function of the cortex was affected by *Tsc1* deletion in the developing thalamus. We showed that there were secondary patterning defects as a result of the primary genetic lesion in the thalamus (See Figure 2, above). We also showed that compared to wildtype controls (Figure 5A), the deletion of *Tsc1* in the thalamus disrupted the cerebral cortex functionally as shown by local field potential analysis, which revealed abnormal 3Hz oscillations consistent with epileptiform activity in mutant mice (Figure 5B). Finally, consistent with the changes in neuronal physiology, circuitry, and local field potentials, the early deletion of *Tsc1* in the thalamus results in a pronounced over-grooming phenotype and robust seizures, which we quantified (Figure 5C).

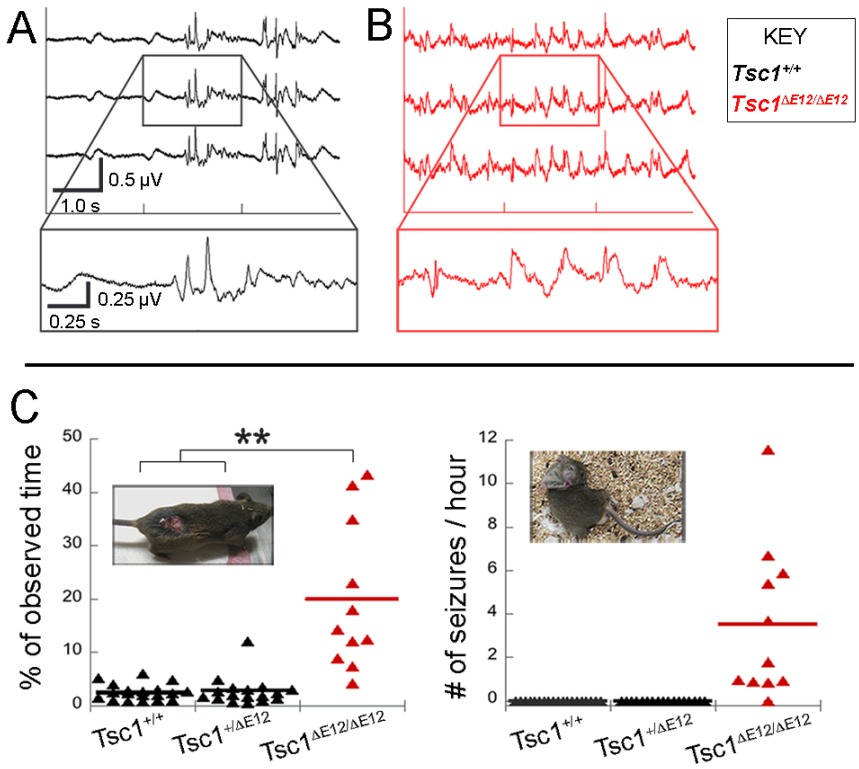

Figure 5. Abnormal brain activity and behaviors caused by thalamic *Tsc1* deletion. (A,B) Local field potentials in primary somatosensory neocortex were altered in *Tsc1*$^{\Delta E12/\Delta E12}$ mutants. (C) The percentage of time that each mouse groomed is plotted by genotype (left). Number of seizures per hour of observation time for each mouse is plotted by genotype (right). Insets show a *Tsc1*$^{\Delta E12/\Delta E12}$ mouse with a wound from overgrooming and a mutant with contorted posture during seizure.

A product/deliverable that was described in our initial Statement of Work that has been provided through this grant period is linking *Tsc1* function to specific intrinsic physiological properties and global brain function. We produced a top tier publication regarding this work. The first is a direct application of temporal gene deletion and neuronal function within a well-defined neural circuit to show a specific time period during which *Tsc1* deletion causes neural circuit

changes and behavioral abnormalities (Normand et al., 2013, Appendix 1). We submitted a new application to use these mice and the concept of temporal mosaic gene deletion to ascertain how the mTOR pathway contributes to autism-like repetitive behavior and to seizures. Notably, this is the first TS mouse model to capture both of these features. (See Reportable Outcomes).

KEY RESEARCH ACCOMPLISHMENTS

- Developed quantitative analysis of mosaicism in thalamus
- Thalamic relay neurons have ectopic parvalbumin expression
- Thalamic axons are do not properly innervate cerebral cortical target areas
- Somatosensory representation in the cerebral cortex is secondarily affected
- Genetic circuit mapping links mutant thalamic neurons and axon deficiencies
- Early *Tsc1* deletion in the thalamus causes alterations in intrinsic neuronal membrane properties
- Early *Tsc1* deletion in thalamus causes alterations in thalamic neuron burst and tonic firing properties
- Early *Tsc1* deletion in the thalamus causes global neural dysfunction and changes in cortical local field potentials
- Early *Tsc1* deletion causes seizures and excessive repetitive grooming
- *Tsc1* deletion causes cell non-autonomous consequences in addition to the primary genetic lesion

REPORTABLE OUTCOMES

Manuscripts (in chronological order)

Normand EA, Crandall SR, Thorn CA, Murphy EM, Voelcker B, Browning C, Machan JT, Moore CI, Connors BW, Zervas M* (2013) Temporal and mosaic *Tsc1* deletion in the developing thalamus disrupts thalamocortical circuitry, neural function, and behavior. *Neuron*, 78:895-909. Selected for epub ahead of printed journal and highlighted in "Spotlight On" feature. http://dx.doi.org/10.1016/j.neuron.2013.03.030 (NIHMS 463956). *corresponding author.

Normand E, Browning C, Hagan N, **Zervas M** (2013) Genetic marking of neural circuits. *Gene Exp Patterns,* Manuscript# MODGEP1128, Under Revision.

Abstracts (in chronological order)

Normand E, **Zervas M** (2011) Developmental and behavioral results of a Tsc1-null thalamus in an otherwise normal brain. *International TSC Research Conference: Summit for Drug Discovery in TSC and Related Disorders.* July 6-9, 2011, Washington DC. Student Travel Award.

Rios M, Normand E, **Zervas M** (2011) The effects of rapamycin treatment on *Tsc1*-deficient neurons in the thalamus. *BP-ENDURE at Hunter/NYU Neuroscience Research* Symposium. July 29-31, 2011.

Normand E, **Zervas M** (2011) mTOR pathway dysregulation during thalamic development leads to severe behavioral abnormalities in adult mice. *Mammalian Development Meeting.* September 2, 2011, UCHC, CT. Student Presentation.

Normand E, Browning C, **Zervas M** (2012) Cellular and behavioral consequences of mTOR pathway dysregulation within a population of subcortical neurons during mouse embryogenesis. Keystone Symposia: *Synapses and Circuits: From Formation to Disease*, Apr 1-6 2012, Steamboat Springs, Colorado. (* student travel award recipient).

Abstracts (continued)

Normand E, Browning C, **Zervas M** (2012) Seizures and compulsive grooming behaviors resulting from thalamus-specific *Tsc1* gene inactivation. *Gordon Research Conference: Fragile X and Autism-related Disorders.* June 10-15, 2012, Stonehill College, MA.

Normand E, Browning C, Machan JT, Voelcker B, **Zervas M** (2012) The deletion of *Tsc1* at specific developmental stages and in distinct regions of the thalamus disrupts neural circuit architecture and causes unique behavioral abnormalities. *Gordon Research Conference: Neural Development.* August 12-17, 2012, Salve Regina, RI.

Normand E, Smith J, **Zervas M** (2013) A dynamic developmental requirement for Tsc1 in the embryonic mouse thalamus. *International TSC Research Conference: Summit for Drug Discovery in TSC and Related Disorders.* June 20-23, 2011, Washington DC.

Invited Seminars

Zervas, M. "Determining how the temporal and spatial deletion of *Tsc1* and mTOR dysregulation during brain development causes neurological disease in Tuberous Sclerosis". Honorary Lecturer at 8th Annual Pharmacology Graduate Students' Symposium, Stony Brook University. June 6, 2011 (Invited by Graduate Students).

Zervas, M. "Genetic Approaches in Mouse to Interrogate Brain Development and Disease". University of Massachusetts, Amherst, February 22, 2012.

Zervas, M. "Temporal and mosaic disruption of *Tsc1* causes abnormal thalamocortical circuitry and complex behaviors in murine Tuberous Sclerosis". Brandeis University, Neurobiology Journal Club, Waltham MA, September 11, 2012.

Zervas, M. "Temporal and mosaic disruption of *Tsc1* causes abnormal thalamocortical circuitry and complex behaviors in murine Tuberous Sclerosis". University of Connecticut Health Center, Department of Neuroscience Seminar Series, Farmington CT, September 25, 2012.

Zervas, M. "*Tsc1* deletion with genetic mosaicism alters neural circuits, neuronal physiology, and behaviors". International Research Conference on TSC and Related Disorders: Molecules to Medicines, Washington DC, June 20-23, 2013.

Funding applied for based on work supported by this award

TS110083 (PI: **Zervas, M**)
DOD-CDMRP Idea Development Award
Dates: 2012-2015 (Funded, June 1, 2012 start date)
Temporal loss of Tsc1: Neural development and brain disease in Tuberous Sclerosis
Role: Principal Investigator; Total Award: $450,000 (direct costs)

The major goals of this project are to identify how critical windows of brain development are affected by the loss of *Tsc1,* how normal brain development is impacted by mTOR inhibition, and how the timing and duration of rapamycin ameliorates cellular, neural circuit, and behavioral changes in a conditonal mouse model of Tuberous Sclerosis.

R01 Accession # 3459040 (PI: Zervas M)
NIH R01
Dates: Dec 01, 2012-November 30, 2017
Subcortical brain structures and neurological disease in Tuberous Sclerosis

Role: Principal Investigator; Total Award: $1,250,000 (direct costs)

The major goals of this project are to conditionally delete *Tsc1* in the striatum during embryonic development and ascertain how FMRP phosphorylation and SAPAP3 protein expression are affected to link a molecular pathway to repetitive behaviors in a mouse model of Tuberous Sclerosis.

Scored: 39 Percentile

SFARI ID#: 275701 (PI: **Zervas, M**)
Simons Foundation Autism Research Initiative Annual RFA (2013)
Linking genetic mosaicism, neural circuit abnormalities and behavior. Simons Foundation Autism Research Initiative (SFARI) 2013 RFA.
Dates: July 01, 2013-June 30, 2015
Role: Principal Investigator; Total Award: $250,000 (direct costs)
Status: Scored, Under review for final award.

Training supported by this award

Elizabeth Normand, Graduate Student in the Brown Neuroscience Graduate Program has been supported in part by this grant and has conducted the experiments described in this report. Elizabeth is also the first author on two recently submitted manuscripts that are related to this award. Elizabeth has presented her findings at three meetings and has received travel awards because of the high quality data and impact of her work.

CONCLUSION

Our research proposal used an innovative approach that tested novel ideas, developed new animal model systems, and modified existing molecular approaches to specifically address hypotheses relevant to neural circuitry and neuronal dysfunction in TS. It is clear that TS is a multi-systemic disorder that affects cognitive processing in a substantial cohort of TS patients. However, a thorough understanding of the affected brain regions, neuronal cell types, and neural circuits has not been ascertained in TS. Finally, the developmental mechanisms causing brain disease in TS have not been carefully linked to aberrant neurological function at the cellular, circuit, or behavioral level. We have established an animal model that mimics salient features of TS and is an innovative advance to address deficiencies in TS research. Genetic approaches in mice allow us to test hypotheses that are central to understanding TS and we are using a sophisticated genetic method that I helped pioneer (Zervas et al., 2004, Brown et al., 2009, Ellisor et al., 2009, Ellisor et al., 2010; Hagan et al., 2012, Yang et al., 2013) to induce genetic mutations and mark mutant neuronal populations with spatial and temporal control *in vivo*. We successfully applied this methodology to inactivate *Tsc1* and mark mutant neurons including their axonal projections to target sites in development. Thus, innovative conceptual issues we addressed during our funding period are the following: 1. Physiological properties of a specific population of neurons are affected by *Tsc1* loss of function; 2. Structural alterations of thalamic neuron projections are affected in TS. 3. *Tsc1* loss of function also affects the cerebral cortex structurally and functionally in a cell non-autonomous manner. This project created a new paradigm in which select neural circuits that have been shown to be affected in human TS were manipulated in mice. The findings represent more than an incremental understanding of TS by further delineating brain regions that may contribute to TS and by establishing which functionally connected regions are affected at the cellular level. In addition, the combination of mouse lines we used will be beneficial to screen for therapeutic compounds in a recently funded project that is designed to treat specific types of neurons and distinct neural circuits in TS. The highly

innovative nature of our approach is exemplified by performing the first temporally and spatially controlled biallelic deletion of *Tsc1* and establishing the first link between one specific brain region and a prominent behavioral change relevant to human TS. Notably, this research project led to new funding opportunities and to a new manuscript recently published in *Neuron.*

This project is clinically relevant to TS because the gene that we are deleted (*Tsc1*) encodes hamartin (TSC1 protein) that forms a heterodimeric complex with tuberin (TSC2 protein). Together these proteins regulate downstream mammalian target of rapamycin (mTOR). The “mTOR pathway” is a central hub of intracellular signaling that is vital for cellular processes including cell growth, axon guidance, and transcriptional regulation (Crino 2004, Ess et al., 2006, de Vries et al., 2007, Swiech et al., 2008). Signal transduction through mTOR culminates in the phosphorylation of the ribosomal protein S6 (pS6), which is elevated to high levels when mTOR signaling is dysregulated (Crino et al., 2010). We elucidated the role of *Tsc1*/mTOR in thalamic neurons and identified a developmental time point that is sensitive to *Tsc1* deletion.

This project has made original and important contributions to advancing TS related research. First, we mutated neurons in selective brain regions with temporal control to isolate a critical time point that *Tsc1* inactivation is most pathogenic *in vivo*. Notably, this time point in mice is equivalent to 8-9 weeks of human gestation and is a time where mutations in *TSC1* could make significant contributions to brain dysfunction. Second, we simultaneously marked mutant cells and traced axonal projections to identify changes in developing neural circuits related the loss of *Tsc1*. Third, we showed physiological changes occurring in mutant thalamic neurons. This project will positively affect TS research and possibly patient care by having developed an animal model with both temporal and spatial control of *Tsc1* deletion that we will use to test therapeutic approaches in a cell-type specific manner. This approach will be a foundation to test whether rapamycin is a viable treatment strategy to ameliorates specific features of TS and may be helpful to identify and test novel therapeutic targets for TS. My background in using animal models of neurological developmental brain disorders and therapeutic intervention in Niemann-Pick Disease Type C (NPC) led directly to human clinical trials to NPC. Thus, we have a track record of successfully conducting innovative approaches to understand brain diseases and show that our potential gains to uncover novel aspects of the developmental mechanisms underpinning TS warranted our use of a complex genetic strategy. We have begun to establish a correlation between gene inactivation, changes in neural circuit structure, and physiology. Our animal model system will allow us to test the feasibility of pharmacological treatment strategies in ameliorating features of TS with an emphasis on how specific brain regions (thalamus) respond to rapamycin administration. We were recently awarded a grant to conduct the drug treatment studies.

REFERENCES

Agmon, A., and Connors, B.W. (1991). Thalamocortical responses of mouse somatosensory (barrel) cortex in vitro. Neuroscience *41*, 365-379.

Asano, E., Chugani, D.C., Muzik, O., Behen, M., Janisse, J., Rothermel, R., Mangner, T.J., Chakraborty, P.K., and Chugani, H.T. (2001). Autism in tuberous sclerosis complex is related to both cortical and subcortical dysfunction. Neurology *57*, 1269-1277.

Brown A, Brown B, Ellisor D, Hagan, N, Normand, E, **Zervas, M**. (2009) A Practical Approach to Genetic Inducible Fate Mapping: A Visual Guide to Mark and Track Cells *In Vivo. J Vis Exp*, **43:** pii: 1687, doi: 10.3791/1687 (PMCID: PMC2846818**)**.

Crino, P.B. (2004). Molecular pathogenesis of tuber formation in tuberous sclerosis complex. J Child Neurol *19*, 716-725.

Crino, P.B., Aronica, E., Baltuch, G., and Nathanson, K.L. (2010). Biallelic TSC gene inactivation in tuberous sclerosis complex. Neurology *74*, 1716-1723.

de Vries, P.J., and Howe, C.J. (2007). The tuberous sclerosis complex proteins--a GRIPP on cognition and neurodevelopment. Trends Mol Med *13*, 319-326.

Ellisor, D., Koveal, D., Hagan, N., Brown, A., and **Zervas, M.** (2009). Comparative analysis of conditional reporter alleles in the developing embryo and embryonic nervous system. Gene Expr Patterns *9*, 475-489.

Ellisor D, **Zervas, M** (2010) Tamoxifen dose response and conditional cell marking: Is there control? *Mol Cell Neurosci* 45:132-138. Selected scientific image featured on cover (PMID: 20600933).

Ess, K.C. (2006). The neurobiology of tuberous sclerosis complex. Semin Pediatr Neurol *13*, 37-42.

Hagan N, **Zervas M** (2012) *Wnt1* expression temporally allocates upper rhombic lip progenitors and defines their terminal cell fate in the cerebellum. *Mol Cell Neurosci* 49:217-229. PMID: 22173107 (manual entry for PMCID, ID pending).

Madisen, L., Zwingman, T.A., Sunkin, S.M., Oh, S.W., Zariwala, H.A., Gu, H., Ng, L.L., Palmiter, R.D., Hawrylycz, M.J., Jones, A.R., Lein, E.S., and Zeng, H. (2010). A robust and high-throughput Cre reporting and characterization system for the whole mouse brain. Nat Neurosci *13*, 133-140.

Normand EA, Crandall SR, Thorn CA, Murphy EM, Voelcker B, Browning C, Machan JT, Moore CI, Connors BW, **Zervas M** (2013) Temporal and mosaic *Tsc1* deletion in the developing thalamus disrupts thalamocortical circuitry, neural function, and behavior. *Neuron*, 78:895-909. Selected for epub ahead of printed journal and highlighted in “Spotlight On” feature. http://dx.doi.org/10.1016/j.neuron.2013.03.030 (NIHMS 463956).

Normand E‡, Browning C[i], Hagan N[ii], **Zervas M** (2012) The timing and duration of *Gbx2* expression delineates thalamocortical or dopamine medial forebrain bundle circuitry. *Gene Expr Patterns*, Manuscript #MODGEP1128, Under revision.

Ridler, K., Bullmore, E.T., De Vries, P.J., Suckling, J., Barker, G.J., Meara, S.J., Williams, S.C., and Bolton, P.F. (2001). Widespread anatomical abnormalities of grey and white matter structure in tuberous sclerosis. Psychol Med *31*, 1437-1446.

Swiech, L., Perycz, M., Malik, A., and Jaworski, J. (2008). Role of mTOR in physiology and pathology of the nervous system. Biochim Biophys Acta *1784*, 116-132.

Zervas, M., Millet, S., Ahn, S., and Joyner, A.L. (2004). Cell behaviors and genetic lineages of the mesencephalon and rhombomere 1. Neuron *43*, 345-357.

Neuron
Article

Temporal and Mosaic *Tsc1* Deletion in the Developing Thalamus Disrupts Thalamocortical Circuitry, Neural Function, and Behavior

Elizabeth A. Normand,[1] Shane R. Crandall,[1] Catherine A. Thorn,[1] Emily M. Murphy,[1] Bettina Voelcker,[2] Catherine Browning,[2] Jason T. Machan,[3] Christopher I. Moore,[1] Barry W. Connors,[1] and Mark Zervas[2,*]
[1]Department of Neuroscience
[2]Department of Molecular Biology, Cell Biology and Biochemistry
Division of Biology and Medicine, Brown University, 70 Ship Street, Providence, RI 02903, USA
[3]Departments of Orthopedics and Surgery at Rhode Island Hospital and the Warren Alpert Medical School at Brown University, Providence, RI 02903, USA
*Correspondence: mark_zervas@brown.edu
http://dx.doi.org/10.1016/j.neuron.2013.03.030

SUMMARY

Tuberous sclerosis is a developmental genetic disorder caused by mutations in *TSC1*, which results in epilepsy, autism, and intellectual disability. The cause of these neurological deficits remains unresolved. Imaging studies suggest that the thalamus may be affected in tuberous sclerosis patients, but this has not been experimentally interrogated. We hypothesized that thalamic deletion of *Tsc1* at distinct stages of mouse brain development would produce differential phenotypes. We show that mosaic *Tsc1* deletion within thalamic precursors at embryonic day (E) 12.5 disrupts thalamic circuitry and alters neuronal physiology. *Tsc1* deletion at this early stage is unique in causing both seizures and compulsive grooming in adult mice. In contrast, only a subset of these phenotypes occurs when thalamic *Tsc1* is deleted at a later embryonic stage. Our findings demonstrate that abnormalities in a discrete population of neurons can cause global brain dysfunction and that phenotype severity depends on developmental timing and degree of genetic mosaicism.

INTRODUCTION

Tuberous sclerosis (TS) is a complex mosaic genetic disorder that affects one in 6,000 children and commonly presents in infancy or early childhood, suggesting an early developmental basis for the disease. TS is characterized by benign hamartomas in multiple organs, but neurological involvement is common and debilitating. Patients may experience seizures (70%–90%), intellectual disability (50%), autism (25%–50%), and sleep disturbances (McClintock, 2002). Hamartomas in the brain were thought to cause neurological symptoms, but the extent of hamartomas does not necessarily correlate with the severity of neurological impairment (Wong and Khong, 2006). This suggests that subtle aspects of brain development or function are perturbed in TS.

Genetically, TS is caused by mutations in either of two tumor suppressor genes, *TSC1* or *TSC2*, and is inherited in an autosomal dominant manner. In addition to the inherited mutation, a somatic mutation in the remaining functional allele results in loss of heterozygosity and gives rise to isolated TSC null cells that proliferate and contribute to the formation of hamartomas (Au et al., 1999). This "two-hit" mechanism results in a mosaic population of cells in a patient's organs: a discrete population that has undergone a second hit to become null for *TSC1* or *TSC2* and surrounding heterozygous cells. However, it is unclear whether this two-hit mechanism underlies neurocognitive aspects of TS (Crino et al., 2010). To experimentally emulate this mosaic state within the brain and to test whether targeted disruption of *Tsc1* in a focal manner can disrupt global brain function, we employed an inducible CreER/*loxP*-based method of gene inactivation in mice, which produces a spatially restricted, mosaic population of *Tsc1* mutant cells surrounded by genetically unaffected cells.

The TSC1 and TSC2 proteins form a heterodimer that negatively regulates the mTOR pathway, which in turn modulates a wide array of cellular processes (Hay and Sonenberg, 2004). The multifaceted nature of the mTOR pathway raises the possibility that the effects of TSC loss of function vary depending on a cell's identity, functional role, or developmental state at the time of *TSC* mutation. During brain development, cell fate specification, cell growth, differentiation, and axonal connectivity are tightly regulated to establish proper brain architecture and function. Thus, spatially and temporally controlling *Tsc1* deletion in targeted cell types and comparing the resulting phenotypes will be instructive to our understanding of this complex disease. Because our CreER/*loxP* experimental system is temporally inducible, we are able to target *Tsc1* inactivation at distinct stages of brain development.

Numerous studies have evaluated how *Tsc1/2* deletion affects the cerebral cortex. Subcortical regions have not been extensively evaluated thus far, although one such structure that warrants investigation based on previous findings is the thalamus. MRI-imaging studies of TS patients show that changes in

thalamic gray matter volume correlate with poor cognitive performance (Ridler et al., 2007). Thalamic involvement in TS is relevant because the thalamus provides specific, information-carrying afferents to the cerebral cortex and plays a crucial role in higher-order cognitive processes (Saalmann and Kastner, 2011). The thalamus also projects robustly to the striatum, a pathway implicated in attentional orientation (Smith et al., 2004). Notably, dysfunction of the thalamus and striatum are implicated in obsessive compulsive disorder and autism (Hardan et al., 2008; Fitzgerald et al., 2011). The relay cells of the thalamus receive extensive excitatory feedback from the neocortex and inhibitory inputs from the thalamic reticular nucleus (TRN). Due, in part, to this extensive reciprocal connectivity, the thalamus plays a key role in oscillatory neocortical dynamics and in the generation of low-frequency rhythms, which are prominent in specific forms of epileptic activity (Blumenfeld, 2003). We have used spatially and temporally controlled *Tsc1* gene deletion to address how altered thalamic development has the potential to perturb widespread neural function and behavior.

RESULTS

Spatiotemporal Contribution of the *Gbx2* Lineage to Adult Thalamic Neurons

To temporally and spatially control *Tsc1* gene deletion, we combined three genetically modified mouse alleles (see Figure S1A available online): (1) $Gbx2^{CreER}$, which targets CreER expression to thalamic cells (Chen et al., 2009); (2) $Tsc1^{fl}$, which is converted into a null allele ($Tsc1^{\Delta}$) by Cre-mediated recombination (Kwiatkowski et al., 2002); and (3) either $R26^{LacZ}$ (Soriano, 1999) or $R26^{tdTomato}$ (Madisen et al., 2010), which produce β-galactosidase (β-gal) or red fluorescent protein (RFP), respectively, upon Cre-mediated recombination. CreER remains quiescent until it is transiently activated by tamoxifen. Subsequently, the $Tsc1^{fl}$ gene is permanently converted to $Tsc1^{\Delta}$ and the conditional reporter genes are permanently activated in the thalamus (Figures S1B and S1C). $Gbx2^{CreER}$ expression has been reported in the spinal cord (Luu et al., 2011) but, within the brain, regions outside of the thalamus had only very sparse recombination with tamoxifen at E12.5 (Figure S1). We validated the fidelity of $Tsc1^{fl}$ recombination in the thalamus compared to the neocortex (Figures S1D and S1E). Operationally, we use $Tsc1^{\Delta E12/\Delta E12}$ to indicate mutant animals that received tamoxifen on embryonic day (E) 12.5 and $Tsc1^{\Delta E18/\Delta E18}$ to indicate mutants that received tamoxifen on E18.5. We first performed genetic inducible fate mapping on $Gbx2^{CreER};R26^{LacZ}$ animals to characterize the extent, spatial distribution, and molecular identity of recombined cells (Figure 1). We administered tamoxifen to pregnant females carrying $Gbx2^{CreER};R26^{LacZ}$ embryos at E12.5 or E18.5 and determined the long-term lineage contribution to the thalamus. Postnatal brain sections were analyzed by immunohistochemistry (IHC) for β-gal expression from the activated $R26^{LacZ}$ allele. E12.5 fate-mapped cells (green) were distributed widely throughout the full medial-lateral extent of the thalamus (Figures 1A–1F). In animals that received tamoxifen at E18.5, the spatial extent of recombination was reduced (Figures 1G–1L). Regions that underwent recombination at both E12.5 and E18.5 include the anteromedial and mediodorsal nuclei. The ventrolateral, ventromedial, ventrobasal, laterodorsal, and the lateral geniculate nuclei underwent recombination at E12.5 but were not marked at E18.5. Nuclei that underwent extensive recombination early (E12.5) and moderate mosaic recombination later (E18.5) include the posterior nucleus and the medial geniculate nucleus. We investigated whether recombination occurred in a particular cell type by IHC for β-gal in combination with parvalbumin (PV, red, Figures 1A–1C and 1G–1I) or calbindin (Calb, red, Figures 1D–1F and 1J–1L). Within relay nuclei, β-gal+ cells contributed to both Calb− and Calb+ cells at both E12.5 and E18.5 (Figures 1D–1F and 1J–1L, arrowheads). Although most excitatory relay neurons did not express any PV+ within their soma, there were a few examples of neurons with low PV+ levels that also expressed β-gal at E12.5 (Figures 1A–1C, arrowheads). Notably, the highly PV+ inhibitory thalamic reticular nucleus (TRN) did not undergo recombination at either stage.

mTOR Pathway Dysregulation Occurs Rapidly after *Tsc1* Recombination

We used the inducible nature of our system to control the timing of *Tsc1* gene deletion and determine how rapidly mTOR dysregulation occurs. We administered tamoxifen to E12.5 embryos with $Gbx2^{CreER}$ and either $Tsc1^{+/+}$ or $Tsc1^{fl/fl}$. E12.5 is a stage when thalamic neurons have differentiated and are beginning to extend axonal projections toward the cortex (Molnár et al., 1998). We compared mTOR activity in the $Tsc1^{+/+}$ and $Tsc1^{\Delta E12/\Delta E12}$ thalamus at E14.5 by IHC for the S6 protein phosphorylated at Ser240/244 (pS6), which is a reliable readout of mTOR pathway activity. We observed basal pS6 expression in the E14.5 $Tsc1^{+/+}$ brain (Figure 2A), consistent with the requirement for mTOR activity during early development (Hentges et al., 2001). Nevertheless, in the E14.5 $Tsc1^{\Delta E12/\Delta E12}$ thalamus, there was an increase in thalamic pS6 levels over controls (Figure 2B). In E17.5 $Tsc1^{\Delta E12/\Delta E12}$ embryos, thalamic levels of pS6 were also dramatically increased compared to controls (Figures 2C and 2D). These experiments show how rapidly neurons respond to *Tsc1* gene inactivation in vivo during embryogenesis. mTOR dysregulation persisted in the postnatal $Tsc1^{\Delta E12/\Delta E12}$ thalamus but was negligible in the $Tsc1^{+/+}$ and $Tsc1^{+/\Delta E12}$ controls (Figures 2E–2G). $R26^{LacZ}$ reporter activation (β-gal, green) validated that all genotypes had a similar extent of CreER-mediated recombination. Similar results were seen with IHC for pS6(Ser235/236), another mTOR-dependent S6 phosphorylation site (data not shown).

E12.5 *Tsc1* Deletion Alters Morphology and Circuitry in Mature Thalamic Neurons

To determine whether mTOR dysregulation affected the morphology of adult thalamic neurons, we quantified soma size based on the somatodendritic marker microtubule-associated protein 2 (MAP2). Sections were also stained for pS6 (red). CreER-mediated recombination produced mTOR dysregulation in 70% of thalamic neurons in $Tsc1^{\Delta E12/\Delta E12}$ mice (621 out of 878 MAP2+ neurons). We took advantage of this mosaicism and sorted neurons into two populations: dysregulated $Tsc1^{\Delta E12/\Delta E12}$ neurons (pS6+, filled arrowheads) and unaffected neurons (pS6−, open arrowheads, Figure 3B). The geometric mean soma area of pS6+ $Tsc1^{\Delta E12/\Delta E12}$ neurons was 403 μm, which was

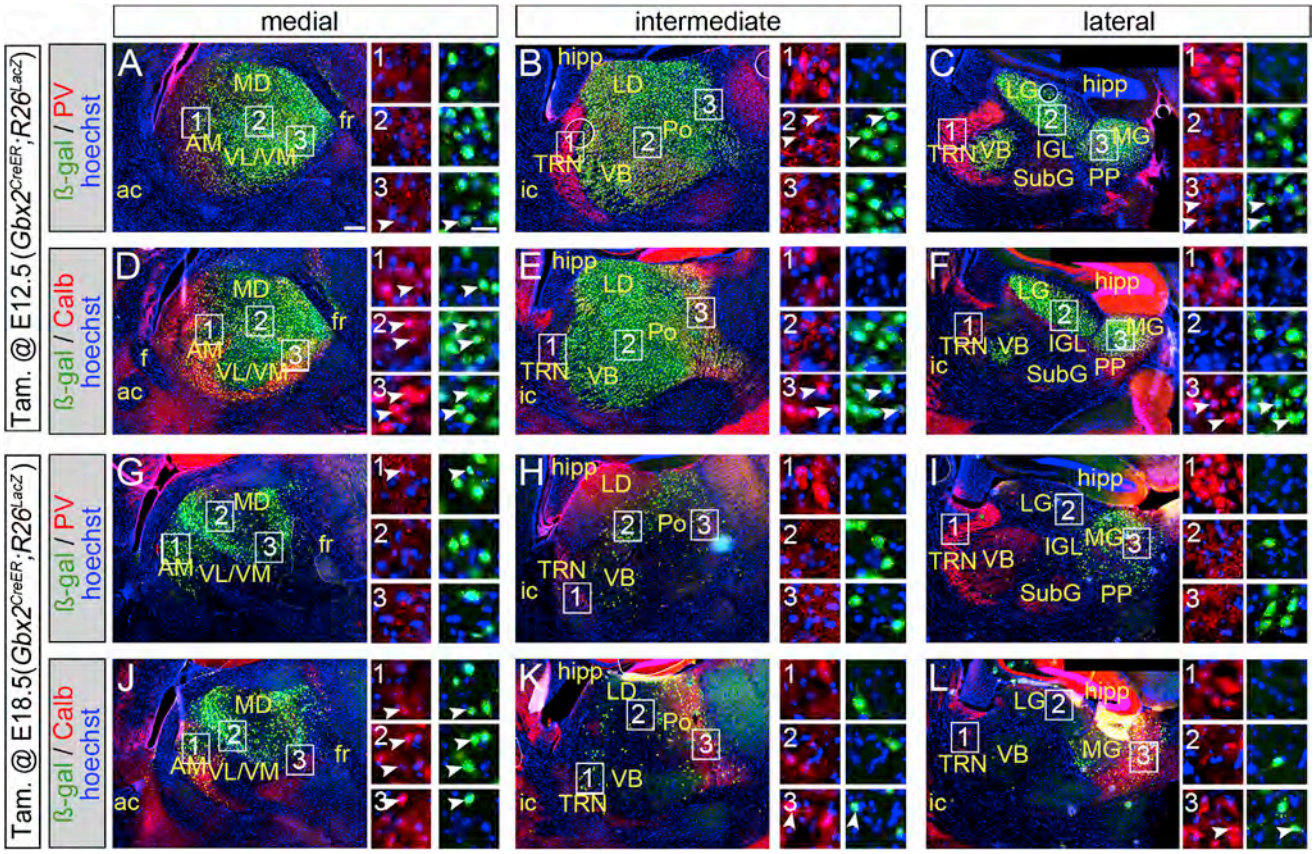

Figure 1. *Gbx2*^{CreER}-Mediated Recombination in Thalamic Neurons

(A–F) Tamoxifen at E12.5. Expression of β-gal (green) in medial (A and D), Intermediate (B and E), and lateral (C and F) sagittal sections of adult thalamus. Colocalization with parvalbumin (PV, red; A, B, and C) or calbindin (Calb, red; D, E, and F) is indicated by arrowheads.

(G–L) Tamoxifen at E18.5. Recombination in medial (G and J), Intermediate (H and K), and lateral (I and L) sagittal section of adult thalamus showing recombined cells (β-gal, green) and PV+ (G–I) or Calb+ (J–L) neurons. Scale bar in (A) (270 μm) applies to low-magnification panels; scale bar in (A3) (30 μm) applies to high-magnification panels. Thalamic nuclei: AM, anteromedial; LD, laterodorsal; LG, lateral geniculate; MD, mediodorsal; MG, medial geniculate; Po, posterior; PP, peripeduncular; SubG, subgeniculate; TRN, thalamic reticular; VB, ventrobasal; VL, ventrolateral; VM, ventromedial; a.c., anterior commissure; f, fornix; fr, fasciculus retroflexus; hipp, hippocampus; i.c., internal capsule; IGL, intergeniculate leaflet. See also Figure S1.

significantly larger than *Tsc1*$^{+/+}$ (220 μm^2), *Tsc1*$^{\Delta E12/+}$ (209 μm^2), and pS6− *Tsc1* $^{\Delta E12/\Delta E12}$ (203 μm^2) neurons ($p = 0.003$, $n = 3$ mice per genotype, Figure 3B, see Table S1 for variability estimates). Because normal-sized pS6− cells neighbored enlarged pS6+ cells, we conclude that neuron overgrowth occurs in a cell-autonomous manner. We also detected substantial PV expression in fibers within the internal capsule of *Tsc1*$^{\Delta E12/\Delta E12}$ brains (Figures 3E and 3E′), which was absent in controls (Figures 3C and 3C′). Because corticothalamic and thalamocortical axons (TCAs) intermingle in the internal capsule, we assayed for *R26*^{tdTomato} expression. Comparison of RFP/PV colocalization in the fibers (Figures 3C, 3C′ and 3E, 3E′) and cell bodies of thalamic relay neurons (Figures 3D, 3D′, 3F, and 3F′) confirmed that the PV+ signal was from the *Tsc1*$^{\Delta E12/\Delta E12}$ relay neurons and their TCAs. Because previous TS mouse models have described myelination defects and astrocytosis (Meikle et al., 2008; Way et al., 2009; Carson et al., 2012), we assayed for myelin basic protein (MBP) and glial fibrillary acidic protein (GFAP). Control mice had clear MBP labeling throughout the brain, including within the thalamus and the internal capsule, and this did not differ between mutants and controls (Figure S2). Only sporadic GFAP+ cells were observed in the thalamus of both mutants and controls (Figure S2). Because the enlarged *Tsc1*$^{\Delta E12/\Delta E12}$ thalamic neurons were reminiscent of dysmorphic neurons in neuronal storage disorders, we assayed for GM2 ganglioside, which accumulates in these disorders (Zervas et al., 2001). GM2 was not detected in *Tsc1*$^{+/+}$ or *Tsc1*$^{\Delta E12/\Delta E12}$ thalamic neurons (data not shown).

We next investigated whether deleting *Tsc1* at E12.5 affected thalamocortical circuit development. We took advantage of the highly organized and stereotyped projections from the thalamic ventrobasal nuclear complex (VB) to the vibrissa barrels in layer IV of primary somatosensory cortex (SI) (Woolsey and Van der Loos, 1970). We used *R26*^{tdTomato} to label thalamic projections for neural circuit analysis. In control animals (adults), TCAs innervated layer IV of somatosensory cortex in discrete clusters corresponding to individual vibrissae (Figure 4A, region 1), similar to descriptions using nongenetic labeling (Wimmer et al., 2010). In

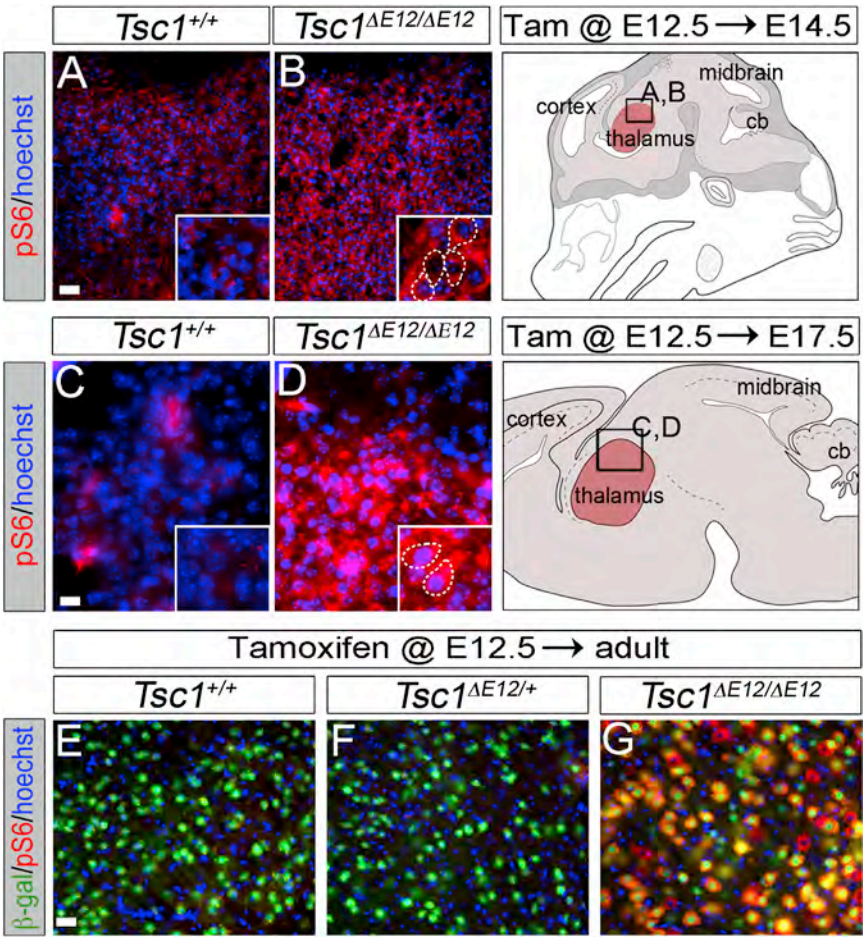

Figure 2. Conditional Deletion of *Tsc1* in the Thalamus Causes Rapid mTOR Dysregulation

(A and B) pS6 (red) immunolabeling in E14.5 $Tsc1^{\Delta E12/\Delta E12}$ embryos.

(C and D) E17.5 $Tsc1^{\Delta E12/\Delta E12}$ embryos had a robust increase in pS6 (red) compared to controls. (E–G) Adult $Tsc1^{\Delta E12/\Delta E12}$ mutants had high pS6 levels (red). $R26^{LacZ}$ (β-gal, green) independently showed similar recombination efficiency across genotypes. Control and mutant sections were imaged with identical exposure settings. $n \geq 3$ animals per genotype per stage. Scale bars represent 30 μm in (A), (B), and (E)–(G) and 15 μm in (C) and (D).

contrast, $Tsc1^{\Delta E12/\Delta E12}$ mice (adults) had a diffuse pattern of cortical innervation: individual barrels were indistinguishable in layer IV (Figure 4B, region 1) and projections were overabundant in the deep layers (arrow). Within the internal capsule, TCA fascicles appeared less sharply defined compared to controls (Figures 4A and 4B, region 2). We confirmed these findings by stereotaxic injection of lentiviral-GFP into VB in control and mutant animals (Cruikshank et al., 2010), which filled infected neurons with GFP, including their axons and terminal projections (Figure S3).

To assess the effect of the disorganized TCAs on genetically normal cortical targets, we used cytochrome oxidase (CO) staining, which is enriched in the dendritic mitochondria of layer IV spiny stellate barrel neurons (Wong-Riley and Welt, 1980) and nicely delineates the barrel hollow structures (Figures 4C–4J). In controls, RFP+ TCAs were enriched in the CO+ barrel hollows and largely excluded from the surrounding septa (Figure 4E, asterisks and arrowheads, respectively). In $Tsc1^{\Delta E12/\Delta E12}$ mutants, the TCAs were not only localized to barrel hollows (Figure 4I, asterisks) but were also heavily distributed throughout the septal regions (arrowheads). The CO staining pattern was also altered in $Tsc1^{\Delta E12/\Delta E12}$ brains, suggesting that the cortical barrels were improperly patterned (Figure 4, compare 4C and 4D to 4G and 4H). The small vibrissa barrels were particularly indistinct in the $Tsc1^{\Delta E12/\Delta E12}$ cortex (Figures 4D and 4H, gray regions), which was a phenotype reminiscent of that described in *mGluR5* knockout mice (She et al., 2009). To quantitatively assess the large barrels (Figures 4D and 4H, orange regions), we outlined the limits of the SI vibrissa region and the individual barrels based on CO staining in a genotype-blinded manner. The average barrel size was larger in mutants (58 mm^2) compared to controls (37 mm^2, $p < 0.001$, $n \geq 72$ barrels across 3 mice per genotype, two-sample two-tailed t test; Figure 4K). Quantification of the septal proportion of the barrel region based on CO staining showed no significant difference between $Tsc1^{\Delta E12/\Delta E12}$ (21%) and controls (25%, $p = 0.16$, $n = 3$ mice per genotype, two-sample two-tailed t test; Figure 4L). To determine whether the organization of the cortical cell bodies was altered, we combined NeuN antibody labeling with CO staining to quantify cell density in the barrel hollows (outer limit of the CO+ barrel hollow is indicated by the dashed lines in Figures 4F and 4J) and the surrounding barrel wall region (indicated by the solid lines in Figures 4F and 4J) (Narboux-Nême et al., 2012). Mutants had lower neuron density in the barrel wall region (3.7 neurons/mm^2) than controls (Figure 4M; 4.5 neurons/mm^2). This same trend applied to the barrel hollow region ($Tsc1^{\Delta E12/\Delta E12}$ 3.2 neurons/mm^2; $Tsc1^{+/+}$ 3.5 neurons/mm^2, $p_{wall} < 0.001$, $p_{hollow} = 0.020$, $n \geq 20$ nonadjacent barrels across 3 animals per genotype, two-sample two-tailed t test; Figure 4M). Together, these experiments confirmed that thalamic *Tsc1* inactivation causes mTOR dysregulation, cell overgrowth, aberrant PV expression, and altered thalamocortical projections that affect the genetically normal neocortex.

Later Deletion of *Tsc1* Causes More Subtle Cellular Changes than Those Arising from Early Inactivation

We administered tamoxifen at E18.5 to compare the effects of thalamic *Tsc1* inactivation at a later developmental stage. By E18.5, thalamic neurons have fully differentiated, their axonal

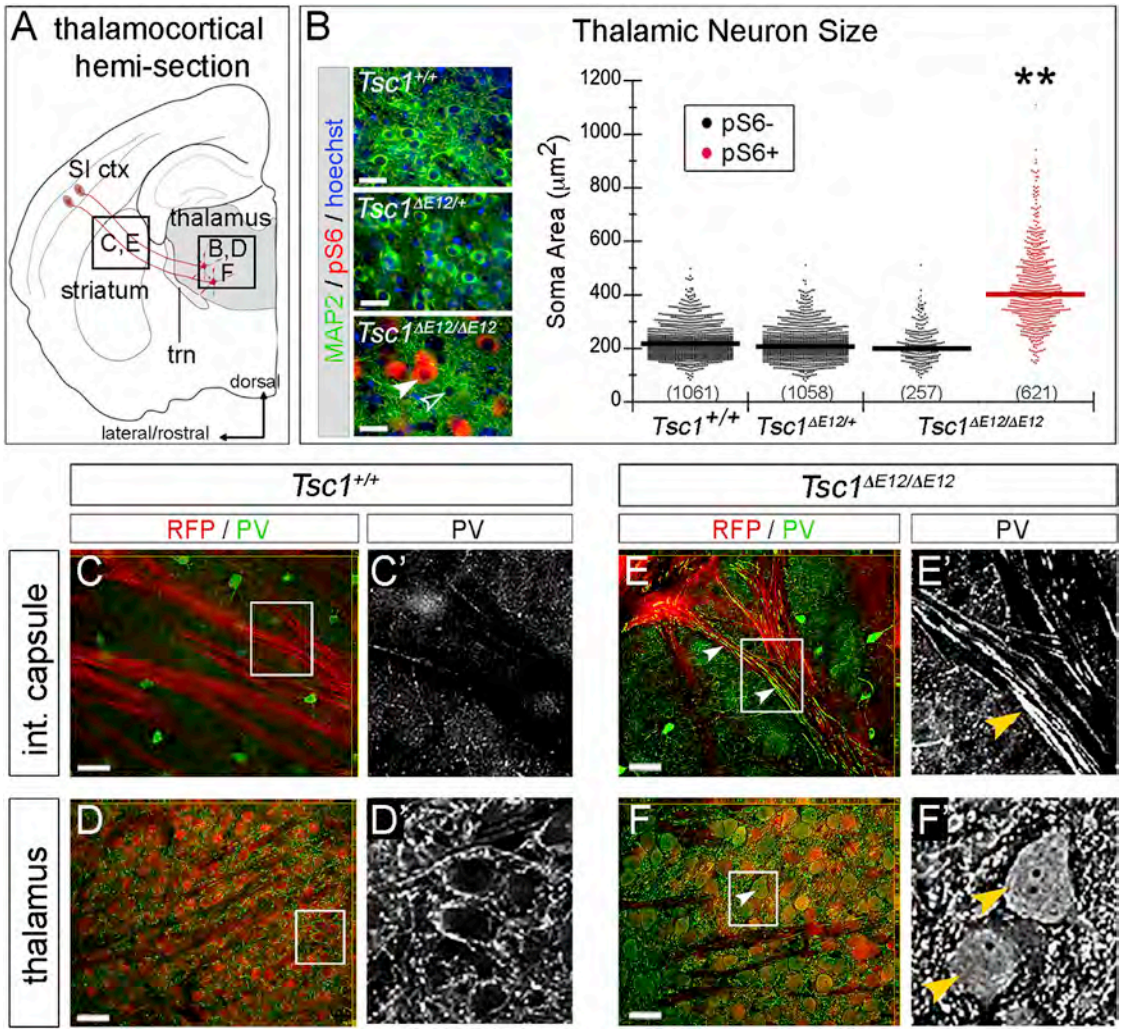

Figure 3. Cellular Phenotypes Caused by *Tsc1* Deletion in Thalamus at E12.5

(A) Thalamocortical regions of interest.

(B) Sections from adult mice were immunolabeled for MAP2 (green), pS6 (red), and counterstained with hoechst (blue). Thalamic neurons of $Tsc1^{+/+}$ and $Tsc1^{\Delta E12/+}$ mice were pS6−. Recombination produced a mosaic thalamus of unaffected (pS6−, open arrowhead) and affected (pS6+, filled arrowhead) neurons. Soma area is plotted by genotype and pS6 status. Numbers of neurons are listed and geometric means are indicated by horizontal lines.

(C–F′) Analysis of PV (green) and RFP (red) revealed PV+ fibers in the internal capsule of $Tsc1^{\Delta E12/\Delta E12}$ mice (E and E′, arrowheads), but not in controls (C and C′). Soma of $Tsc1^{\Delta E12/\Delta E12}$ RFP+ neurons were also PV+ (F and F′, arrowheads, which was not seen in controls (D and D′)). n = 3 animals per genotype. Scale bars represent 32 μm in (B) and 48 μm in (C)–(F). **$p < 0.005$. See also Figure S2.

projections have accumulated in the subplate of their cortical target regions, and they are beginning to invade the cortical layers (Molnár et al., 1998). Upon reaching adulthood, $Tsc1^{\Delta E18/\Delta E18}$ brains were analyzed for mTOR activity and cell size (Figure 5A). mTOR was dysregulated in 29% of neurons (221 out of 542 MAP2+ cells) in the $Tsc1^{\Delta E18/\Delta E18}$ thalamus, as evidenced by increased pS6 (Figure 5A). We analyzed cell size as described in Figure 3. Although some pS6+ $Tsc1^{\Delta E18/\Delta E18}$ neurons skewed toward larger cell sizes than pS6− neurons, on average, pS6+ $Tsc1^{\Delta E18/\Delta E18}$ neurons (359 μm^2) were not significantly larger than pS6− $Tsc1^{\Delta E18/\Delta E18}$ (246 μm^2), $Tsc1^{\Delta E18/+}$ (242 μm^2), or $Tsc1^{+/+}$ (253 μm^2) cells ($p = 0.11$; Figure 5A). We observed rare pS6+ neurons in the $Tsc1^{+/+}$ (2 out of 632 cells, average size 304 μm^2, data not shown) and $Tsc1^{\Delta E18/+}$ (8 out of 1,069 cells, average size: 277 μm^2) thalamus, which were not graphed for clarity. Unlike the E12.5 findings, aberrant PV expression was not apparent in either axons or cell bodies of $Tsc1^{\Delta E18/\Delta E18}$ thalamic neurons (Figures 5B and 5C, region 3, data not shown). $Tsc1^{\Delta E18/\Delta E18}$ thalamocortical projections appeared coarse within the internal capsule and overabundant within deep cortical layers (Figures 5B and 5C, arrows), similar to the E12.5 findings. Because of the different recombination pattern, the vibrissal barrel-projecting neurons in VB did not undergo substantial recombination and thus were not labeled by the $R26^{tdTomato}$ reporter. For this reason, TCA innervation of the vibrissa barrels could not be

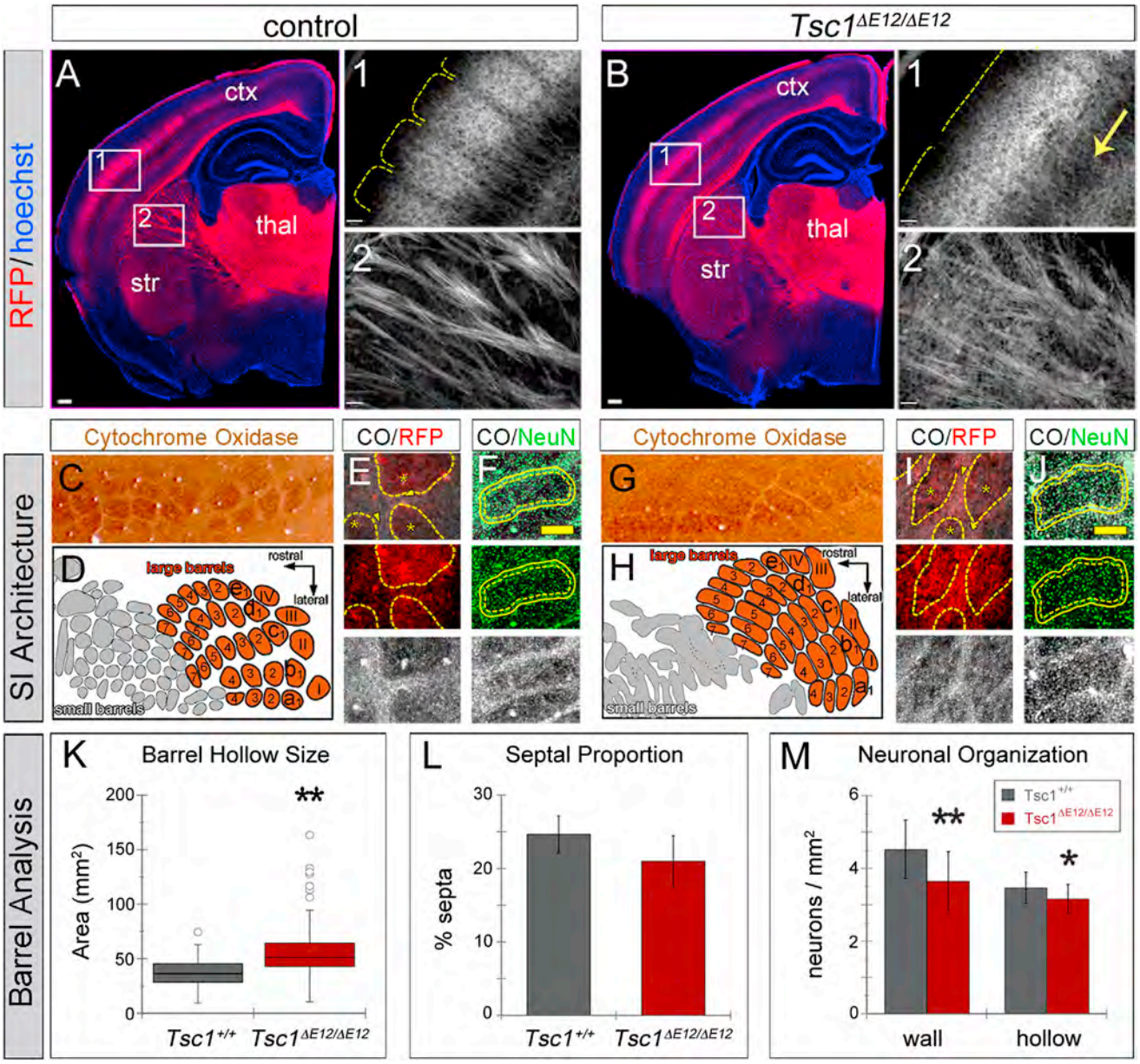

Figure 4. *Tsc1*$^{\Delta E12/\Delta E12}$ Mutants Have Abnormal Thalamocortical Circuits

(A and B) RFP+ TCAs (red) delineated individual vibrissa barrels in adult *Tsc1*$^{+/+}$ neocortex but were diffuse in *Tsc1*$^{\Delta E12/\Delta E12}$ mutants (region 1). Mutants had excess axonal processes in deep cortical layers (arrow) and RFP+ TCA fascicles that were less defined in the internal capsule (region 2).

(C–J) Cortical vibrissa barrels stained with cytochrome oxidase (CO).

(C and D) Controls had well-defined CO+ barrels (brown) separated by CO negative septa.

(E and I) *Tsc1*$^{+/+}$ RFP+ TCAs (red) targeted the CO+ barrel hollows (black, asterisks) but were less restricted in *Tsc1*$^{\Delta E12/\Delta E12}$ mice.

(F and J) Barrel neurons (NeuN+, green) clustered around the perimeter of CO+ barrel hollows (black). Dashed line represents extent of CO+ barrel hollow. Solid line represents 15 μm outer perimeter ("wall") used for quantification in (M).

(G and H) *Tsc1*$^{\Delta E12/\Delta E12}$ cortex had misshapen barrels (brown) and small vibrissa barrels were nearly indistinguishable (gray).

(K) Average CO+ barrel size was larger in *Tsc1*$^{\Delta E12/\Delta E12}$ mutants.

(L) The septa proportion showed no difference.

(M) *Tsc1*$^{\Delta E12/\Delta E12}$ mice had lower neuron density in the barrel wall and hollow versus *Tsc1*$^{+/+}$ animals. Scale bars represent 240 μm in (A) and (B), 61 μm in (A1), (A2), (B1), and (B2), and 130 μm in (F) and (J). thal, thalamus; str, striatum; ctx, neocortex. *$p < 0.05$, **$p < 0.005$. Data are represented as mean ± SD. See also Figure S3.

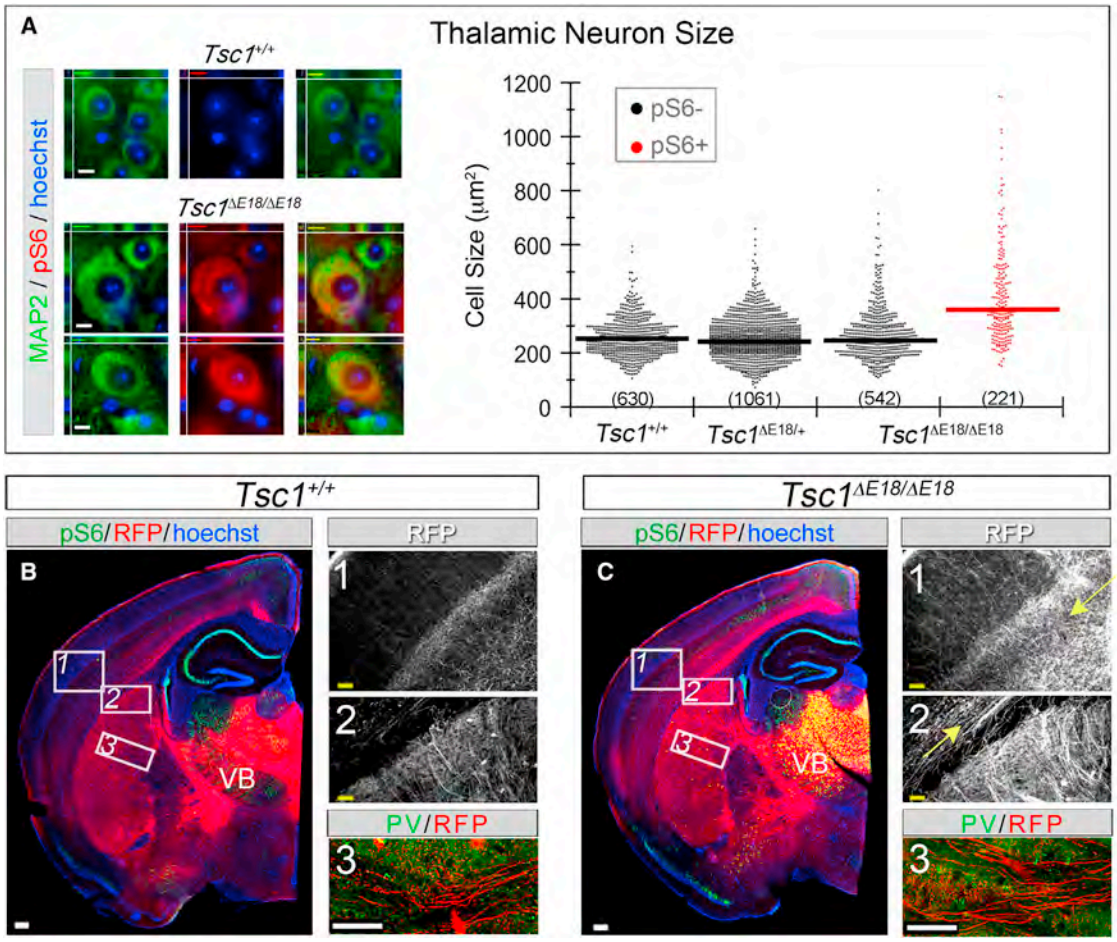

Figure 5. *Tsc1* Deletion at E18.5 in the Thalamus Causes Excessive Thalamic Axons

(A) Control and $Tsc1^{\Delta E18/\Delta E18}$ sections from adults were immunostained for MAP2 (green) and pS6 (red). Soma size was graphed by genotype and pS6 expression and showed no significant difference. Note that pS6+ neurons were rarely observed in $Tsc1^{+/+}$ (two cells) and $Tsc1^{\Delta E18/+}$ brains (eight cells) and were not graphed for clarity.

(B and C) $Tsc1^{+/+}$ (B) and $Tsc1^{\Delta E18/\Delta E18}$ (C) sections were immunolabeled for pS6 (green) and RFP (red). $Tsc1^{\Delta E18/\Delta E18}$ TCAs were superfluous and disorganized in deep cortical layers (region 1, arrow) and internal capsule (region 2, arrow). PV (region 3, green, from adjacent sections) was absent from $Tsc1^{\Delta E18/\Delta E18}$ and $Tsc1^{+/+}$ TCAs (red). Scale bars represent 8 μm in (A), 240 μm in (B) and (C), 61 μm in (B1), (B2), (C1), and (C2), and 57 μm in (B3) and (C3). See also Figure S4.

visualized by RFP expression. Nevertheless, we assessed vibrissa barrel formation using CO staining, which showed that the $Tsc1^{\Delta E18/\Delta E18}$ somatosensory cortex did not have any patterning disruptions (Figure S4).

Intrinsic Physiology Is Abnormal in $Tsc1^{\Delta E12/\Delta E12}$, but Not $Tsc1^{\Delta E18/\Delta E18}$ Thalamic Neurons

To interrogate the functional effects of *Tsc1* deletion at E12.5 versus E18.5 on individual cells, we performed whole-cell patch-clamp recordings on thalamic VB neurons in mature thalamocortical slices (Figure 6). (For all data in this section, see Table S1 for variability estimates, nonsignificant means, and p values.) We recorded from VB because it is easily identifiable and its relay neurons exhibit stereotyped, well-characterized physiological properties (Landisman and Connors, 2007). We used RFP fluorescence from the $R26^{tdTomato}$ reporter allele to target our recordings to recombined neurons. Biocytin was added to the recording pipette to identify neurons post hoc, reconstruct their morphology, and confirm mTOR dysregulation in mutant neurons (Figure 6A). We characterized the intrinsic membrane properties of $Tsc1^{\Delta E12/\Delta E12}$ and $Tsc1^{\Delta E18/\Delta E18}$ VB neurons compared to neurons from their respective $Tsc1^{+/+}$ littermates. $Tsc1^{\Delta E12/\Delta E12}$ VB neurons had significantly lower input resistance than neurons in $Tsc1^{+/+}$ littermates (72.6 MΩ versus 137.2 MΩ, p = 0.001; Figure 6B). In addition, $Tsc1^{\Delta E12/\Delta E12}$ VB neurons had a higher capacitance than $Tsc1^{+/+}$ neurons (417.6 pF versus 219.7 pF, p = 0.004, Figure 6B). In contrast, $Tsc1^{\Delta E18/\Delta E18}$ neurons did not differ from their controls in either resistance or capacitance (Figure 6B). The membrane time constant was unchanged in $Tsc1^{\Delta E12/\Delta E12}$ and $Tsc1^{\Delta E18/\Delta E18}$ compared to controls (Figure 6B), because the decrease in resistance offset the increase in capacitance.

We also analyzed the properties and dynamics of action potentials in VB neurons (Figure 6C). Action potential thresholds

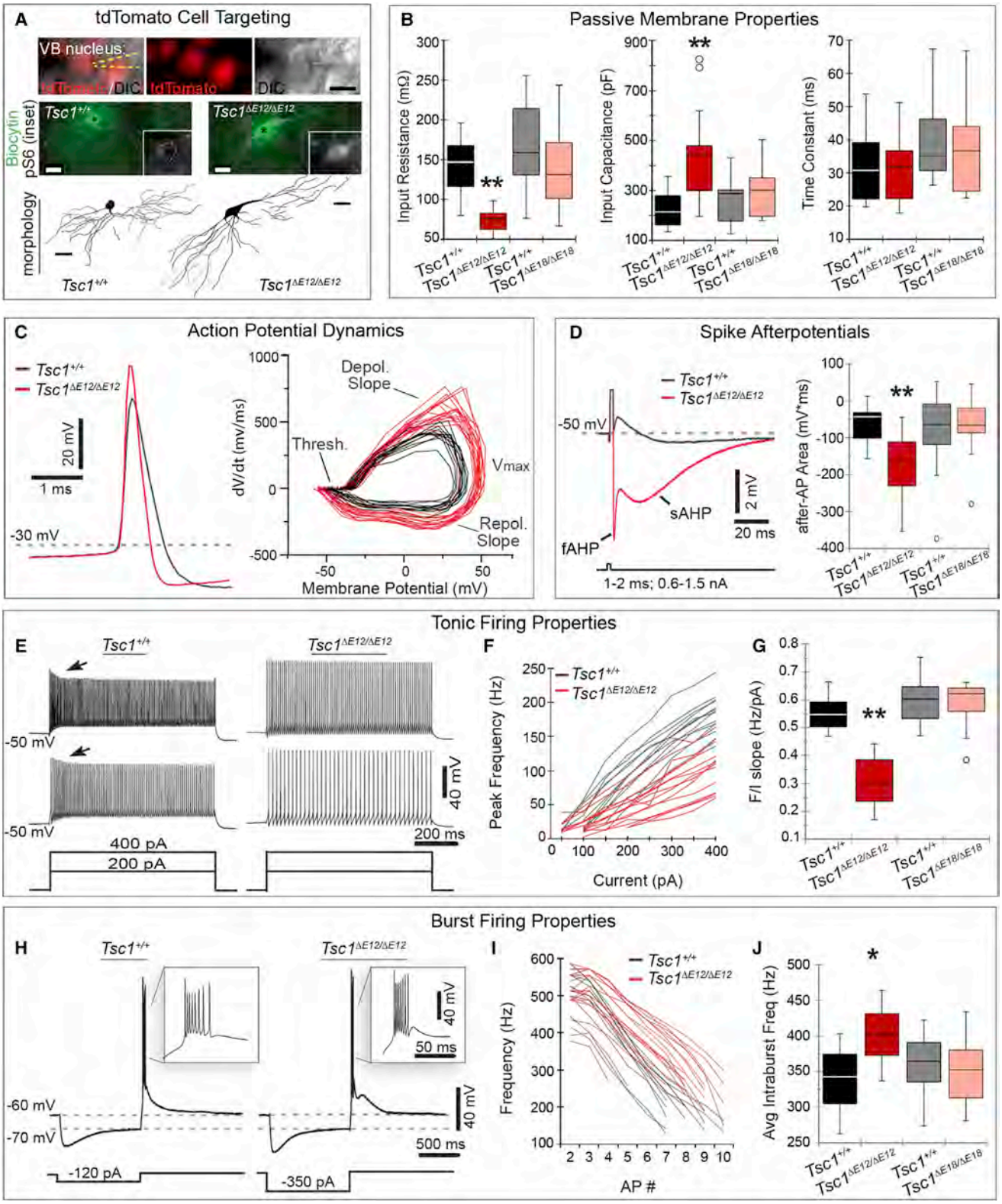

Figure 6. *Tsc1*$^{\Delta E12/\Delta E12}$ Thalamic Neurons Have Altered Electrophysiological Properties

(A) DIC/fluorescence shows electrode (yellow dashed lines) targeted to a RFP+ (red) VB neuron. Neurons were filled with biocytin (green) and immunostained for pS6 (white, insets). Morphology was reconstructed as shown below each filled neuron.

(legend continued on next page)

in $Tsc1^{\Delta E12/\Delta E12}$ neurons were similar to those of $Tsc1^{+/+}$. However, $Tsc1^{\Delta E12/\Delta E12}$ neurons, when compared to $Tsc1^{+/+}$ neurons, had significantly larger spike amplitude (82 mV versus 70 mV, p = 0.0002) and faster rates of depolarization (618 mV/ms versus 423 mV/ms, p = 0.0001) and repolarization (−263 mV/ms versus −151 mV/ms, p < 0.0001) (Figure 6C). $Tsc1^{\Delta E18/\Delta E18}$ spikes did not differ significantly from those of $Tsc1^{+/+}$ neurons in terms of amplitude, depolarization rate, or repolarization rate (Figure S5). VB action potentials are typically followed by fast and slow afterhyperpolarizations (AHPs) and an afterdepolarization (ADP) of intermediate duration (Figure 6D, black trace). To compare these events, we summed the total area under the postaction potential trajectory, which revealed that the $Tsc1^{\Delta E12/\Delta E12}$ neurons had significantly more negative afterpotentials compared to controls (−177 mV*ms versus −64 mV*ms, p = 0.0026; Figure 6D). The $Tsc1^{\Delta E18/\Delta E18}$ afterpotentials did not differ significantly from controls (Table S1).

Thalamic relay neurons fire in both tonic and bursting modes, depending on the state of the resting membrane potential. We characterized tonic firing by holding the membrane potential at −50 mV and applying steps of depolarizing current. While the amplitudes of $Tsc1^{+/+}$ action potentials declined over the first 100 ms of spiking (adaptation), the amplitudes of $Tsc1^{\Delta E12/\Delta E12}$ action potentials remained constant (Figure 6E, arrows). The relationship between firing frequency and stimulus current was roughly linear for both $Tsc1^{+/+}$ and $Tsc1^{\Delta E12/\Delta E12}$ cells (Figure 6F). The average slope of the frequency/current relationship for $Tsc1^{\Delta E12/\Delta E12}$ cells (0.27 Hz/pA) was significantly lower than that of $Tsc1^{+/+}$ cells from littermate controls (0.53 Hz/pA, p < 0.001, n ≥ 11 cells recorded from n ≥ 3 animals per group; Figure 6G). Frequency/current relationships of $Tsc1^{\Delta E18/\Delta E18}$ cells did not differ from those of littermate controls (Figures 6G and S5). We next characterized the cells' burst firing by holding membrane potentials initially at −60 mV, then injecting a 1 s step of current sufficient to bring the membrane to −70 mV. Upon release of the current, VB neurons fired a single burst of spikes (Figure 6H). Each burst comprised a similar number of action potentials that did not vary by genotype; however, the mean duration of the $Tsc1^{\Delta E12/\Delta E12}$ bursts were shorter. Figure 6I plots the intraburst frequency as a function of spike number within the bursts; $Tsc1^{\Delta E12/\Delta E12}$ neurons had a significantly higher mean spiking frequency throughout the burst (401 Hz) compared to $Tsc1^{+/+}$ littermate controls (mean of 339 Hz, p = 0.026). $Tsc1^{\Delta E18/\Delta E18}$ neurons were not significantly different from neurons of $Tsc1^{+/+}$ littermates (Figures 6J and S5). These experiments revealed that the enlarged $Tsc1^{\Delta E12/\Delta E12}$ neurons require stronger input currents to modify their membrane potentials, have larger, faster action potentials, and have altered firing properties in both tonic and bursting mode, compared to wild-type VB neurons, whereas $Tsc1^{\Delta E18/\Delta E18}$ neurons were unaltered.

Thalamic *Tsc1* Deletion at E12.5 and E18.5 Causes Abnormal Neural Activity and Behavior

To determine whether the changes in thalamic development and physiology impact neocortical physiology, we recorded local field potentials (LFPs) in the vibrissal representation of primary SI of adult anesthetized mice. We chose SI because it receives robust input from VB, where we detected changes in circuit organization and whole-cell physiology. We confirmed targeting to barrel cortex by stimulating vibrissae to drive sensory-evoked responses (data not shown). We observed prominent low-frequency oscillations in both $Tsc1^{\Delta E12/\Delta E12}$ and $Tsc1^{\Delta E18/\Delta E18}$ mice (Figures 7A–7C, n = 6 $Tsc1^{+/+}$, n = 3 $Tsc1^{\Delta E12/\Delta E12}$, n = 5 $Tsc1^{\Delta E18/\Delta E18}$ mice). Quantitative analysis of LFP activity showed that mutants had higher power across multiple frequencies, particularly in the 3 Hz range (Figure 7D). This is a frequency associated with spike-and-wave epileptiform activity, which is related to altered thalamic dynamics (Blumenfeld, 2003). Mutants had significantly higher 3 Hz power than controls (p = 0.008, Figure 7E), which was evident in the comparison across all individuals (controls in black/gray, mutants in red/pink triangles). Further, the number of epochs of high-power 3 Hz activity lasting ≥20 s was significantly higher in $Tsc1^{\Delta E12/\Delta E12}$ (red triangles) and $Tsc1^{\Delta E18/\Delta E18}$ (pink triangles) mutant animals compared to controls (p = 0.028, Figure 7F). Older (>8 months) $Tsc1^{\Delta E18/\Delta E18}$ animals and controls were also assessed to account for possible age-related differences in brain activity. These data points are differentiated by black outlines in Figures 7E and 7F.

We addressed whether there were any behavioral ramifications of this altered brain activity. At 2 months of age, $Tsc1^{\Delta E12/\Delta E12}$ mice seemed to groom more frequently than control littermates and developed severe skin lesions (Figure 7G, inset). Because control littermates never developed lesions but were housed in the same cage as affected mice, we hypothesized that the lesions were due to the excessive self-grooming, rather than environmental factors, fighting, or allogrooming. Importantly, overgrooming was apparent before wounds

(B) $Tsc1^{\Delta E12/\Delta E12}$ neurons (red) had lower membrane input resistance and higher input capacitance but unchanged time constants compared to littermate controls (black). Note that $Tsc1^{\Delta E18/\Delta E18}$ mutants (pink) and their controls (gray) are also plotted.
(C) Representative traces from control and $Tsc1^{\Delta E12/\Delta E12}$ neurons (left) show that $Tsc1^{\Delta E12/\Delta E12}$ action potentials were faster and larger. $Tsc1^{\Delta E12/\Delta E12}$ action potential dynamics (right) were significantly different with respect to depolarization rate, maximum amplitude, and repolarization rate.
(D) $Tsc1^{\Delta E12/\Delta E12}$ spike afterpotentials (red) were more negative during the fast (fAHP) and during the slow phase (sAHP) compared to controls (black). Total postspike membrane potential was integrated over time and quantified by integrating the voltage signal over 280 ms (right).
(E) Representative tonic voltage response of a $Tsc1^{+/+}$ and $Tsc1^{\Delta E12/\Delta E12}$ neuron to current injections (400 pA, top and 200 pA, bottom).
(F) Peak firing frequency per current step (F/I) is plotted for $Tsc1^{+/+}$ (black, n = 12) and $Tsc1^{\Delta E12/\Delta E12}$ (red, n = 17) neurons.
(G) Linear slopes of the F/I curves are quantified.
(H) Representative voltage response of a $Tsc1^{+/+}$ and a $Tsc1^{\Delta E12/\Delta E12}$ thalamic neuron to hyperpolarizing current step. Insets show rebound bursts.
(I) Intraburst firing frequency as a function of spike number within each burst is plotted for $Tsc1^{+/+}$ (black, n = 11) and $Tsc1^{\Delta E12/\Delta E12}$ (red, n = 18) neurons.
(J) Mean intraburst firing frequencies are quantified. Note that $Tsc1^{\Delta E18/\Delta E18}$ mutants (pink) did not significantly differ from their controls (gray; B, D, G, and J). Box plots represent minimum, first quartile (Q1), median, Q3, and maximum. Outliers (open circles) were >Q3 + 1.5*IQR or <Q1 − 1.5*IQR. Scale bars in (A) represent 20 μm (DIC) and 30 μm (biocytin/morphology). *p < 0.05, **p < 0.005. See also Figure S5 and Table S1.

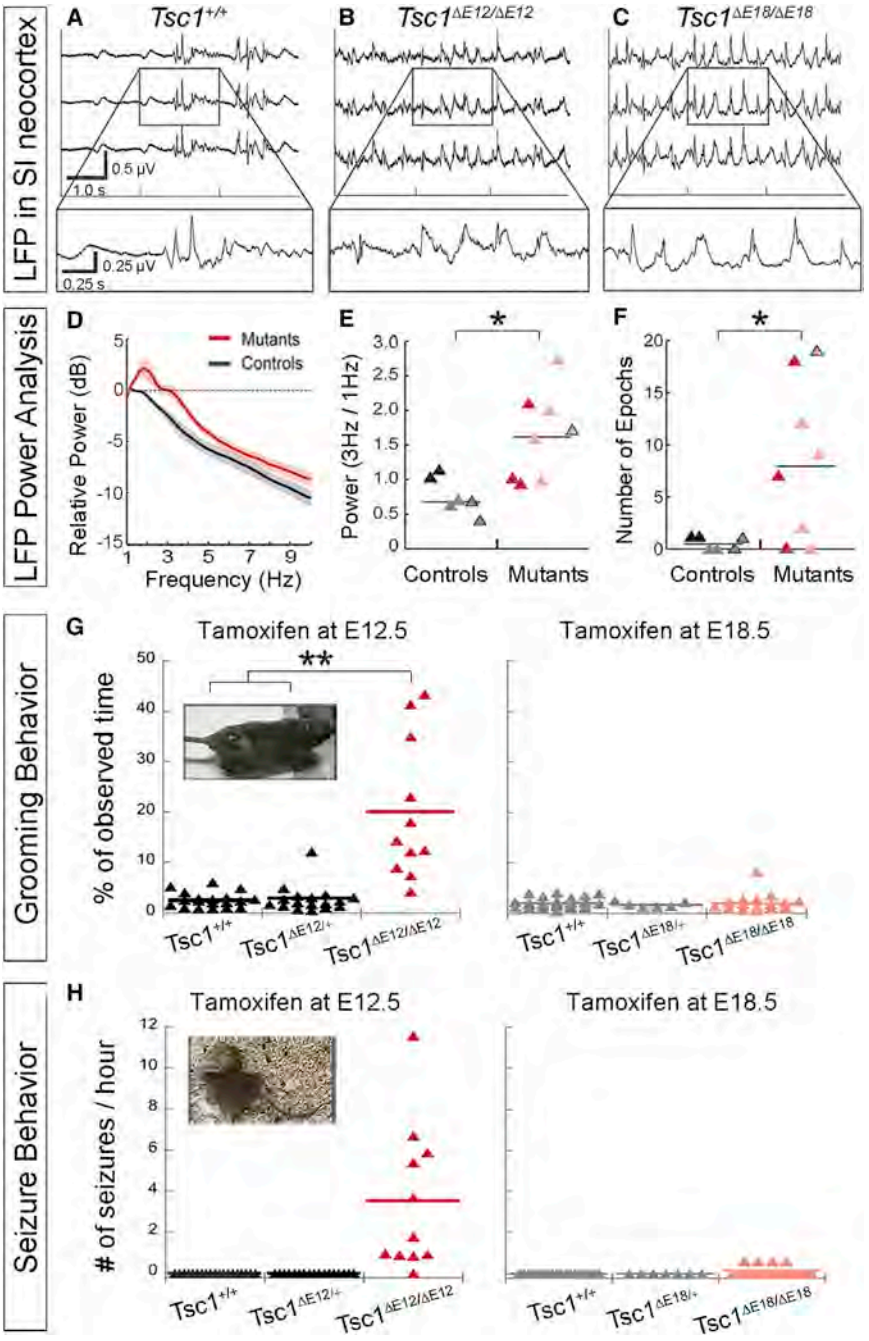

Figure 7. Abnormal Brain Activity and Behaviors Caused by Thalamic *Tsc1* Deletion

(A–C) LFPs in primary somatosensory neocortex were altered in adult $Tsc1^{\Delta E12/\Delta E12}$ and $Tsc1^{\Delta E18/\Delta E18}$ mutants.

(D) Average power spectra of mutants and controls (tamoxifen at E12.5 and E18.5 experiments were pooled together) shows increased power between 2–4 Hz. Lines and shading represent mean ± SEM.

(E) Three hertz was normalized to 1 Hz power for controls (black, E12.5; gray, E18.5) and mutants (red, $Tsc1^{\Delta E12/\Delta E12}$; pink, $Tsc1^{\Delta E18/\Delta E18}$). Data points with black outlines represent recordings performed on aged animals (>8 months).

(F) Greater than or equal to twenty second epochs of high-power 3 Hz activity are plotted.

(G) The percentage of time spent grooming is plotted by genotype. Tamoxifen at E12.5 and E18.5 graphs share a y axis. Inset: a $Tsc1^{\Delta E12/\Delta E12}$ mouse that developed a wound from overgrooming.

(H) Number of seizures per hour of observation time is plotted by genotype. Tamoxifen at E12.5 and E18.5 graphs share a y axis. Inset: contorted posture typically observed during seizures. *$p < 0.05$, **$p < 0.005$. See also Figure S6.

developed, indicating that the wound was not the trigger for the grooming but rather a result of it. To confirm this, animals were videotaped for 8 min periods twice a week in their homecage before wounds appeared. An observer scored the amount of time spent grooming by each mouse in a genotype-blinded manner. $Tsc1^{\Delta E12/\Delta E12}$ mice spent significantly more of their time grooming (24.1%, 95% confidence interval (CI_{95}): 21.8%–26.5%) than $Tsc1^{+/+}$ (3.0%, CI_{95}: 2.4%–3.9%) and $Tsc1^{\Delta E12/+}$ (3.8%, CI_{95}: 3.0%–4.9%) mice ($p < 0.0001$, $n \geq 11$ mice per genotype; Figure 7G). In contrast, $Tsc1^{\Delta E18/\Delta E18}$ mice displayed no overt phenotypes by 3 months of age (n = 17) and did not develop wounds or groom more often than $Tsc1^{+/+}$ or $Tsc1^{\Delta E18/+}$ littermates, regardless of age (n = 25 and n = 6 respectively, Figure 7G).

$Tsc1^{\Delta E12/\Delta E12}$ mice also exhibited spontaneous seizures beginning around 2 months of age, consistent with the increase in 3 Hz LFP activity. The seizure events were highly stereotyped and began with prolonged grooming of the hindlimb, followed by loss of upright posture, then a tonic-clonic state during which the body entered into a convulsive, twisted posture typically lasting 10 s (Figure 7H, inset; Movie S1). An observer blinded to genotype quantified the frequency and duration of seizures. The $Tsc1^{\Delta E12/\Delta E12}$ mice averaged 3.7 seizures/hr (CI_{95}: 2.0–6.9 seizures/hr), while control littermates never exhibited seizures (Figure 7H). Ninety-one percent of the $Tsc1^{\Delta E12/\Delta E12}$ mice (10/11) that were analyzed experienced convulsive seizures as described above during the observation periods. While the remaining mouse did not have overt seizures, it did display abnormal behavior in that it remained in a motionless, sleep-like state for minutes at a time, which may have been absence seizures. In contrast, $Tsc1^{\Delta E18/\Delta E18}$ mice did not exhibit seizures at 2 months of age. However, by 8 months of age, four of the 17 $Tsc1^{\Delta E18/\Delta E18}$ mice had experienced a seizure (Figure 7H, Movie S2), but these rare seizure events only occurred upon handling. Thus, we conclude that 100% of $Tsc1^{\Delta E12/\Delta E12}$ mice and 24% of $Tsc1^{\Delta E18/\Delta E18}$ mice displayed

abnormal behavior, with some variation in form and severity. Notably, the severity of the grooming and the seizure phenotypes was not correlated within individuals.

Because *Gbx2*^{CreER} mediates recombination in the spinal cord at E12.5 (Luu et al., 2011), we tested peripheral sensory and motor function (Figure S6). We did not detect a significant difference in tactile sensitivity (von Frey filament test, $p = 0.315$) or motor function (wire hang assay, $p = 0.134$) between control and *Tsc1*$^{\Delta E12/\Delta E12}$ animals. We also showed that thermal pain sensitivity was unaffected in *Tsc1*$^{\Delta E12/\Delta E12}$ mutants (hot plate test, $p = 0.188$). Because *Gbx2*^{CreER} is no longer expressed in the spinal cord after E14.5 (John et al., 2005), we did not perform similar tests on *Tsc1*$^{\Delta E18/\Delta E18}$ animals. Taken together, our collective analysis of thalamocortical circuitry, neuronal physiology, and neocortical local field potentials strongly suggest that the primary drive of these *Tsc1*$^{\Delta E12/\Delta E12}$ or *Tsc1*$^{\Delta E18/\Delta E18}$ phenotypes is mTOR dysregulation in the thalamus.

DISCUSSION

TS is a developmental mosaic genetic disorder caused by disrupting the TSC/mTOR pathway. In this study, we tested the hypothesis that disrupting the mTOR pathway elicits different phenotypes depending on the identity and developmental state of cells in which *Tsc1* is deleted and mTOR is dysregulated.

Genetic circuit tracing showed that *Tsc1*$^{\Delta E12/\Delta E12}$ thalamic projections are disorganized and have excessive processes that innervate layer IV septal regions of the somatosensory barrel cortex. This phenotype may result from the lack of activity-dependent pruning or excess axonal ramifications filling intrabarrel spaces. Our observations are consistent with previous reports describing abnormal axonal targeting of retinal projections in both the *Drosophila* and mouse brain, in which *Tsc1* mutant axons overshoot their target and have branches that terminate outside the normal target regions (Knox et al., 2007; Nie et al., 2010). It is probable that other cortical areas receive similarly disorganized *Tsc1*$^{\Delta E12/\Delta E12}$ thalamic inputs. We also analyzed *Tsc1*$^{\Delta E18/\Delta E18}$ TCA projections as they traversed the striatum and entered the cortex. Similar to *Tsc1*$^{\Delta E12/\Delta E12}$, there was a qualitative excess of RFP+ *Tsc1*$^{\Delta E18/\Delta E18}$ TCA projections within the deep cortical layers. However, a direct comparison of *Tsc1*$^{\Delta E18/\Delta E18}$ and *Tsc1*$^{\Delta E12/\Delta E12}$ vibrissa barrel innervation was precluded because of their different recombination patterns. Regardless, these thalamocortical projection phenotypes in deep layers are consistent with disrupted neuronal processes in response to mTOR dysregulation (Choi et al., 2008).

We uncovered multiple electrophysiological alterations upon early deletion of *Tsc1*. The increased input capacitance and reduced input resistance are both consistent with increased membrane as a result of cell growth. Notably, action potential dynamics were also altered, yet spike threshold potentials were unaffected. The altered action potentials of *Tsc1*$^{\Delta E12/\Delta E12}$ neurons may partially compensate for the changes in passive properties. As the input resistance of a neuron falls, larger synaptic currents are required to modify membrane voltage. Mutant *Tsc1*$^{\Delta E12/\Delta E12}$ neurons also have larger amplitude, briefer action potentials with normal thresholds, and rates of rise and fall that are considerably faster than normal. The maximum rate-of-rise of an action potential is proportional to peak inward sodium current in many neurons (Cohen et al., 1981). Therefore, these changes in spike kinetics strongly suggest that voltage-gated sodium and potassium channels are altered in the mutant cells. The spike shapes are consistent with either higher membrane channel densities or altered single-channel properties, such as subunit composition or phosphorylation, that affect conductance and gating dynamics. In support of these possibilities, the mTOR pathway has been reported to control expression levels and subunit composition of some voltage-gated ion channels (Raab-Graham et al., 2006). Multiple ion channel involvement is further suggested by changes in both the tonic and burst firing modes of mutant cells. The reduced slope of the tonic frequency/current relationship in mutant cells is most easily explained as a consequence of their lower input resistance, while more rapid intraburst spiking is likely due to changes in ion channels. In addition to altered spike-related sodium and potassium channels, it is possible that the rapid intraburst spiking in *Tsc1*$^{\Delta E12/\Delta E12}$ cells is caused by altered density or kinetics of low-threshold calcium channels. Additionally, the ectopic production of PV, a protein that acts as a slow Ca^{2+} buffer, in *Tsc1*$^{\Delta E12/\Delta E12}$ thalamic relay neurons may disrupt internal Ca^{2+} dynamics, which can affect gene transcription, synaptic function, and membrane potential and could contribute to some of the physiological changes we describe (Schwaller, 2010).

Importantly, our data show that the effects of early mutation spread well beyond the cells with the *Tsc1* deletion. Individually mutated neurons ensnare the neocortex into hyperexcitable networks, as evidenced by abnormal LFPs in SI. Thus, disruption of an anatomically distinct but functionally connected node within a circuit can propagate the disease phenotype. Comparing the effects of early and late *Tsc1* deletion is informative. We did not detect abnormal physiological properties of *Tsc1*$^{\Delta E18/\Delta E18}$ VB neurons, which indicates that, at least for VB neurons, there is a critical window of *Tsc1*/mTOR required to establish proper intrinsic excitability properties. Nevertheless, a striking finding is that neocortical (SI) LFP activity was altered in some E18.5 deletion animals. The most likely reason for the global abnormalities is that feedback loops involving multiple thalamic nuclei have altered physiology, which is propagated both locally and to other brain regions. The sources of altered feedback may involve thalamic nuclei that undergo substantial recombination at E18.5 (such as Po) and that subsequently disrupt the reticulothalamic or the corticothalamic loops. By comparing the early versus later deletion of *Tsc1*, we are able to discern that abnormalities, even in a small proportion of cells, can cause reverberating global changes in neural activity.

Comparison of our thalamic *Tsc1* mutant phenotypes to other mouse models can be informative in considering the contribution of individual brain regions to global neural dysfunction. Behaviorally, *Tsc1*$^{\Delta E12/\Delta E12}$ animals groomed excessively, to the extent that they gave themselves severe lesions. A similar overgrooming phenotype has been described in genetic mouse models of autism and obsessive compulsive disorder in which *Slitrk5*, *Shank3*, or *Sapap3* is deleted (Welch et al., 2007; Shmelkov et al., 2010; Peça et al., 2011). Because striatum-specific gene rescue can ameliorate the phenotype, these groups implicate the corticostriatal circuit in causing abnormal repetitive behaviors. The thalamus projects both directly and indirectly, via

neocortex, to the striatum (Smith et al., 2004), suggesting that abnormal thalamic modulation of the striatum in our mice contributes to the repetitive grooming phenotype. However, it is possible that sparse recombination in other subcortical brain structures, such as the striatum and hindbrain, may also contribute to the behavioral changes. *Tsc1* or *Tsc2* knockout in Purkinje cells of the cerebellum also causes repetitive grooming (Tsai et al., 2012; Reith et al., 2013), possibly by disrupting signals from the cerebellum to the motor cortex, which are relayed by the ventrolateral thalamus. In addition, all $Tsc1^{\Delta E12/\Delta E12}$ and some $Tsc1^{\Delta E18/\Delta E18}$ mice experience seizures and abnormal neural activity with epileptiform features. Seizures are a common feature of TS clinically. *Tsc1* knockout in forebrain neurons leads to seizures in 10% of mice (Meikle et al., 2007), while *Tsc1* deletion in astrocytes (and likely neurons as well; Casper and McCarthy, 2006) causes frequent seizures and premature death (Uhlmann et al., 2002). Widespread deletion of *Tsc1* in neural progenitors has also been shown to cause spontaneous seizures in adult mice (Goto et al., 2011). Ours, however, is a conditional *Tsc1* knockout that causes both seizures and overgrooming. Although one may presume that this is simply because the thalamus is a central structure and its dysregulation therefore compromises multiple functional circuits, the explanation cannot be that simple; in the Meikle et al. and Goto et al. studies, *Tsc1* recombination occurs in the thalamus as well as the rest of the forebrain. The fact that more comprehensive *Tsc1* knockouts do not produce similar overgrooming suggests that perturbing a single node of a neural network has the potential to be more deleterious than disrupting the entire network, perhaps because global homeostatic mechanisms are not invoked when only part of a highly interconnected and integrative system is dysregulated. This is an important consideration for brain structures, such as the thalamus, which feature complex feedback loops and widespread reciprocal connectivity that could amplify and spread the effects of a slight functional imbalance. This concept is particularly relevant given the mosaic nature of TS in humans, in which subsets of cells undergo biallelic *TSC1/2* mutations, leading to discrete cohorts of mutant cells (Crino et al., 2010). It is important to note, however, that while thalamic *Tsc1* knockout replicates salient features of TS, we are not implying that TS is a disease of the thalamus. Rather, our findings suggest that the thalamus and other subcortical regions warrant further investigation and that the complex nature of disorders like TS involve multiple brain regions that may respond differentially to the same genetic insult.

The phenotypes related to E12.5 versus E18.5 *Tsc1* inactivation suggest three contributing factors: the spatial pattern of recombination, the overall number of affected cells, and the developmental timing of *Tsc1* inactivation. The spatial pattern of recombination is clearly important and experimentally arises from the dynamic expression of the *Gbx2* gene regulatory elements that drive *CreER* expression (Chen et al., 2009). The dynamic recombination pattern causes the MD, MG, and AM nuclei to undergo recombination at both E12.5 and E18.5. In contrast, the Pf and VB nuclei are largely spared by recombination at E18.5. This differential involvement of nuclei probably leads to distinct consequences. The Pf and VB nuclei project, either directly or indirectly, to the dorsolateral striatum (Pan et al., 2010), which is a central component in a circuit that regulates a syntactic chain of grooming behaviors (Cromwell and Berridge, 1996). Disruption of this circuit at E12.5, but not at E18.5, could underlie the compulsive grooming behavior in $Tsc1^{\Delta E12/\Delta E12}$, but not $Tsc1^{\Delta E18/\Delta E18}$, mutant animals. Alternatively, there may be a threshold extent of mosaicism that can be tolerated and compensated for by the brain, above which compensatory mechanisms become ineffective. In this regard, the lower overall number of recombined cells in the $Tsc1^{\Delta E18/\Delta E18}$ thalamus might place the system near the tolerance threshold, resulting in abnormal neural activity but with only a subset of animals experiencing overt seizures and only upon external stimulation. In contrast, the extensive recombination within the $Tsc1^{\Delta E12/\Delta E12}$ thalamus may be above the tolerance threshold, resulting in unmitigated disruption of thalamic development and function. Finally, because mTOR regulates many developmental cellular programs including proliferation, cell growth, axon formation, and synapse formation and maintenance, it is also possible that the later deletion of *Tsc1* results in a diminished phenotype simply because there is a critical period during which thalamic neurons require functional *Tsc1*. By E18.5, thalamic neurons have already extended their axons to their cortical target regions, so this developmental event would be spared when *Tsc1* inactivation occurs at E18.5 but may be affected by earlier *Tsc1* inactivation. This idea is consistent with the fact that, at the single-cell level, recombined VB neurons display aberrant protein expression and altered electrophysiological properties when recombination occurs at E12.5, while VB neurons are apparently unaffected when recombination occurs at E18.5.

It is likely that all three of these factors—the specific cells that suffer the genetic insult, the number of cells that are affected, and the developmental stage at which the genetic hit occurs—contribute to the distinct E12.5 and E18.5 phenotypes to some degree. Although this complex interplay of multiple factors precludes making simple conclusions about mechanisms, it does nicely mimic the complex nature of mosaic disorders such as TS. Mosaic genetic diseases can have extremely variable penetrance, expressivity, and severity. The factors that can contribute to this disease variability, similar to those in our mouse model, include (1) when during development the initial genetic mutation occurs, (2) in which cell that mutation happens (and how the gene functions in that cell type), and (3) how extensively that initial cell's lineage contributes to the final organism (Hall, 1988). Our temporally and spatially controllable mouse model of TS allows us to manipulate where and when the *Tsc1* gene is deleted, which is instructive in understanding the consequences of mosaic genetic insults at distinct stages of development. Future studies that further parse the contributions of these factors will be instrumental for understanding the developmental underpinnings and mechanisms that contribute to tuberous sclerosis and to mosaic diseases in general.

EXPERIMENTAL PROCEDURES

Mice, Tissue Processing, and Cellular Analysis

$Tsc1^{fl}$, $Rosa26^{loxP\text{-}STOP\text{-}loxP\text{-}LacZ}$ ($R26^{LacZ}$), $R26^{loxP\text{-}STOP\text{-}loxP\text{-}tdTomato}$ ($R26^{tdTomato}$), and $Gbx2^{CreER\text{-}IRES\text{-}eGFP}$ ($Gbx2^{CreER}$) mice were described

previously (Soriano, 1999; Kwiatkowski et al., 2002; Chen et al., 2009; Madisen et al., 2010). Mice were housed and handled in accordance with Brown University Institutional Animal Care and Use Committee guidelines. Genotyping, tamoxifen, immunohistochemistry (IHC), antibodies, and cytochrome oxidase (CO) staining are described in Brown et al. (2009) and Ellisor et al. (2009) and Supplemental Experimental Procedures. Identical exposure settings were used when comparing labeling intensity across the three genotypes. For neuron density analysis, a barrel outline was created based on CO+ staining ("barrel hollow") and a perimeter was made 15 μm outside the inner outline ("barrel wall"). The area and the number of NeuN-positive objects in the barrel hollow and wall regions were determined and analyzed for significance by Student's t test. For cell size analysis, five thalamic regions from five medial-to-lateral brain sections were assessed. The measure function (Volocity) was used to calculate the perimeter and area of all outlined cell bodies. Generalized estimating equations (log-normal generalized model) were used to compare genotypes with regards to neuronal size. Pairwise comparisons were made using orthogonal contrast statements, with p values adjusted using the Holm test to maintain family-wise alpha at 0.05. Statistical and experimental details are provided in the Supplemental Experimental Procedures.

Whole-Cell Recordings

Brain slice preparation, solutions, and recording conditions (Agmon and Connors, 1991; Cruikshank et al., 2010, 2012) are provided in detail in the Supplemental Experimental Procedures. Data were collected with Clampex 10.0 and analyses were performed post hoc using Clampfit 10.0. Resting membrane potentials (R_m), input resistances (R_{in}), membrane time constants (τ_m), and input capacitances (C_{in}) were determined as described in the Supplemental Experimental Procedures. Burst properties were characterized by holding the soma at a membrane potential of −60 mV with intracellular current and subsequently injecting large negative currents. Tonic and single action potential properties were characterized by holding the soma at a membrane potential of −50 mV with intracellular current and injecting suprathreshhold positive current. Single action potential data were obtained by injecting the minimum current needed to elicit an action potential. Afterhyperpolarizations were evoked by injecting a 2 ms suprathreshold positive current. Generalized hierarchical linear modeling was used to test for differential effects of gene deletion. Comparisons by genotype were made using orthogonal linear comparisons.

LFP Recordings

Surgical procedures, recordings, and analysis are described in the Supplemental Experimental Procedures. NeuroNexus probes were used for recording sessions. LFP signals were sampled, filtered, and recorded using a Cheetah Data Acquisition System (NeuraLynx). The probe was lowered 1,600 μm and responses to vibrissa deflections confirmed electrode placement in SI. Ten minutes of pre- and postbaseline activity and a stimulus period were recorded. Stimuli periods had a mean period of 5 s. For each animal, a single SI recording session was selected for LFP analysis using the layer IV contact. Recorded signals were low-pass filtered, downsampled, and clipping artifacts were removed. Data were analyzed using MATLAB. The power spectral density (PSD) for 20 s nonoverlapping time windows was estimated using Welch's method with a 4,096 point FFT, normalized by dividing by the sum of the PSD across all frequencies and smoothed using a 5 pt moving average filter. Relative power at 3 Hz was calculated as the ratio of the normalized PSD at 3 Hz by the value at 1 Hz for each time window, averaged across the session. The number of 20 s epochs that exceeded 97.5th percentile of normalized 3 Hz power was counted. Two-tailed two-sample t tests were performed by grouping all controls versus all mutants (significance level, α of 0.05).

Behavioral Analysis

An independent observer assessed videos to score seizures and overgrooming as detailed in the Supplemental Experimental Procedures. Generalized estimating equations were used to compare genotypes with regards to percent minutes grooming (binomial generalized model grooming/total minutes) and seizure frequency (negative-binomial generalized model offset by log total hours). Pairwise comparisons were made using orthogonal contrast statements, with p values adjusted using the Holm test to maintain family-wise alpha at 0.05. Sensorimotor testing details are described in the Supplemental Experimental Procedures.

SUPPLEMENTAL INFORMATION

Supplemental Information includes six figures, one table, Supplemental Experimental Procedures, and two movies and can be found with this article online at http://dx.doi.org/10.1016/j.neuron.2013.03.030.

ACKNOWLEDGMENTS

This work was supported by the Department of Defense Congressionally Directed Medical Research Program awards (W8 1XWH-11-1-0241 and W8 1XWH-12-1-0187, M.Z.). Additional personnel support includes: Brown Institute for Brain Science (E.A.N., C.I.M.), NIH NSGP training grant (NS062443-02, E.A.N.), NIH/NIMH Conte Center grant (P50 MH086400-03, B.W.C.), EFRI-BioSA/NSF (B.W.C.), and NIH (7-R01NS045130-08, C.I.M.). M.Z. and E.A.N. conceived of the project and wrote the manuscript. M.Z. oversaw all experiments and analysis. E.A.N. conducted and oversaw primary experiments and data analysis. S.R.C. conducted and analyzed whole-cell electrophysiology data with E.A.N. C.A.T. and E.M.M. conducted and analyzed LFPs. C.I.M. and B.W.C. consulted on electrophysiology experimental design and analysis. J.T.M. conducted biostatistics with E.A.N. and M.Z. C.B. analyzed grooming and seizures under the supervision of E.A.N. and M.Z. B.V. performed barrel analysis with E.A.N. and M.Z. Sensorimotor function was tested and analyzed by K. Bath (http://rndb.clps.brown.edu). We thank S. Cruikshank for his help with the lentiviral experiments.

Accepted: March 25, 2013
Published: May 9, 2013

REFERENCES

Agmon, A., and Connors, B.W. (1991). Thalamocortical responses of mouse somatosensory (barrel) cortex in vitro. Neuroscience *41*, 365–379.

Au, K.S., Hebert, A.A., Roach, E.S., and Northrup, H. (1999). Complete inactivation of the TSC2 gene leads to formation of hamartomas. Am. J. Hum. Genet. *65*, 1790–1795.

Blumenfeld, H. (2003). From molecules to networks: cortical/subcortical interactions in the pathophysiology of idiopathic generalized epilepsy. Epilepsia *44*(*Suppl 2*), 7–15.

Brown, A., Brown, S., Ellisor, D., Hagan, N., Normand, E., and Zervas, M. (2009). A practical approach to genetic inducible fate mapping: a visual guide to mark and track cells *in vivo*. J. Vis. Exp. *43*, pii: 1687.

Carson, R.P., Van Nielen, D.L., Winzenburger, P.A., and Ess, K.C. (2012). Neuronal and glia abnormalities in Tsc1-deficient forebrain and partial rescue by rapamycin. Neurobiol. Dis. *45*, 369–380.

Casper, K.B., and McCarthy, K.D. (2006). GFAP-positive progenitor cells produce neurons and oligodendrocytes throughout the CNS. Mol. Cell. Neurosci. *31*, 676–684.

Chen, L., Guo, Q., and Li, J.Y.H. (2009). Transcription factor Gbx2 acts cell-nonautonomously to regulate the formation of lineage-restriction boundaries of the thalamus. Development *136*, 1317–1326.

Choi, Y.J., Di Nardo, A., Kramvis, I., Meikle, L., Kwiatkowski, D.J., Sahin, M., and He, X. (2008). Tuberous sclerosis complex proteins control axon formation. Genes Dev. *22*, 2485–2495.

Cohen, I., Attwell, D., and Strichartz, G. (1981). The dependence of the maximum rate of rise of the action potential upstroke on membrane properties. Proc. R. Soc. Lond. B Biol. Sci. *214*, 85–98.

Crino, P.B., Aronica, E., Baltuch, G., and Nathanson, K.L. (2010). Biallelic TSC gene inactivation in tuberous sclerosis complex. Neurology *74*, 1716–1723.

Cromwell, H.C., and Berridge, K.C. (1996). Implementation of action sequences by a neostriatal site: a lesion mapping study of grooming syntax. J. Neurosci. *16*, 3444–3458.

Cruikshank, S.J., Ahmed, O.J., Stevens, T.R., Patrick, S.L., Gonzalez, A.N., Elmaleh, M., and Connors, B.W. (2012). Thalamic control of layer 1 circuits in prefrontal cortex. J. Neurosci *32*, 17813–17823.

Cruikshank, S.J., Urabe, H., Nurmikko, A.V., and Connors, B.W. (2010). Pathway-specific feedforward circuits between thalamus and neocortex revealed by selective optical stimulation of axons. Neuron *65*, 230–245.

Ellisor, D., Koveal, D., Hagan, N., Brown, A., and Zervas, M. (2009). Comparative analysis of conditional reporter alleles in the developing embryo and embryonic nervous system. Gene Expr. Patterns *9*, 475–489.

Fitzgerald, K.D., Welsh, R.C., Stern, E.R., Angstadt, M., Hanna, G.L., Abelson, J.L., and Taylor, S.F. (2011). Developmental alterations of frontal-striatal-thalamic connectivity in obsessive-compulsive disorder. J. Am. Acad. Child Adolesc. Psychiatry *50*, 938–948, e3.

Goto, J., Talos, D.M., Klein, P., Qin, W., Chekaluk, Y.I., Anderl, S., Malinowska, I.A., Di Nardo, A., Bronson, R.T., Chan, J.A., et al. (2011). Regulable neural progenitor-specific Tsc1 loss yields giant cells with organellar dysfunction in a model of tuberous sclerosis complex. Proc. Natl. Acad. Sci. USA *108*, E1070–E1079.

Hall, J.G. (1988). Review and hypotheses: somatic mosaicism: observations related to clinical genetics. Am. J. Hum. Genet. *43*, 355–363.

Hardan, A.Y., Minshew, N.J., Melhem, N.M., Srihari, S., Jo, B., Bansal, R., Keshavan, M.S., and Stanley, J.A. (2008). An MRI and proton spectroscopy study of the thalamus in children with autism. Psychiatry Res. *163*, 97–105.

Hay, N., and Sonenberg, N. (2004). Upstream and downstream of mTOR. Genes Dev. *18*, 1926–1945.

Hentges, K.E., Sirry, B., Gingeras, A.C., Sarbassov, D., Sonenberg, N., Sabatini, D., and Peterson, A.S. (2001). FRAP/mTOR is required for proliferation and patterning during embryonic development in the mouse. Proc. Natl. Acad. Sci. USA *98*, 13796–13801.

John, A., Wildner, H., and Britsch, S. (2005). The homeodomain transcription factor Gbx1 identifies a subpopulation of late-born GABAergic interneurons in the developing dorsal spinal cord. Dev. Dyn. *234*, 767–771.

Knox, S., Ge, H., Dimitroff, B.D., Ren, Y., Howe, K.A., Arsham, A.M., Easterday, M.C., Neufeld, T.P., O'Connor, M.B., and Selleck, S.B. (2007). Mechanisms of TSC-mediated control of synapse assembly and axon guidance. PLoS ONE *2*, e375.

Kwiatkowski, D.J., Zhang, H., Bandura, J.L., Heiberger, K.M., Glogauer, M., el-Hashemite, N., and Onda, H. (2002). A mouse model of TSC1 reveals sex-dependent lethality from liver hemangiomas, and up-regulation of p70S6 kinase activity in Tsc1 null cells. Hum. Mol. Genet. *11*, 525–534.

Landisman, C.E., and Connors, B.W. (2007). VPM and PoM nuclei of the rat somatosensory thalamus: intrinsic neuronal properties and corticothalamic feedback. Cereb. Cortex *17*, 2853–2865.

Luu, B., Ellisor, D., and Zervas, M. (2011). The lineage contribution and role of Gbx2 in spinal cord development. PLoS ONE *6*, e20940.

Madisen, L., Zwingman, T.A., Sunkin, S.M., Oh, S.W., Zariwala, H.A., Gu, H., Ng, L.L., Palmiter, R.D., Hawrylycz, M.J., Jones, A.R., et al. (2010). A robust and high-throughput Cre reporting and characterization system for the whole mouse brain. Nat. Neurosci. *13*, 133–140.

McClintock, W.M. (2002). Neurologic manifestations of tuberous sclerosis complex. Curr. Neurol. Neurosci. Rep. *2*, 158–163.

Meikle, L., Talos, D.M., Onda, H., Pollizzi, K., Rotenberg, A., Sahin, M., Jensen, F.E., and Kwiatkowski, D.J. (2007). A mouse model of tuberous sclerosis: neuronal loss of Tsc1 causes dysplastic and ectopic neurons, reduced myelination, seizure activity, and limited survival. J. Neurosci. *27*, 5546–5558.

Meikle, L., Pollizzi, K., Egnor, A., Kramvis, I., Lane, H., Sahin, M., and Kwiatkowski, D.J. (2008). Response of a neuronal model of tuberous sclerosis to mammalian target of rapamycin (mTOR) inhibitors: effects on mTORC1 and Akt signaling lead to improved survival and function. J. Neurosci. *28*, 5422–5432.

Molnár, Z., Adams, R., and Blakemore, C. (1998). Mechanisms underlying the early establishment of thalamocortical connections in the rat. J. Neurosci. *18*, 5723–5745.

Narboux-Nême, N., Evrard, A., Ferezou, I., Erzurumlu, R.S., Kaeser, P.S., Lainé, J., Rossier, J., Ropert, N., Südhof, T.C., and Gaspar, P. (2012). Neurotransmitter release at the thalamocortical synapse instructs barrel formation but not axon patterning in the somatosensory cortex. J. Neurosci. *32*, 6183–6196.

Nie, D., Di Nardo, A., Han, J.M., Baharanyi, H., Kramvis, I., Huynh, T., Dabora, S., Codeluppi, S., Pandolfi, P.P., Pasquale, E.B., and Sahin, M. (2010). Tsc2-Rheb signaling regulates EphA-mediated axon guidance. Nat. Neurosci. *13*, 163–172.

Pan, W.X., Mao, T., and Dudman, J.T. (2010). Inputs to the dorsal striatum of the mouse reflect the parallel circuit architecture of the forebrain. Front. Neuroanat. *4*, 147.

Peça, J., Feliciano, C., Ting, J.T., Wang, W., Wells, M.F., Venkatraman, T.N., Lascola, C.D., Fu, Z., and Feng, G. (2011). Shank3 mutant mice display autistic-like behaviours and striatal dysfunction. Nature *472*, 437–442.

Raab-Graham, K.F., Haddick, P.C.G., Jan, Y.N., and Jan, L.Y. (2006). Activity- and mTOR-dependent suppression of Kv1.1 channel mRNA translation in dendrites. Science *314*, 144–148.

Reith, R.M., McKenna, J., Wu, H., Hashmi, S.S., Cho, S.-H., Dash, P.K., and Gambello, M.J. (2013). Loss of Tsc2 in Purkinje cells is associated with autistic-like behavior in a mouse model of tuberous sclerosis complex. Neurobiol. Dis. *51*, 93–103.

Ridler, K., Suckling, J., Higgins, N.J., de Vries, P.J., Stephenson, C.M., Bolton, P.F., and Bullmore, E.T. (2007). Neuroanatomical correlates of memory deficits in tuberous sclerosis complex. Cereb. Cortex *17*, 261–271.

Saalmann, Y.B., and Kastner, S. (2011). Cognitive and perceptual functions of the visual thalamus. Neuron *71*, 209–223.

Schwaller, B. (2010). Cytosolic Ca2+ buffers. Cold Spring Harb. Perspect. Biol. *2*, a004051.

She, W.-C., Quairiaux, C., Albright, M.J., Wang, Y.-C., Sanchez, D.E., Chang, P.-S., Welker, E., and Lu, H.-C. (2009). Roles of mGluR5 in synaptic function and plasticity of the mouse thalamocortical pathway. Eur. J. Neurosci. *29*, 1379–1396.

Shmelkov, S.V., Hormigo, A., Jing, D., Proenca, C.C., Bath, K.G., Milde, T., Shmelkov, E., Kushner, J.S., Baljevic, M., Dincheva, I., et al. (2010). Slitrk5 deficiency impairs corticostriatal circuitry and leads to obsessive-compulsive-like behaviors in mice. Nat. Med. *16*, 598–602, 1p, 602.

Smith, Y., Raju, D.V., Pare, J.-F., and Sidibe, M. (2004). The thalamostriatal system: a highly specific network of the basal ganglia circuitry. Trends Neurosci. *27*, 520–527.

Soriano, P. (1999). Generalized lacZ expression with the ROSA26 Cre reporter strain. Nat. Genet. *21*, 70–71.

Tsai, P.T., Hull, C., Chu, Y., Greene-Colozzi, E., Sadowski, A.R., Leech, J.M., Steinberg, J., Crawley, J.N., Regehr, W.G., and Sahin, M. (2012). Autistic-like behaviour and cerebellar dysfunction in Purkinje cell Tsc1 mutant mice. Nature *488*, 647–651.

Uhlmann, E.J., Wong, M., Baldwin, R.L., Bajenaru, M.L., Onda, H., Kwiatkowski, D.J., Yamada, K., and Gutmann, D.H. (2002). Astrocyte-specific TSC1 conditional knockout mice exhibit abnormal neuronal organization and seizures. Ann. Neurol. *52*, 285–296.

Way, S.W., McKenna, J., 3rd, Mietzsch, U., Reith, R.M., Wu, H.C.-J., and Gambello, M.J. (2009). Loss of Tsc2 in radial glia models the brain pathology of tuberous sclerosis complex in the mouse. Hum. Mol. Genet. *18*, 1252–1265.

Welch, J.M., Lu, J., Rodriguiz, R.M., Trotta, N.C., Peça, J., Ding, J.-D., Feliciano, C., Chen, M., Adams, J.P., Luo, J., et al. (2007). Cortico-striatal synaptic defects and OCD-like behaviours in Sapap3-mutant mice. Nature *448*, 894–900.

Wimmer, V.C., Bruno, R.M., de Kock, C.P.J., Kuner, T., and Sakmann, B. (2010). Dimensions of a projection column and architecture of VPM and POm axons in rat vibrissal cortex. Cereb. Cortex *20*, 2265–2276.

Wong, V., and Khong, P.-L. (2006). Tuberous sclerosis complex: correlation of magnetic resonance imaging (MRI) findings with comorbidities. J. Child Neurol. *21*, 99–105.

Wong-Riley, M.T., and Welt, C. (1980). Histochemical changes in cytochrome oxidase of cortical barrels after vibrissal removal in neonatal and adult mice. Proc. Natl. Acad. Sci. USA *77*, 2333–2337.

Woolsey, T.A., and Van der Loos, H. (1970). The structural organization of layer IV in the somatosensory region (SI) of mouse cerebral cortex. The description of a cortical field composed of discrete cytoarchitectonic units. Brain Res. *17*, 205–242.

Zervas, M., Somers, K.L., Thrall, M.A., and Walkley, S.U. (2001). Critical role for glycosphingolipids in Niemann-Pick disease type C. Curr. Biol. *11*, 1283–1287.

SUPPLEMENTAL FIGURES and LEGENDS

Neuron, Volume *78*

Supplemental Information

Temporal and Mosaic Tsc1 Deletion in the Developing Thalamus Disrupts Thalamocortical Circuitry, Neural Function, and Behavior

Elizabeth A. Normand, Shane R. Crandall, Catherine A. Thorn, Emily M. Murphy, Bettina Voelcker, Catherine Browning, Jason T. Machan, Christopher I. Moore, Barry W. Connors, and Mark Zervas

SUPPLEMENTAL FIGURES and LEGENDS

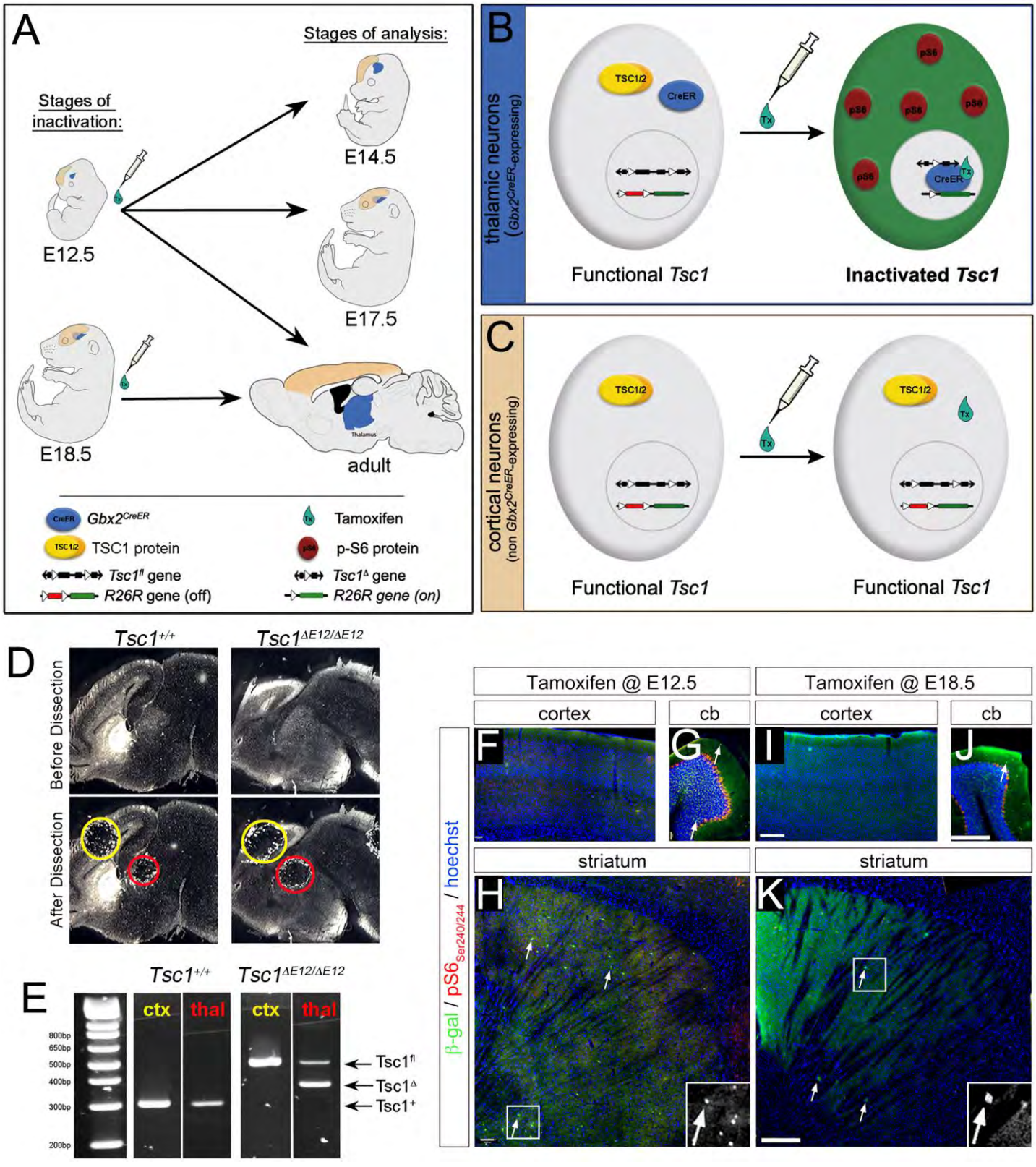

SUPPLEMENTAL FIGURES and LEGENDS

Figure S1, related to Figure 1. Spatial control over *Tsc1^{fl}* allele recombination. (A) Experimental approach. Tamoxifen is administered at E12.5 or E18.5 and mice are analyzed at E14.5, E17.5, or postnatally. Thalamus is shown in blue, cerebral cortex is in tan. (B) Within thalamic *Gbx2^{CreER}*-expressing cells, tamoxifen activates the CreER protein (blue), allowing it to translocate into the nucleus, where it has access to the genome and mediates recombination of *loxP* sites (triangles), thereby deleting the *Tsc1^{fl}* allele (black) and activating the reporter allele (green). (C) In cells, such as cortical neurons, that do not express *Gbx2^{CreER}*, the *Tsc1^{fl}* allele remains functional and the reporter allele remains quiescent, despite being exposed to tamoxifen. (D) Controls (*Tsc1$^{+/+}$*) and mutants (*Tsc1$^{\Delta E12/\Delta E12}$*) were harvested at E17.5. Sagittal brain sections (12 µm) were manually microdissected to collect thalamic tissue (red circle) as well as control tissue from the cerebral cortex (yellow circle). (E) Tissue was lysed and PCR was performed to detect three alleles of *Tsc1*: *Tsc1^{+}* (295bp), *Tsc1^{fl}* (486bp), or *Tsc1$^{\Delta}$* (368bp). Conversion of the *Tsc1^{fl}* allele into the *Tsc1$^{\Delta}$* allele is seen only in the thalamic tissue where *Gbx2^{CreER}* is expressed, but not in the cortical tissue, where there is no CreER expression. *Tsc1^{+}* is unaffected in both the cortical and thalamic tissue samples, as expected. (F-H) IHC was performed on *Gbx2^{CreER};R26^{LacZ};Tsc1$^{+/+}$* animals that received tamoxifen at E12.5 (F-H) or E18.5 (I-K). ß-gal labeling (green) indicates sparse recombination within the cerebellum (arrows) and striatum and a lack of any recombination in the cortex. Purkinje cells of the cerebellum express high basal levels of p-S6.

SUPPLEMENTAL FIGURES and LEGENDS

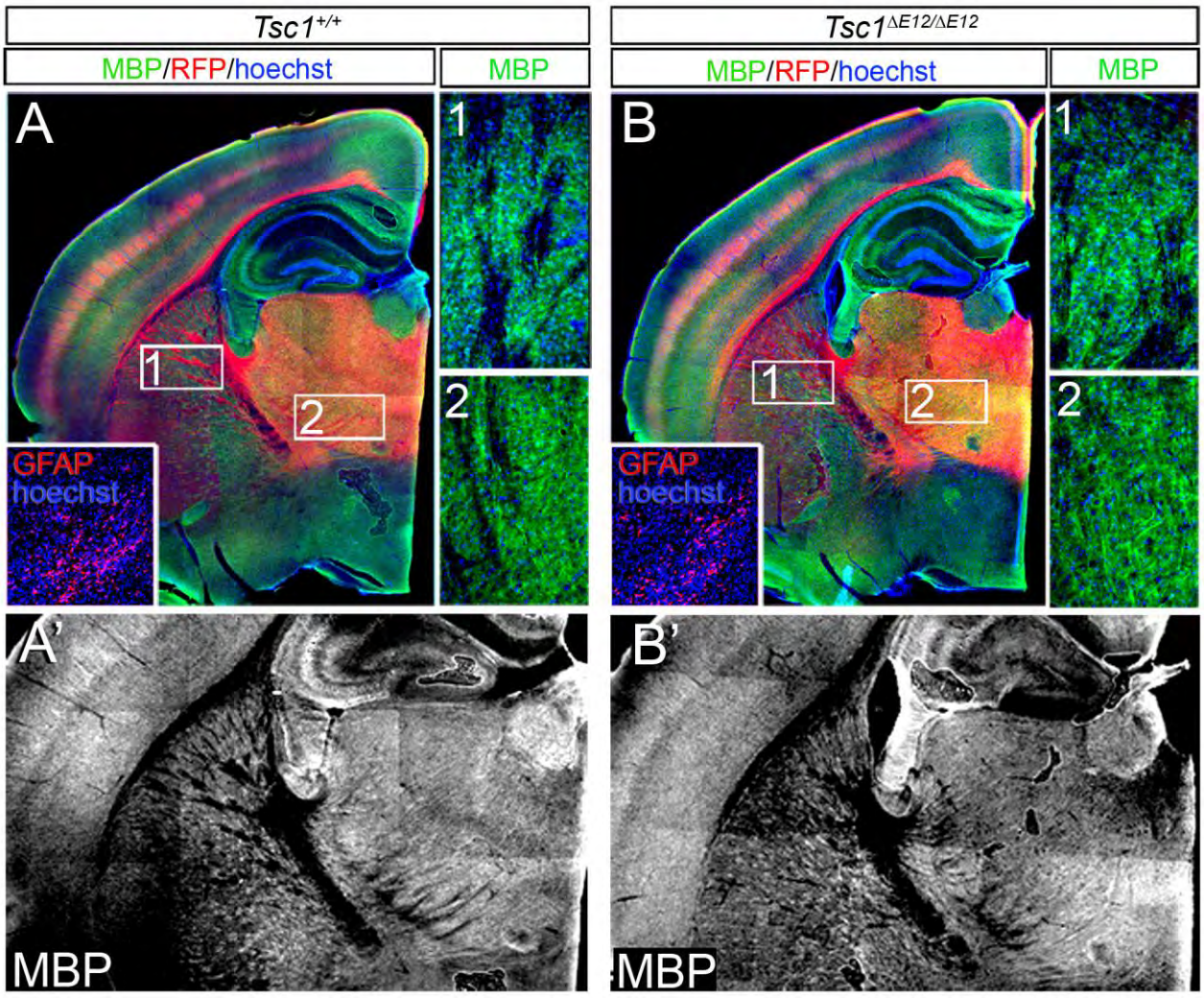

Figure S2, related to Figure 3. Myelination and astrocytes are unaffected in *Tsc1*$^{\Delta E12/\Delta E12}$ mutants. *Tsc1*$^{+/+}$ (A and A') and *Tsc1*$^{\Delta E12/\Delta E12}$ (B and B') adult brain sections were stained for myelin basic protein (MBP, green) and RFP (red). MBP staining was present throughout the brain, as expected, and there were no apparent differences between control and mutant staining patterns. High magnification panels show details of MBP labeling (green) within the internal capsule (region 1) and thalamus (region 2). Insets: IHC for GFAP (red), an astrocyte marker, was also performed on thalamic sections to determine if gliosis occurred as a result of early *Tsc1* deletion. GFAP+ astrocytes were sparse in the thalamus, and no differences in staining were observed between control and *Tsc1*$^{\Delta E12/\Delta E12}$ thalamus. MBP is isolated and shown in A' and B'.

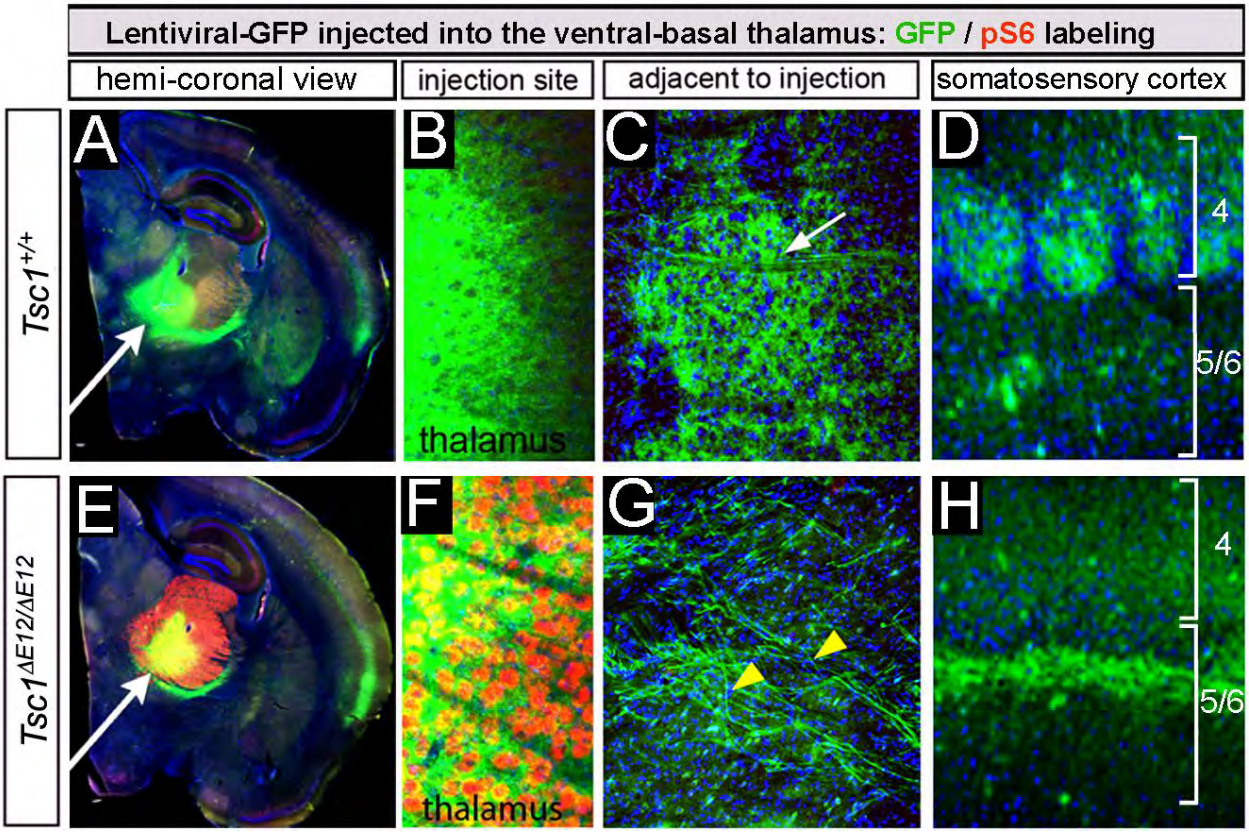

Figure S3, related to Figure 4. Altered distribution of thalamic projections in the internal capsule and cerebral cortex of *Tsc1*$^{\Delta E12/\Delta E12}$ mutants. Lentiviral-GFP was stereotactically injected into the ventrobasal region of the thalamus. After waiting two weeks for expression, the brains were harvested, sectioned, and immunostained for GFP (green) and pS6 (red). GFP+ thalamic axons can be seen exiting the control (A and B) or mutant thalamus (E and F), traversing the striatum (C and G), and entering the cerebral cortex (D and H). Characteristic whisker barrels of the somatosensory cortex can be clearly delineated by the preferential thalamocortical innervation in control brains (D), whereas this barrel pattern is much less apparent in the *Tsc1*$^{\Delta E12/\Delta E12}$ brain (H) and the GFP+ projections instead stratify in deeper cortical layers.

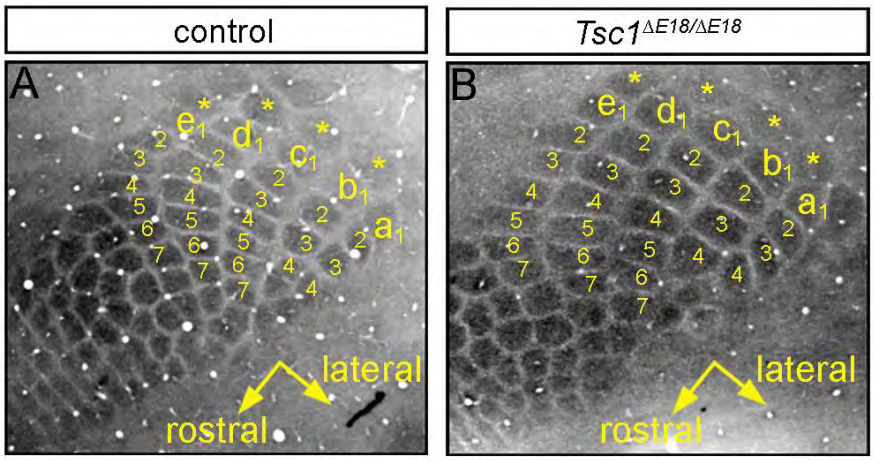

Figure S4, related to Figure 5. *Tsc1*$^{\Delta E18/\Delta E18}$ animals have normal whisker barrel structure. Tangential sections through layer IV somatosensory cortex stained for cytochrome oxidase (black) showed well-organized barrel fields in both control (A) and *Tsc1*$^{\Delta E18/\Delta E18}$ (B) mutant brains. Conventional vibrissae identifiers are indicated.

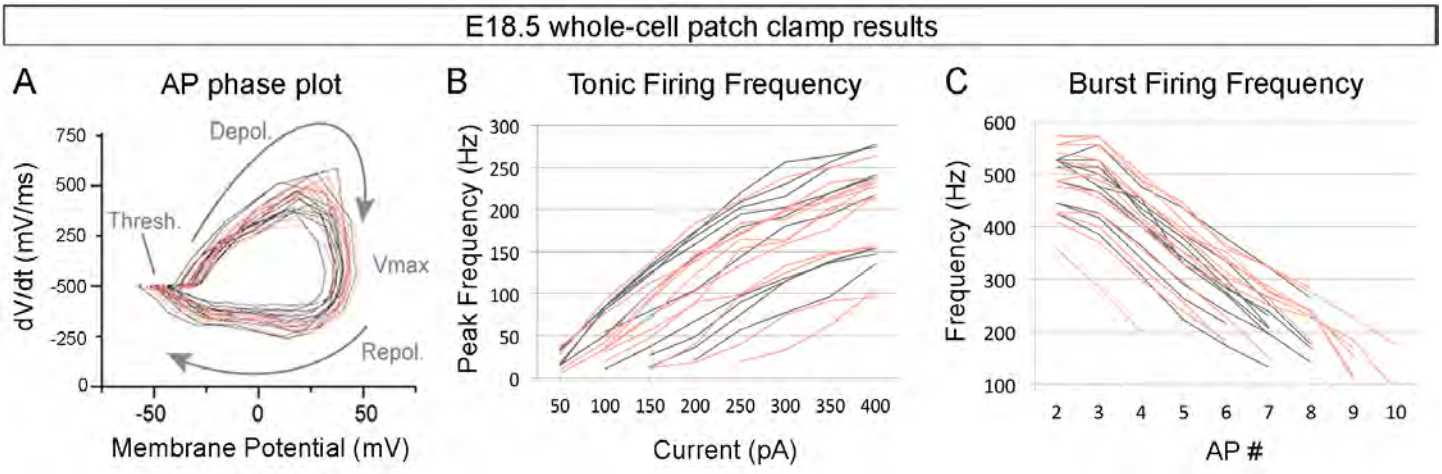

Figure S5, related to Figure 6. Whole-cell physiology of *Tsc1*$^{\Delta E18/\Delta E18}$ mutant thalamic neurons. (A) AP dynamics are shown in a phase plot for *Tsc1*$^{+/+}$ and *Tsc1*$^{\Delta E18/\Delta E18}$, similar to Figure 6C. There was no difference in any of the AP properties analyzed. (B) Peak firing frequency per current injection was plotted, similar to Figure 6F. *Tsc1*$^{\Delta E18/\Delta E18}$ VB neurons (pink lines) have firing frequency similar to *Tsc1*$^{+/+}$ neurons (gray lines). (C) Firing frequency per AP within a post-hyperpolarization rebound burst is plotted, similar to Figure 6I. There was no difference between the *Tsc1*$^{\Delta E18/\Delta E18}$ neurons and the *Tsc1*$^{+/+}$ neurons. See Figure 6 and Table S1 for means and statistics.

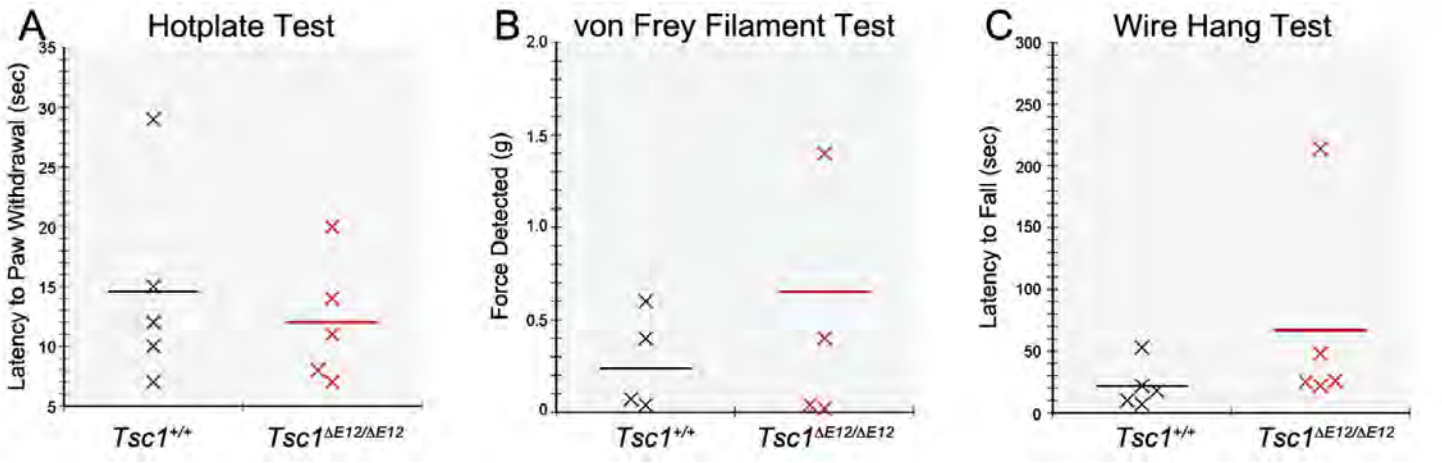

Figure S6, related to Figure 7. Sensory and motor function is unaffected in *Tsc1*$^{\Delta E12/\Delta E12}$ mice. Sensory perception and motor function in *Tsc1*$^{\Delta E12/\Delta E12}$ mice and their littermate controls were compared using the hotplate test (A), von Frey filaments (B), and a wire hang assay (C) to test thermal pain sensitivity, tactile sensitivity, and motor function, respectively. *Tsc1*$^{\Delta E12/\Delta E12}$ (n=5) did not differ significantly from control animals (n=5) in any of the assays (two-tailed t-tests, $p>0.05$), indicating that their sensorimotor functions are not compromised. Data points indicate performance level for individual mice. Horizontal lines indicate population means.

Table S1. Mean Values, Sample Sizes, and Statistical Analysis of Cellular Properties

Property	Tamoxifen	Genotype	number of cells	mean	geometic mean	s.e.m. (lower)	s.e.m. (upper)	95% CI (lower)	95% CI (upper)	p value (if adjusted, with Holm)
Soma area (μm^2)	E12.5	Tsc1+/+ (pS6-)	1061		220.02	-1.96	1.97	211.73	228.62	0.181 (adj.)
	E12.5	Tsc1ΔE12/+ (pS6-)	1058		209.47	-1.86	1.88	201.58	217.69	**0.003 (adj.)**
	E12.5	Tsc1ΔE12/ΔE12, (pS6-)	257		203.73	-3.66	3.73	188.45	220.26	**0.004 (adj.)**
	E12.5	Tsc1ΔE12/ΔE12, (pS6+)	621		403.51	-4.67	4.73	383.77	424.24	
	E18.5	Tsc1+/+ (pS6-)	630		253.36	-16.53	17.67	204.42	314.00	n.d.
	E18.5	Tsc1+/+ (pS6+)	2		304.81	n.d.	n.d.	n.d.	n.d.	
	E18.5	Tsc1ΔE18/+ (pS6-)	1061		242.38	-17	18.28	192.30	305.45	0.142 (adj.)
	E18.5	Tsc1ΔE18/+ (pS6+)	8		277.30	-33.1	37.58	185.03	415.59	
	E18.5	Tsc1ΔE18/ΔE18, (pS6-)	542		246.73	-16.09	17.22	199.06	305.82	0.110 (adj.)
	E18.5	Tsc1ΔE18/ΔE18, (pS6+)	221		358.53	-33.87	37.39	358.52	491.67	
Resting Membrane Potential (mV)	E12.5	Tsc1+/+	12	-61.81		-0.43	0.43	-62.81	-60.82	**0.006**
	E12.5	Tsc1ΔE12/ΔE12	18	-58.06		-0.92	0.92	-60.17	-55.94	
	E18.5	Tsc1+/+	12	-61.86		-0.94	0.94	-64.03	-59.70	0.155
	E18.5	Tsc1ΔE18/ΔE18	13	-60.14		-0.57	0.57	-61.46	-58.81	
Input Resistance (mΩ)	E12.5	Tsc1+/+	12		137.20	-15.648	17.662	103.76	181.15	**0.001**
	E12.5	Tsc1ΔE12/ΔE12	18		72.59	-3.098	3.236	65.64	80.27	
	E18.5	Tsc1+/+	12		157.75	-15.14	16.748	125.01	199.06	0.318
	E18.5	Tsc1ΔE18/ΔE18	13		132.22	-16.292	18.583	97.64	179.06	
Input Capacitance (pF)	E12.5	Tsc1+/+	12		219.66	-28.066	32.178	160.28	301.09	**0.004**
	E12.5	Tsc1ΔE12/ΔE12	18		417.63	-35.789	39.143	339.71	513.47	
	E18.5	Tsc1+/+	12		237.75	-30.397	34.853	173.45	325.40	0.439
	E18.5	Tsc1ΔE18/ΔE18	13		267.47	-12.303	12.896	239.94	298.15	
Membrane Time Constant (msec)	E12.5	Tsc1+/+	12		30.14	-4.252	4.951	21.22	42.80	0.958
	E12.5	Tsc1ΔE12/ΔE12	18		30.43	-2.787	3.068	24.39	37.98	
	E18.5	Tsc1+/+	12		37.51	-1.322	1.37	34.53	40.74	0.647
	E18.5	Tsc1ΔE18/ΔE18	13		35.03	-4.54	5.217	25.43	48.26	
Max AP Rise (mV/msec)	E12.5	Tsc1+/+	12		423.41	-11.86	11.86	396.07	450.76	**<0.001**
	E12.5	Tsc1ΔE12/ΔE12	18		618.44	-26.36	26.36	557.64	679.25	
	E18.5	Tsc1+/+	12		451.44	-19.06	19.06	407.50	495.38	0.478
	E18.5	Tsc1ΔE18/ΔE18	12		472.56	-21.01	21.01	424.10	521.02	
Max AP Fall (mV/msec)	E12.5	Tsc1+/+	12		-151.54	-12.69	12.69	-180.81	-122.27	**<0.001**
	E12.5	Tsc1ΔE12/ΔE12	18		-262.75	-8.39	8.39	-282.10	-243.40	
	E18.5	Tsc1+/+	12		-175.72	-5.36	5.36	-188.09	-163.35	0.603
	E18.5	Tsc1ΔE18/ΔE18	12		-182.88	-12.07	12.07	-210.71	-155.05	
AP amplitude (mV)	E12.5	Tsc1+/+	12		70.39	-1.72	1.72	66.43	74.36	**<0.001**
	E12.5	Tsc1ΔE12/ΔE12	18		82.40	-0.74	0.74	80.71	84.10	
	E18.5	Tsc1+/+	12		71.69	-0.66	0.66	70.17	73.21	0.135
	E18.5	Tsc1ΔE18/ΔE18	12		74.10	-1.29	1.29	71.13	77.06	
AP Half-width (msec)	E12.5	Tsc1+/+	12	0.43		-0.0234	0.0256	0.39	0.49	**0.002**
	E12.5	Tsc1ΔE12/ΔE12	18	0.32		-0.008	0.008	0.31	0.34	
	E18.5	Tsc1+/+	12	0.41		-0.016	0.016	0.37	0.44	0.955
	E18.5	Tsc1ΔE18/ΔE18	12	0.40		-0.022	0.024	0.35	0.46	
Peak fAHP Potential (mV)	E12.5	Tsc1+/+	11	-0.10		0.98	0.98	-2.37	2.17	**0.005**
	E12.5	Tsc1ΔE12/ΔE12	17	-4.24		0.45	0.45	-5.28	-3.21	
	E18.5	Tsc1+/+	11	-0.11		0.96	0.96	-2.31	2.10	0.871
	E18.5	Tsc1ΔE18/ΔE18	12	0.12		0.92	0.92	-2.00	2.23	
ADP+AHP area (mV)	E12.5	Tsc1+/+	11	-63.72		14.73	14.73	-97.70	-29.75	**0.003**
	E12.5	Tsc1ΔE12/ΔE12	17	-177.15		21.89	21.89	-227.63	-126.68	
	E18.5	Tsc1+/+	11	-81.95		9.60	9.60	-104.08	-59.82	0.623
	E18.5	Tsc1ΔE18/ΔE18	12	-69.86		21.60	21.60	-119.66	-20.06	
Tonic F/I slope (Hz*pA)	E12.5	Tsc1+/+	12	0.53		0.01	0.01	0.50	0.56	**<0.001**
	E12.5	Tsc1ΔE12/ΔE12	16	0.27		0.03	0.03	0.21	0.33	
	E18.5	Tsc1+/+	10	0.59		0.04	0.04	0.50	0.69	0.278
	E18.5	Tsc1ΔE18/ΔE18	12	0.52		0.04	0.04	0.42	0.62	
Peak Tonic Firing Frequency @ 400pA (Hz)	E12.5	Tsc1+/+	12	188.30		2.15	2.15	183.34	193.25	**0.001**
	E12.5	Tsc1ΔE12/ΔE12	16	120.74		12.41	12.41	92.13	149.35	
	E18.5	Tsc1+/+	10	210.30		17.02	17.02	171.05	249.55	0.557
	E18.5	Tsc1ΔE18/ΔE18	12	195.35		17.50	17.50	154.99	235.71	
Mean Intraburst Spike Frequency (Hz)	E12.5	Tsc1+/+	12	339.27		21.43	21.43	289.85	388.70	**0.026**
	E12.5	Tsc1ΔE12/ΔE12	18	400.89		7.03	7.03	384.68	417.09	
	E18.5	Tsc1+/+	10	355.99		12.16	12.16	327.95	384.03	0.585
	E18.5	Tsc1ΔE18/ΔE18	13	346.78		10.70	10.70	322.09	371.46	
# of spikes per burst	E12.5	Tsc1+/+	12		7.38	-0.704	0.778	5.86	9.30	0.409
	E12.5	Tsc1ΔE12/ΔE12	18		8.28	-0.682	0.744	6.79	10.10	
	E18.5	Tsc1+/+	10		7.27	-0.079	0.08	7.09	7.46	0.738
	E18.5	Tsc1ΔE18/ΔE18	13		7.43	-0.454	0.484	6.43	8.60	
Peak Burst Firing Frequency (Hz)	E12.5	Tsc1+/+	12		496.21	-29.0023	29.0023	429.33	563.09	0.514
	E12.5	Tsc1ΔE12/ΔE12	18		519.79	-18.681	18.681	476.71	562.87	
	E18.5	Tsc1+/+	10		493.73	-15.6677	15.6677	457.60	529.86	0.719
	E18.5	Tsc1ΔE18/ΔE18	13		485.54	-15.3921	-15.3921	450.04	521.03	

Supplemental Experimental Procedures

Mice

Tsc1^{fl} (Kwiatkowski et al., 2002) and *R26*$^{loxP\text{-}STOP\text{-}loxP\text{-}tdTomato}$ (*R26*^{tdTomato}) (Madisen et al., 2010) mice were obtained from Jackson laboratories (stock # 005680 and #007905, respectively). *Gbx2*$^{CreER\text{-}IRES\text{-}eGFP}$ mice (*Gbx2*^{CreER}) (Chen et al., 2009) and *Rosa26*$^{loxP\text{-}STOP\text{-}loxP\text{-}LacZ}$ reporter (*R26*^{LacZ}) mice (Soriano, 1999) were generously provided by J. Li (UConn Health Center) and P. Soriano (Mt. Sinai School of Medicine), respectively. *Gbx2*^{CreER} mice were bred with *Tsc1*$^{fl/fl}$ mice and either *R26*^{LacZ} or *R26*^{tdTomato} mice to maintain a compound line. Genotyping was performed as previously described for the *CreER* and *R26*^{LacZ} alleles (Ellisor et al., 2009). Genotyping for the *R26*^{tdTomato} allele was performed as described on the jax.org website. Genotyping for the *Tsc1*$^{+}$, *Tsc1*^{fl}, and *Tsc1*$^{\Delta}$ allele was performed as previously described (Figure S1) (Kwiatkowski et al., 2002). *Tsc1*^{fl} inactivation experiments were conducted by crossing *Gbx2*^{CreER};*R26*^{LacZ};*Tsc1*$^{fl/+}$ or *Gbx2*^{CreER};*R26*^{tdTomato};*Tsc1*$^{fl/+}$ males with *Tsc1*$^{fl/+}$ females. The morning (0900) of the day a vaginal plug was detected was designated as embryonic day (E)0.5. 4mg of tamoxifen (20mg/mL in corn oil) was administered by oral gavage (Brown et al., 2009) to the pregnant females harboring embryos at embryonic stage (E)12.5 or E18.5 to simultaneously activate the *R26*^{LacZ} or *R26*^{tdTomato} allele and induce recombination of the *Tsc1*^{fl} allele into the *Tsc1*$^{\Delta}$ allele within the embryos (Figure S1). Mice were housed and handled in accordance with Brown University Institutional Animal Care and Use Committee guidelines.

Tissue Processing, Immunohistochemistry (IHC), and cytochrome oxidase staining

For embryonic analysis, timed-pregnant females harboring embryos at the desired pregnancy stage (E14.5 or E17.5; n≥3 each stage and genotype) were sacrificed at 0900, the uterine chain was dissected out, embryos were genotyped, immersion-fixed in 4% paraformaldehyde (PFA), cryoprotected in 30% sucrose, frozen in Optimal Cutting Temperature (OCT, Fisher), and sectioned on a Leica cryostat as previously described (Ellisor et al., 2009). For postnatal tissue analysis, animals were deeply anesthetized with 195mg/kg Beuthanasia-D (Schering-Plough Animal Health Corp.) and intracardially perfused. Craniotomies were performed as previously described (Brown et al., 2009). Brains were sectioned at a sagittal angle (40 µm) or a thalamocortical angle (60 µm) (Agmon and Connors, 1991) using a Leica vibratome. Embryonic sections and adult free-floating sections were matched based on morphology and processed for IHC by standard methods (Ellisor et al., 2009) using primary antibodies raised against the following antigens: phosphorylated S6 ribosomal protein at Ser240/244 (pS6, rabbit, 1:800, Cell Signaling), phosphorylated S6 ribosomal protein at Ser235/236 (1:100, rabbit, Cell Signaling), ß-galactosidase (1:500, goat, Biogenesis or 1:500, chicken, Abcam), GFP (1:500, rat, Nacalai Tesque or 1:600, rabbit, Invitrogen), RFP (1:1000, chicken, VWR), MAP-2 (1:500, mouse, Sigma), calbindin D-28K (1:1000, rabbit, Swant), parvalbumin (mouse, 1:1000, Sigma), myelin basic protein (MBP, rabbit, 1:500, Millipore), glial fibrillary acidic protein (GFAP, rabbit, 1:500, Millipore), Neuronal Nuclei (NeuN, mouse,1:500, Millipore). The following secondary antibodies from Invitrogen were used at a 1:500 dilution in 1% normal donkey serum/PBS-Triton X-100: Alexa 488 donkey anti-rabbit IgG, Alexa 555 donkey anti-rabbit IgG, Alexa 488 donkey anti-rat IgG, Alexa 555 donkey anti-goat IgG, and Alexa 488 donkey anti-mouse IgG (Molecular Probes) and DyLight 549 donkey anti-chicken IgG (Jackson ImmunoResearch). All sections were counterstained using the Hoechst 33342 (Molecular Probes) and mounted on ColorFrost Plus Slides (Fisher) using Fluoromount-G mounting media (Southern Biotech).

For cytochrome oxidase (CO) staining of vibrissa barrels, mice were deeply anesthetized and intracardially perfused with 4% paraformaldehyde/1% glutaraldehyde in PBS. The brains were obtained and the two hemispheres were separated by a longitudinal cut along the midline. The cerebellum, brainstem, thalamus, hippocampus, olfactory bulb, temporal lobe and most of the subcortical white matter were removed. The two hemispheres were flattened between two glass slides in fix solution (4% PFA, 1% gluteraldehyde in PBS) for 1 hour at 4^{O}C. The flattened hemispheres were cryoprotected in 30% sucrose solution at 4^{O}C, frozen in OCT, and sectioned on a Leica cryostat at 50 µm (*Tsc1*$^{\Delta E12/\Delta E12}$ samples) or 100 µm (*Tsc1*$^{\Delta E18/\Delta E18}$ samples). The sections were incubated with 5 mg DAB (Sigma), 2mg Cytochrome C (Sigma), and 0.4g sucrose in 10mL PBS at 37^{O}C in the dark for 1-3 hours, washed with PBS, and mounted on slides with Fluoromount-G. Adobe Illustrator was used for outlining the barrels stained with CO on different sections. The outlines from all of the

barrel-containing sections were co-registered based on morphological landmarks and/or blood vessel locations, and collapsed to form a representative map of the full barrel field.

For neuron density analysis, a barrel outline was created based on CO+ staining ("barrel hollow") and a perimeter was made 15 µm outside the inner outline ("barrel wall") using Adobe Illustrator's offset path function. The area and the number of NeuN-positive objects in the barrel hollow and wall regions were determined using the automated "measure area" and "find points" function in Volocity software (Improvision). Quantative barrel analysis was analyzed for significance by Student's t-test.

Microscopy and Cell Size Analysis

Sections were imaged on a Leica DM6000B epifluorescent microscope with Volocity 5.2 imaging software (Improvision). Red, green, and blue channels were imaged separately and pseudocolored as part of the acquisition palettes. Identical exposure settings were used across the three genotypes to allow for direct comparison of labeling intensity. Post-acquisition image processing was performed in Adobe Photoshop, with control and experimental data processed identically. For cell size analysis, free-floating adult sagittal sections from *Tsc1*$^{+/+}$, *Tsc1*$^{\Delta E12+}$, and *Tsc1*$^{\Delta E12/\Delta E12}$ animals (n=3 each genotype) were processed for IHC using primary antibodies to MAP-2 and p-S6$_{Ser240/244}$, as described above. Five thalamic regions (dorsal, ventral, anterior, posterior, and center) from five medial-to-lateral brain levels were imaged at 40x magnification. After the red channel was cloaked to blind the observer to p-S6 levels, the green MAP-2 signal was used to manually outline the edges of clearly labeled neuronal cell bodies using Volocity's Freehand Tool. The Measure function was used to calculate the perimeter and area of all outlined cell bodies, which were exported to Microsoft Excel for data analysis. After analysis, the red p-S6 channel was unmasked in order to sort cells into "p-S6 positive" and "p-S6 negative" cohorts, based on p-S6 immunolabeling intensity. Numbers of measured cells per cohort are indicated in Figures 3 and 5. Generalized Estimating Equations (log-normal generalized model) were used to compare genotypes with regards to neuronal size. Each mouse had multiple cells, which were treated as having correlated error. Cells were divided into those expressing pS6 and those not expressing pS6. Comparison between sizes of pS6-positive and pS6-negative cells within the knock-outs was a within-subjects comparison, while those between genotypes were between-subjects comparisons. Pair-wise comparisons were made using orthogonal contrast statements, with p-values adjusted using the Holm test to maintain family-wise alpha at 0.05.

Whole-cell Recordings

Slice Preparation: Brain sections were prepared from young mice (postnatal age: 20-23 days) of either sex as previously described (Agmon and Connors, 1991; Cruikshank et al., 2010; Cruikshank et al., 2012). Briefly, mice were deeply anesthetized with isofluorane, then decapitated. The brains were quickly removed and placed in cold (4°C) oxygenated (5% CO_2, 95% O_2) slicing solution containing (in mM): 3.0 KCl, 1.25 NaH_2PO_4, 10.0 $MgSO_4$, 0.5 $CaCl_2$, 26.0 $NaHCO_3$, 10.0 Glucose, and 234.0 sucrose. Brains were then mounted, using a cyanoacrylate adhesive, onto the stage of a vibrating tissue slicer and horizontal brain slices (275-300 µm) containing the VB nucleus were obtained. Slices were immediately transferred to a holding chamber containing oxygenated, physiological saline solution maintained at 32 ± 1 °C. The oxygenated physiological solution (5% CO_2, 95% O2) contained (in mM): 126.0 NaCl, 3.0 KCl, 1.25 NaH_2PO_4, 2.0 $MgSO_4$, 2.0 $CaCl_2$, 26.0 $NaHCO_3$, and 10.0 glucose. After 15-20 min, the temperature was reduced to room temperature and the slices were allowed to incubate for an additional 60 min.

Whole-Cell Recording Procedure: Individual brain slices were placed in a submersion-type recording chamber maintained at 32 ± 1 ºC and continuously superfused (2.5-3 ml/min) with oxygenated physiological saline. VB neurons were visualized using a Zeiss Axioskop fixed-stage microscope equipped with IR-DIC optics and a water-immersion objective (40X, 0.75 NA, Zeiss). All but 6 mutant neurons were identified visually by expression of *R26*^{tdTomato}. Electrophysiological data were acquired using an Axoclamp-2B amplifier, filtered at 10 kHz and digitized at 20 kHz using a Digidata 1322A digitizer in combination with pClamp10 software (Molecular Devices). For whole-cell recordings, patch pipettes had tip resistances of 3-6 MΩ when filled with a potassium-based internal solution containing (in mM): 130.0 K-gluconate, 4.0 KCl, 2.0 NaCl, 10 HEPES, 0.2

EGTA, 4.0 ATP-Mg, and 0.3 GTP-Tris, 14.0 phosphocreatine-K (pH 7.25, ~290 mOsm). During all recordings the pipette capacitance was neutralized and access resistance was continually monitored. Membrane potentials were not corrected for liquid junction potentials.

Data Analyses: Data were collected with protocols made with Clampex 10.0 and analyses were performed post-hoc using Clampfit 10.0. Resting membrane potentials (R_m) were measured within 2 min of break-in. Input resistances (R_{in}) were estimated as the slope of the voltage-current relationship obtained with current pulses (-50 to +50 pA, 25-50 pA increments, 800 ms duration). Membrane time constants (τ_m) were calculated from voltage responses to small negative current injections (3-5 pA, 500 ms duration). For τ_m, the voltage responses were fitted with a single exponential to the initial 150 ms of the responses. Input capacitances (C_{in}) were calculated as τ_m /R_{in}. Burst properties were characterized by holding the soma at a membrane potential of -60 mV with intracellular current and subsequently injecting large negative currents (400-1000 pA, 40-100 pA increments, 800 ms duration). When comparing low-threshold bursts, only trials in which the steady-state potential reached -70 ± 2 mV were used. Tonic and single action potential properties were characterized by holding the soma at a membrane potential of -50 mV with intracellular current and injecting suprathreshhold positive current. Frequency-current relationships were obtained using large positive current injections (50-400 pA, 50 pA increments, 800 ms duration). Single action potential data were obtained by injecting the minimum current needed to elicit an action potential (10-200 pA, 10-15 pA increments, 800 ms duration). Action potential thresholds were calculated as the voltage difference between the steady-state potential and the point at which the rate of rise was greater than 15 mV/ms. Action potential amplitudes and half-widths were measured relative to threshold potential. After-hyperpolarizations (AHPs) were evoked by injecting a 2 ms suprathreshold positive current (600-1500 pA).

Generalized Hierarchical Linear Modeling was use to test for differential effects of *Tsc1* gene deletion at E12.5 and E18.5, while appropriately accounting for nested measurement of multiple cells within-mouse (up to 6 cells sampled in 12 mice for a total of 55). The choice of distribution on which the statistical model was based was chosen based on model diagnostic residual visualizations. Cell genotype and stage of tamoxifen were treated as fixed effects with cell genotype also treated as a random effect with a compound symmetry variance-covariance structure. Any model misspecification was adjusted for using classical sandwich estimation. Individual comparisons by cell genotype within tamoxifen time-points (i.e. $Tsc1^{\Delta E12/\Delta E12}$ mutants versus $Tsc1^{+/+}$ littermates) were made using orthogonal linear comparisons. The interaction effect of the omnibus represented the comparison of these effects.

In vivo Extracellular Recordings

Head-post Surgery and Craniotomy: Animals were anesthetized under 3.0% isoflurane (Isothesia, Butler Schein, Dublin OH) in O_2 within a plastic induction chamber and fitted into a stereotaxic apparatus (David Kopf Instruments, Tujunga CA). Throughout surgery, animals received 0.5-2.0% isoflurane in 1.0% O_2; levels were controlled with the use of an Isotec vaporizer (SurgiVet, Waukesha WI). Body temperature was maintained at 36-38°C with a heating pad (Cara, Inc., Warwick RI) during both surgery and recording sessions. Animals received 0.05 mL intraperitoneal injections of atropine sulfate (0.54 mg/mL, Med-Pharmex, Pomona CA) and buprenorphine hydrochloride (.03 mg/mL, Reckitt-Benckiser, Richmond VA), and a 0.025 mL intraperitoneal injection of dexamethasone (2 mg/mL, VEDCO, St. Joseph MO).

The dorsal surface of the head was shaved with a standard razor, and any residual fur was removed using a depilatory agent (Nair). Skull was exposed under aseptic conditions, and the center of the planned craniotomy was marked (AP: -1.2, L: 3.5). A custom-designed titanium head-post was affixed to the skull with C&B metabond (Parkell Inc., Edgewood NY) perpendicular to the sagittal plane. Posts can be clamped for quick and consistent head-fixing. Dental cement (Lang Dental, Wheeling IL) was used to form a surface within the head-post interior for a saline well. The tissue surrounding the head-post was reattached to the head-post exterior edge using superglue (Loctite instant adhesive 454, Rocky Hill CT). An air-powered drill (Midwest Tradition Highspeed Handpiece, Dentsply Professional, Des Plaines IL) outfitted with a 0.5 mm regular carbide bur (Shank Type FGSS, Dentsply Professional) was used to clean away cement at the craniotomy site and thin the

skull. The bone was removed, and the exposed brain was covered with saline. All recording equipment was secured onto a vibration isolation table (Technical Manufacturing Corporation, Peabody MA) to minimize noise and artifact. Animals were head-fixed, and anesthesia was maintained through infusion of 0.5-2.0% isoflurane through a nose cone; isoflurane levels were gradually lowered until the animal was just above the threshold at which there existed a paw pinch response.

NeuroNexus probes were used for all recording sessions. In some cases, bad contacts were present on probes, and these data were discarded. Local field potential (LFP) signals were sampled (30303 Hz), filtered (0.9 to 9000 Hz), and recorded using a Cheetah Data Acquisition System (NeuraLynx, Bozeman, MT). A four-axis micromanipulator (Siskiyou, Grants Pass OR) was used to clamp the probe, which was manually lowered to the brain surface. Prior to thalamic recordings, the probe angle was adjusted to approximately 25°. The probe was grounded on the head-post mount, and a reference wire was placed within the saline well. The probe was lowered at a controlled rate to depths of 1600 μm or 2500 μm for cortical and thalamic recordings, respectively. An air puffer, gated by a solenoid, was positioned above contralateral vibrissae and used to test for response to vibrissa deflection: application of such deflections was used to confirm electrode placement in SI and to ensure consistent quality of recording. After validation of probe location, ten minutes of baseline activity was recorded. A stimulus period consisting of 500 air puff trials followed; inter-trial periods were of randomly selected lengths between 2 and 8 seconds long, with a mean period of 5 seconds. At the end of the stimulus period, a 10 minute post-stimulus baseline period was recorded. Following recordings, the saline well was filled with a silicone elastomer (KwikCast, World Precision Instruments, Sarasota FL) to cap and protect the craniotomy between recording sessions. At the start of subsequent recording sessions, KwikCast was removed and the craniotomy area was inspected for bleeding, inflammation, and bone growth. Recordings then proceeded as previously described.

Recording Analysis: For each animal, a single SI recording session was selected for LFP analysis. The session chosen was that which exhibited the least clipping artifact and the highest amplitude responses following vibrissa deflection across the 16 probe channels. Within each chosen session, the contact exhibiting the largest amplitude and shortest duration responses following vibrissa deflection was identified as a putative layer IV contact and selected for analysis. The recorded signal from this contact was then low-pass filtered (0-150 Hz), downsampled (to 505.05 Hz), and clipping artifacts were removed.

Data from the entire recording session, including baseline (no stimulation) and vibrissa-stimulation periods, were analyzed using Matlab (MathWorks, Natick, MA). Each record was divided into 20-second non-overlapping time windows, and any trailing samples not included in these windows were discarded. The power spectral density (PSD) for each window was estimated using Welch's method (Matlab's pwelch command) with a 4096-point FFT, normalized by dividing by the sum of the PSD across all frequencies, and smoothed using a 5-pt moving average filter. For each animal, the average normalized PSD across the entire recording session was computed by taking the mean of the normalized PSDs across all the 20-second windows. Relative power at 3 Hz was calculated for each 20-second window by dividing the value of the normalized PSD at 3 Hz by the value at 1 Hz, and the average for each animal was taken to be the mean of this ratio across windows. For each animal, the number of 20-second windows in which normalized power at 3 Hz exceeded a threshold was then counted. This threshold was determined as the 97.5th percentile of normalized 3 Hz power across all animals. To test for significant differences between control and mutant subjects, two-tailed two-sample t-tests were performed by grouping all *Tsc1*$^{+/+}$ control animals (tamoxifen delivered at E12.5 and E18.5) and all mutant animals (*Tsc1*$^{\Delta E12/\Delta E12}$ and *Tsc1*$^{\Delta E18/\Delta 18}$), with a significance level, α, of 0.05.

Behavioral Analysis

Seizures and over-grooming: *Tsc1*$^{\Delta E12/\Delta E12}$ mice (n=11) and their littermate controls (*Tsc1*$^{+/+}$ or *Tsc1*$^{fl/fl}$, n=19; *Tsc1*$^{+/\Delta E12}$ n=17) were videotaped in their home cage using a digital camera for 8-minute epochs 2-3 times per week between 2 months of age and 8 months of age. Two *Tsc1*$^{\Delta E12/\Delta E12}$ mice died prematurely of unknown causes and were not included in the behavioral analysis. *Tsc1*$^{\Delta E18/\Delta E18}$ mice (n=17) and their littermate controls (*Tsc1*$^{+/+}$ or *Tsc1*$^{fl/fl}$, n=25; *Tsc1*$^{+/\Delta E18}$, n=6) were observed once per week for 8 minutes, beginning at 2 months of age and continuing through 8 months of age. Videos were analyzed by an observer who was blinded to animal genotypes. Number and duration of all seizures and self-grooming behaviors were manually tallied

(grooming events lasting less than 1 second were rounded up to 1 second duration). An independent observer tallied a subset of videos, and the two observers' tallies had a high level of concordance, confirming the reproducibility of the manual data analysis approach. Animals were euthanized for humane reasons by intracardiac perfusion if they developed severe grooming lesions. Data was analyzed in Excel (Microsoft) and plotted using KaleidaGraph (Synergy). Generalized Estimating Equations were used to compare genotypes with regards to percent minutes grooming (binomial generalized model grooming/total minutes) and seizure event rates (negative-binomial generalized model offset by log total hours). Comparisons represented between-subjects comparisons, with multiple observations within an animal modeled as having correlated error. Pair-wise comparisons were made using orthogonal contrast statements, with p-values adjusted using the Holm test to maintain family-wise alpha at 0.05.

Von Frey Filament test: Withdrawal thresholds from mechanical stimuli of von Frey filaments of ascending bending force (from 0.008 g to 300 g of force) were applied five times to the plantar surface of the bilateral hind paws. A positive response was defined as withdrawal from the von Frey filament on at least 3 of the 5 contacts. Confirmation of threshold was then tested by examining the filament above and below the withdrawal response. Significance was assessed by a one-tailed two-sample t-test, $\alpha=0.05$.

Hot plate test: The test was based on that described by Eddy and Leimbach (1953). A glass cylinder (16 cm high, 16 cm diameter) was used to keep the mice on the heated surface of the plate, which was kept at a temperature of 53°C +/- 0.2°C (Ugo Basile model 7280). The first of two nociceptive thresholds were evaluated: licking of the hind paw or sustained (> 1 s) lifting of the hind paw from the surface. The cut-off for a response was 40 s at which point the trial was terminated. Significance was assessed by a one-tailed two-sample t-test, $\alpha=0.05$.

Wire Hang test: Mice were placed on a wire cage lid, which was then inverted gently 180° so that the mouse gripped the wire at a distance of ~16 cm above the floor of an empty cage. Latency to fall was recorded, with a cut-off time of 300 s. Animals were provided with 4 opportunities to perform on this task and the longest duration to fall was collected. Significance was assessed by a one-tailed two-sample t-test, $\alpha=0.05$.

Elsevier Editorial System(tm) for Gene Expression Patterns
Manuscript Draft

Manuscript Number:

Title: The timing and duration of Gbx2 expression delineates thalamocortical or dopamine medial forebrain bundle circuitry

Article Type: Normal Submission

Keywords: genetic lineage
neural circuits
Gbx2
thalamocortical
dopamine neurons

Corresponding Author: Manning Asisstant Professor of Biology Mark Zervas, Ph.D.

Corresponding Author's Institution: Brown University

First Author: Elizabeth Normand

Order of Authors: Elizabeth Normand; Catherine Browning; Nellwyn Hagan; Mark Zervas, Ph.D.

Abstract: The onset and duration of gene expression is highly coordinated during development to ensure the proper allocation of cell types and tissues. Equally important is how cohorts of neurons establish axonal projections that innervate terminal target sites. We sought to link the temporal dynamics of gene expression within a specific genetic lineage and the establishment of the neuronal circuits. To accomplish this task, we used non-invasive genetic inducible circuit mapping and CreER/loxP technology. Specifically, we genetically marked Gbx2-expressing thalamic neuron progenitors at an early embryonic stage. We subsequently tracked the formation of the lineage-derived thalamocortical axons during embryogenesis and at an early postnatal stage. We show that lineage marking provides a high degree of clarity in following neural circuit development. We also show how the onset and duration of gene expression can be used to delineate subsets of neural circuits within a single lineage. Finally, we uncover a novel contribution of Gbx2-expressing progenitors to midbrain dopamine neurons and dopaminergic axons of the medial forebrain bundle. We anticipate that genetic circuit tracing will be instructive in elucidating changes in neural circuits in the context of normal development and in mutant mice in which circuit formation is altered.

Suggested Reviewers: susan Dymecki M.D., Ph.D.
Department of Genetics, Harvard Medical School
dymecki@genetics.med.harvard.edu
Dr. Dymecki is a an expert in cell fate and lineage decisions. She pioneered the use of intersectional fate mapping and is well qualified to assess timing and lineage as it relates to neural circuit formation.

James Li Ph.D.
Department of Genetics and Developmental Biology , UConn Health Center
jali@uchc.edu
Dr. Li is an expert in Gbx2 lineage and the function of Gbx2. Dr.Li is also an expert on the development of the thalamus and the role of Gbx2 in thalamic development.

John Rubenstein M.D., Ph.D.
Genetics, Development and Behavioral Sciences Building, UCSF
john.rubenstein@ucsf.edu
Dr. Rubenstein is an expert in the development of the thalamus and has contributed tremendously to understanding the role of transcription factors and both brain development and establishment of the thalamus.

Paola Arlotta Ph.D.
Department of Stem Cell and Regenerative Biology, Harvard University and MGH Center for Regenerative Medicine
paola_arlotta@hms.harvard.edu
Dr. Arlotta is an expert on the role of transcription factor regulation of cell fate determination and neural circuit formation.

Cover Letter

Mark Zervas
Manning Assistant Professor of Biology
Laboratory of Developmental Neurobiology, Genetics and Neurological Disease
Department of Molecular Biology, Cell Biology and Biochemistry
Brown University
Providence, RI 02912
Tel: 401-863-6840
Email: Mark_Zervas@brown.edu

BROWN

To: Dr. Wilkinson
Editor-in-Chief
Gene Expression Patterns

Date: July 09, 2012

Re: Manuscript Submission

Dear Wilkinson,

Please consider our manuscript "The timing and duration of *Gbx2* expression delineates thalamocortical or dopamine medial forebrain bundle circuitry." for publication in *Gene Expression Patterns*. This study uses $Gbx2^{CreERT}$ and the $R26^{tdTomato}$ conditional reporter allele to permanently and heritably mark *Gbx2* expressing progenitors at E9.5 using a genetic inducible fate mapping approach. We then demonstrate how axons from neurons derived from the marked *Gbx2* lineage contribute to the formation of thalamocortical circuitry and innervate the cerebral cortex. While it is well known how the thalamocortical circuitry is established during development, we show how lineage tracing and genetics can be coupled to ascertain how neurons from a specific lineage (e.g. *Gbx2*) participates in thalamocortical circuitry. We then take advantage of the genetic components in the alleles used in this system to show how timing of gene expression and lineage can be ascertained simultaneously. With this approach we show that thalamic neurons and their thalamocortical projections that expressed *Gbx2* at E9.5 continued to express *Gbx2* three days later. Interestingly, we also uncovered that midbrain dopamine neurons that project along the medial forebrain bundle are derived from *Gbx2* expressing progenitors that extinguish *Gbx2* within three days. This is the first description of the dopamine neurons being derived from this lineage and provides unique insight into the complexity of the progenitor pool and the timing of gene expression that results in dopamine neuron formation.

We believe this study will be of interest to developmental neurobiologists because it demonstrates the power of combining gene expression analysis, fine temporal fate mapping, and circuit formation in the mouse nervous system. In addition, the findings of *Gbx2* contribution to midbrain dopamine neurons will likely be of interest to the community of biologists interested in dopamine neuron development and cellular programming to generate dopamine neurons from stem cells or induced pluripotent stem cells. We suggest the following people as possible reviewers: Susan Dymecki, James Li, John Rubenstein, and Paola Arlotta.

Thank your for your time in handling our paper.

Sincerely, Mark Zervas

Mark Zervas, Ph.D.
Manning Assistant Professor of Biology

Abstract

The onset and duration of gene expression is highly coordinated during development to ensure the proper allocation of cell types and tissues. Equally important is how cohorts of neurons establish axonal projections that innervate terminal target sites. We sought to link the temporal dynamics of gene expression within a specific genetic lineage and the establishment of the neuronal circuits. To accomplish this task, we used non-invasive genetic inducible circuit mapping and CreER/loxP technology. Specifically, we genetically marked Gbx2-expressing thalamic neuron progenitors at an early embryonic stage. We subsequently tracked the formation of the lineage-derived thalamocortical axons during embryogenesis and at an early postnatal stage. We show that lineage marking provides a high degree of clarity in following neural circuit development. We also show how the onset and duration of gene expression can be used to delineate subsets of neural circuits within a single lineage. Finally, we uncover a novel contribution of Gbx2-expressing progenitors to midbrain dopamine neurons and dopaminergic axons of the medial forebrain bundle. We anticipate that genetic circuit tracing will be instructive in elucidating changes in neural circuits in the context of normal development and in mutant mice in which circuit formation is altered.

Highlights

> Genetic Inducible Circuit Mapping links temporal gene expression to thalamocortical circuitry

> Thalamic neuron progenitors that express Gbx2 at E9.5 persist in Gbx2 expression for three days

> The Gbx2 contributes to midbrain dopamine neurons and projections of the medial forebrain bundle

> Dopamine neuron progenitors express Gbx2 transiently at E9.5

*Manuscript
Click here to view linked References

Title: The timing and duration of *Gbx2* expression delineates thalamocortical or dopamine medial forebrain bundle circuitry.

Elizabeth Normand[1,2], Catherine Browning[3], Nellwyn Hagan[1,4], and Mark Zervas[*,2,3]

[1]Department of Neuroscience, [2]Department of Molecular Biology, Cell Biology and Biochemistry, Division of Biology and Medicine, and [3]Brown University Institute for Brain Science, Brown University, 70 Ship St., Providence, RI 02903, [4]Present address: Department of Neurobiology, Harvard Medical School, 220 Longwood Ave., Boston, MA 02115

*Author for correspondence

Address:

Laboratory of Developmental Neurobiology, Genetics and Neurological Disease
Department of Molecular Biology, Cell Biology and Biochemistry
Division of Biology and Medicine

Box G-E436
Brown University
Providence, RI 02912

Courier delivery:
Laboratories for Molecular Medicine
70 Ship Street, Rm. 436
Providence, RI 02903

email: Mark_Zervas@brown.edu
Tel: 401-863-6840
Fax: 401-863-9653
Web page: http://research.brown.edu/myresearch/Mark_Zervas

Blank Page

Abstract

The onset and duration of gene expression is highly coordinated during development to ensure the proper allocation of cell types and tissues. Equally important is how cohorts of neurons establish axonal projections that innervate terminal target sites. We sought to link the temporal dynamics of gene expression within a specific genetic lineage and the establishment of the neuronal circuits. To accomplish this task, we used non-invasive genetic inducible circuit mapping and CreER/*loxP* technology. Specifically, we genetically marked *Gbx2*-expressing thalamic neuron progenitors at an early embryonic stage. We subsequently tracked the formation of the lineage-derived thalamocortical axons during embryogenesis and at an early postnatal stage. We show that lineage marking provides a high degree of clarity in following neural circuit development. We also show how the onset and duration of gene expression can be used to delineate subsets of neural circuits within a single lineage. Finally, we uncover a novel contribution of *Gbx2*-expressing progenitors to midbrain dopamine neurons and dopaminergic axons of the medial forebrain bundle. We anticipate that genetic circuit tracing will be instructive in elucidating changes in neural circuits in the context of normal development and in mutant mice in which circuit formation is altered.

1. Introduction

The relationship between a specific gene expressed in progenitors during development and the terminal cell fate of these progenitors is referred to a genetic lineage. An important aspect of genetic lineage is how the timing of gene expression within the lineage helps shape the distribution and ultimate cell fate in mature tissues including the nervous system (Dymecki and Kim, 2007; Joyner and Zervas, 2006). An additional component of nervous system development is that axons anatomically bind functional domains through the establishment of neural circuits. Thus a problem in studying neural development is forging a link between progenitors that express genes with temporal precision and establishing neural circuits related to the lineage-derived neurons. There have been recent advances in tackling the problem of neural circuit formation using mice as a model system (reviewed in Luo et al., 2008 and see Lo and Anderson, 2011), but there are relatively few examples of marking neural circuits and establishing easily discernible point to point labeling of axonal connections based on temporal gene expression in mice. Thus, a desirable feature of circuitry mapping would be the use of a genetic based system that can be used to mark progenitors with spatial and temporal control, conferring a high fidelity of marking, and that could be readily used to assess genetic mutant mice. We previously showed that an inducible *CreER* recombinase based system and

conditional GFP reporter allele allowed for the detection of lineage-derived axons (Ellisor et al., 2009; Hagan and Zervas 2011]). Here, we used a well-characterized *CreER* line in combination with a commercially available conditional reporter to characterize distinct stages of axonal development and we specifically mark and track developing thalamic neurons and their emerging circuits during *in vivo* development. We also show that a genetics approach can elucidate temporal dynamics of gene expression and specific neural circuits *in vivo.* We anticipate that the ease and robustness of this approach will advance our understanding of neural circuit formation in normal development and in genetic mutant mice.

2. Results

We administered tamoxifen to E9.5 $Gbx2^{CreER\text{-}ires\text{-}eGFP}$ embryos to mark thalamic progenitors *in vivo* (Chen et al., 2009). We coupled this line with $R26^{tdTomato}$ conditional reporter mice because they provide a robust readout of Cre-mediated recombination (Madisen et al., 2010). In the absence of tamoxifen, CreER protein is sequestered in the cytoplasm and recombination of conditional alleles does not occur (Ellisor et al., 2009; Ellisor and Zervas, 2010). However, by delivering tamoxifen to pregnant female mice we control the release of CreER from sequestration. Once freed CreER translocates to the nucleus where it mediates recombination in same-site oriented *loxP* sites that flank a *stop* cassette in the reporter allele (reviewed in Joyner and Zervas, 2006). Thus, tamoxifen administrations allows us to control the timing of the recombination event and cell marking within the *Gbx2* lineage (Chen et al., 2009; Luu et al., 2009).

We first analyzed embryos at E12.5, which showed thalamic neurons derived from the *Gbx2* lineage marked at E9.5 (Fig. 1A,B). The marked neurons had axons that emerged from the thalamus and formed a thick proximal fascicle (Fig. 1A-C). The *Gbx2*-derived axonal projections terminated at a distal limit in the proximity of the thalamocortical intermediate target zone (Fig. 1D) consistent with thalamocortical axon guidance (Inan and Crair, 2007). A second cohort of *Gbx2*-derived neurons were located in the ganglionic eminence (Fig. 1E). In addition to the thalamocortical projections, there was a more ventrally located loose axonal fiber tract in what appeared to be the medial forebrain bundle (Fig. 1A, MFB). The $Gbx2^{CreER\text{-}ires\text{-}eGFP};R26^{tdTomato}$ allelic configuration allows for the determination of progenitors that expressed *Gbx2* at the stage of marking and whether they continued to express *Gbx2* at the stage of analysis. We previously found that this approach was instructive in determining how the timing and duration of *Gbx2* expression shaped early spinal cord development (Luu et al., 2011). We therefore assessed dynamic gene expression and expanded it to interrogate early thalamic

circuits. Specifically, this analysis identified neural circuits that were derived from early *Gbx2* expressing progenitors marked at E9.5 (tdTomato+ neurons and their axons, red) and neurons that were expressing *Gbx2*(GFP) at the time of analysis (GFP+ neurons and their axons, green). Interestingly, the thalamocortical axons at E12.5 were derived from neurons that had experienced early and persistent *Gbx2* expression (tdTomato+/GFP+, yellow) (Fig. 2A,A'). In contrast, the *Gbx2*-derived axons in the putative medial forebrain bundle that were derived from progenitors expressing *Gbx2* at E9.5 did not continue to express *Gbx2* as evident by their lack of GFP labeling (Fig. 2A). We used an antibody recognizing tyrosine hydroxylase (TH) to label midbrain dopamine neurons and their axons that course along the medial forebrain bundle (Blakely et al., 2011; Vitalis et al., 2000). Surprisingly, the *Gbx2*-derived axons (dsRed+) in the medial forebrain bundle were also TH+, which suggested that dopamine neurons were derived *Gbx2*-expressing progenitors marked at E9.5 (Fig. 2B,B',3). We validated the assertion that midbrain dopamine neurons were derived from the *Gbx2* lineage because the TH+ neurons were also dsRed+ (Fig. 2B*,3).

The *Gbx2* lineage-derived neurons marked at E9.5 continued to populate the thalamus at E18.5 (Fig. 3A,B). These thalamic neurons had axons that exited the thalamus (Fig. 3C) and traversed ventrally and rostrally as fascicles that passed through the ventral half of the striatum (Fig. 3D). The bundles de-fasciculated as they entered the cerebral cortex and formed axonal branches but did not yet innervate the cortical layers (Fig. 3E). In addition, the tdTomato (dsRed+) projections could be used to track entire axonal bundles en route to the deep cortical layers in more lateral sections (Fig. 3F). Finally, by P7 thalamic neurons derived from *Gbx2*-expressing progenitors marked at E9.5 were distributed broadly in the thalamus and had characteristic thalamic morphologies and broad sweeping fascicles that emerged from the lateral extent of the thalamus and entered the internal capsule (Fig. 4A-C). The fascicles remained well organized and appeared as parallel-oriented fibers with numerous small terminal ramifications throughout and at the anterior-dorsal extent of the caudate/putamen (Fig. 4D). Significant cohorts of thalamocortical projections passed through the internal capsule and caudate/putamen as smaller bundles compared to their entrance into the internal capsule, but retained a parallel orientation with each other as they entered into layer 6b of the cerebral cortex (Fig. 4E,F). In parallel sections (Fig. 4H,I) the *Gbx2*-derived axons formed a dense fiber tract with long longitudinal processes positioned along the rostral-caudal axis (Fig. 4I). Once the thalamocortical axons innervated the cerebral cortex, the fibers apparently de-fasciculated and formed numerous fine ramifications in the cortex (Figs 3F and 4). In somatosensory cortex, the

Gbx2-derived projections formed dense axonal clusters that established the rudimentary somatosensory barrels (Fig. 4H).

3. Discussion

The thalamus is composed of both locally projecting interneurons and long-distance projection neurons (Jones 2007). Physical tracing methods have been instructive in elucidating the formation of thalamocortical axons and is a well described process that begins with thalamic axons emanating from the thalamus and halting at intermediate target sites. Subsequently, thalamic axons turn toward an innervate the cerebral cortex (Bayer and Altman, 1991; Adams and Baker, 1995; Inan and Crair, 2007; Vanderhaeghen and Polleux, 2004). It has been shown that the *Gbx2* lineage contributes to thalamic neurons and that *Gbx2* is required for the proper formation of thalamic axonal projections (Hevner et al., 2002; Miyashita-Lin et al., 1999). In addition, *Gbx2* is required cell non-autonomously for thalamic development (Chen et al., 2010). However, establishing a relationship between the timing of gene expression, genetic lineage and neural circuit formation in general using genetic based methods and specifically within the *Gbx2* lineage has not been demonstrated. Thus, we sought to use genetic inducible fate mapping as an approach to demonstrate whether the early expression of *Gbx2* in thalamic neuron progenitors was related to the formation of long distance axonal circuits that eventually innervate cortical targets. We marked *Gbx2* expressing progenitors at E9.5 and analyzed early patterns of axonal growth after three days. We observed clearly labeled *Gbx2* lineage derived thalamocortical axons that exited the thalamus in thick fascicles and were abrogated at the ganglionic eminence consistent with previous physical axonal tracing methods (Jones 2007). By E18.5 the *Gbx2* derived axons entered the striatum as thick fascicles and formed a rich axonal plexus. Upon exiting the caudate/putamen, well-defined axonal tracts entered the deep cortical layers with fine axons that begin to ramify into more superficial layers. At P7, the axons that entered the cortex formed an axonal tract that traversed the rostral-caudal axis. While at E18.5 only fine axons innervated more superficial cortical layers, by P7 the projections establish a broad zone of termination in layer 4 of cortex. In the somatosensory cortex, the projections coalesce as the rudimentary layer 4 barrel structures.

During the course of our analysis, we also observed a second surprising *Gbx2* lineage derived axonal tract located ventrally in the medial forebrain bundle. Thus, we show for the first time that a portion of the medial forebrain bundle axons are derived from *Gbx2* expressing progenitors that contribute to dopamine neurons. It is well known that *Gbx2* expression defines

a domain that is posterior to the germinal zone of ventral midbrain progenitors (Wassarman et al., 1997; Martinez-Barbera et al., 2001; Li and Joyner, 2001; Li et al., 2002) although a recent study showed that *Gbx2* is also transiently expressed in the ventral midbrain primordia (Sunmonu et al., 2011), which is the source of midbrain dopamine neurons (Brown et al., 2011, Hayes et al., 2011). We show here that thalamocortical axons were derived from neurons that had early and persistent expression of *Gbx2* (tdTomato+/GFP+, yellow). In contrast, the dopaminergic axons in the medial forebrain bundle were derived from progenitors that expressed *Gbx2* only early and transiently (at E9.5, but not at E12.5). Thus, this genetic circuit mapping approach makes it possible to link differential timing of gene expression and specific neural circuits within a specific genetic lineage. Finally, we show that a genetic based approach is highly effective at marking and following neural circuit formation *in vivo*. This approach has distinct advantages including that it is not invasive, is highly reproducible forges a link between temporal gene expression during embryogenesis and postnatal neural circuits.

4. Experimental Methods

4.1. Mice and Fate Mapping

Gbx2^{CreER} mice were bred to *R26*^{tdTomato} reporter mice to generate *Gbx2*$^{CreER\text{-}ires\text{-}eGFP}$*;R26*^{tdTomato} mice that were subsequently bred to Swiss Webster mice (Taconic) for genetic inducible fate mapping (GIFM) experiments. *Gbx2*$^{CreER\text{-}ires\text{-}eGFP}$ mice (Chen et al., 2009) were generously provided by James Li (UCHC) and the *Rosa26*^{tdTomato} (*Rosa26*$^{lox\text{-}STOP\text{-}lox\text{-}tdTomato}$) (Madisen et al., 2010) mice were purchased from Jackson Laboratories. Adult mice between four and six weeks of age were set up in breeding pairs at the end of the day (1600-1700 hours) and checked for the presence of a vaginal plug each morning at 0900 hours. The presence of a plug was considered 0.5 days post conceptus or embryonic day (E)0.5. Pregnant female mice harboring embryos at E9.5 mice were administered 4mg (200µl) of tamoxifen from a stock solution of tamoxifen in corn oil (20mg/ml) at 0900 hours by oral gavage as previously described (Ellisor et al., 2009; Brown et al., 2009; Ellisor and Zervas, 2010). Litters were then dissected at E12.5 or E18.5 (n=3 each time point). An additional cohort of mice were allowed to go to term and were sacrificed at postnatal day (P)7 (n=3). All mice were housed, handled, and euthanized in accordance with IACUC guidelines at Brown University.

4.2 Tissue Processing

Embryos were dissected in PBS over ice and a small tail biopsy was used for genotyping. P7 mice were perfused with saline and 4% paraformaldehyde (PFA) and the brains removed as

previously described (Brown et al., 2009; Hagan and Zervas, 2011). Embryos and brains were fixed in PFA overnight at 4 °C. Subsequently, the tissue was rinsed in PBS and immersed in 15% sucrose and 30% sucrose until submerged. Tissues were embedded in Optimal Cutting Temperature (OCT) in cryomolds. Subsequently the OCT/cryomolds were immersed in a polypropylene beaker containing 2-methyl-butane that was immersed in a vessel containing liquid nitrogen until the temperature reached -150°C as described (http://www.adam.com.au/royellis/ fr.htm). Sections were obtained on a Leica cryostat and mounted on slides.

4.3. Immunocytochemistry and microscopy (ICC)

Sections (12µm) were rinsed in PBS for five minutes and fixed in 4% PFA/PBS for 5 min. Slides were then rinsed three times in 0.2% TritonX-100 in PBS (PBT) for 5 min each and blocked in 10% donkey serum in PBT for 2 hours at room temperature in a humid box. Sections were labeled with an anti-DsRed antibody that detects the protein product generated by the recombined *R26*^{tdTomato} reporter allele (anti-dsRed Ab from Clontech, Cat # 632496, 1:500 in 10% donkey serum in PBT). We also used an anti-TH primary antibody (Chemicon; Billerica, MA; Cat# AB152, 1:500 in 10% donkey serum in PBT) to detect dopamine neurons and their axons at E12.5. Appropriate, species matched Alexa secondary antibodies (Molecular Probes) were prepared at a concentration of 1:500 in 1% donkey serum in PBT. Sections were incubated in 300µl of secondary antibody solution for two hours at room temperature, washed with PBT five times for ten minutes each, and counterstained with .01% Hoechst 33342 (Molecular Probes; Cat # H-3570) in PBS for five minutes in the dark. Slides were washed two times with PBS for 2 minutes each, dried and coverslipped. High magnification images were collected with a Leica DM600B epifluorescent microscope using Volocity 5.1 imaging software (Improvision) and were obtained using a motorized stage with a 20x objective. Low magnification images were captured with a Leica MZ16F stereo fluorescent dissecting microscope using PictureFrame software. True magnifications are indicated by scale bars. All images were pseudo colored live as part of the acquisition palettes. Imaging data sets were exported to Adobe Photoshop and montages of representative data were generated.

Acknowledgements

This work was supported by a Department of Defense CDMRP grant (TS110067, MZ) and the Brown University Department of Neuroscience training grant (NS062443-02, LN).

Figure Legends

Fig. 1. Genetic marking uncovers early neural circuit formation

Tamoxifen was administered to *Gbx2*$^{CreER\text{-}ires\text{-}eGFP}$;*R26*^{tdTomato} embryos at E9.5 and analyzed at E12.5. (A) Sagittal section immunolabeled with an anti-dsRed antibody to detect neurons in the thalamus (thal) and ganglionic eminence (ge) that underwent recombination. Neuronal projections were also labeled with the reporter allele and allowed for the detection of a thick fascicle concomitant with the thalamocortical axon bundle (TCA) that coursed rostrally and halted at the ganglionic eminence. A loose axonal bundle was also detected in the vicinity of the medial forebrain bundle (MFB). The inset shows the region of analysis; prosencephalon (pros), mesencephalon (mes), rhombomere 1 (r1). (B) *Gbx2*-derived neurons in the thalamus (dsRed+, arrowheads) and a thick axonal plexus (arrows). (C) TCA of *Gbx2*-derived neurons marked at E9.5 exited the thalamus as a thick bundle. (D) TCA termination at distal to the thalamus. (E) *Gbx2*-derived neurons in the ge. In B-E, sections were counterstained with hoechst (blue).

Fig. 2. Timing of gene expression define subsets of neural circuits within a defined genetic lineage

Tamoxifen was administered to *Gbx2*$^{CreER\text{-}ires\text{-}eGFP}$;*R26*^{tdTomato} embryos at E9.5 and analyzed at E12.5. (A) Sagittal section immunolabeled with anti-dsRed and anti-GFP antibodies to detect thalamic neurons that, respectively, expressed *Gbx2* at E9.5 (dsRed+, red) and currently expressed *Gbx2* at E12.5 (GFP+, green). Sections were counterstained with hoechst (blue). Neurons in the thalamus (thal) and TCA (yellow arrows) were dsRed+/GFP+ (yellow) indicating that they were derived from neuronal progenitors that expressed *Gbx2* at E9.5 and continued to express *Gbx2* at E12.5. The axons in the medial forebrain bundle were dsRed+.GFP- (red arrows) indicating that these projections were related to neurons that expressed *Gbx2* early, but ceased expressing *Gbx2* by E12.5. (A') Thalamus from same sample but at more medial location. (1,2) High magnification panels of regions of interest shown in A. (B) Sagittal section immunolabeled with anti-dsRed and anti-tyrosine hydroxylase (TH) antibodies to detect neurons that expressed *Gbx2* at E9.5 (dsRed+, red) and to identify dopamine neurons (TH+, green), respectively. Neurons in the thalamus and TCAs were dsRed+ consistent with the adjacent section in A. The MFB contained TH+ dopaminergic axons (white arrows). (B') High magnification view of thalamus and dopaminergic axons coursing ventral to the thalamus. Note that the TH+ projections were also dsRed+ but were much fainter than the neurons in the thalamus (the red signal was kept low to prevent saturating the TCAs, See panel 3). (3) High magnification panel of region 3 with the red signal increased to more clearly observe the

projections**.** The asterisk (*****) indicates a reference position to cells that we analyzed caudal and medial to B,B' showing the midbrain dopamine neurons derived from the *Gbx2* lineage marked at E9.5 (dsRed+/TH+, yellow) that projected along the MFB.

Fig. 3. Maturation of lineage derived neural circuits. Genetic marking uncovers early neural circuit formation

Tamoxifen was administered to *Gbx2*$^{CreER\text{-}ires\text{-}eGFP}$*;R26*^{tdTomato} embryos at E9.5 and analyzed at E18.5. (A) Sagittal section immunolabeled with an anti-dsRed antibody to detect neurons in the thalamus (thal) that underwent recombination. Sections were counterstained with hoechst (blue). The thalamocortical axon bundle (TCA) traversed the striatum (str) and entered the deep layers of the cerebral cortex (ctx). (B) Thalamic neurons that expressed *Gbx2* at stage of marking were becoming morphologically distinct. (C) The TCA exited the thal as thick well-defined fascicles that turned rostrally (arrow). (D) The *Gbx2* derived projections entered the striatum (arrows) and formed a fine network of axonal terminals which was in contrast to the TCA marked at the same stage but analyzed at E12.5 (See Fig. 1). (E) TCA that exited the striatum were fine and ramified the the deep cortical layer. (F) In an a section adjacent to panels A-E the *Gbx2*-derived TCA could be followed through the striatum and innervating the deep cortical layers with fine axonal branches that were progressively sparser in layers superficial to cortical layer 6.

Fig. 4. Target innervation of genetic lineage derived neural circuits

Tamoxifen was administered to *Gbx2*$^{CreER\text{-}ires\text{-}eGFP}$*;R26t*^{dTomato} embryos at E9.5 and analyzed at P7. (A) Sagittal section immunolabeled with an anti-dsRed antibody detected neurons and the thalamocortical axon bundle (TCA) derived from the Gbx2 lineage marked at E9.5. Sections were counterstained with hoechst (blue). *Gbx2*-derived TCA traversed the striatum (str) as thick bundles where they branched and formed fine axonal terminations. The TCA exited striatum and innervated the cerebral cortex (ctx). (B) Neuronal progenitors that expressed *Gbx2* at E9.5 contributed to mature thalamic neurons that were distributed in the thal. (C) Numerous thick TCA exited the thal. (D) TCA traversed the entire distance of the str as thick bundles with fine axonal branches that established *Gbx2*-derived plexus in the caudate/putamen of the str. (E,F) Upon exiting the str, the TCA projections were thinner in comparison to when they entered and traversed the str. The TCA then formed a a dense plexus in deep cortical layers. (G) *Gbx2*-derived neurons remaining in close proximity, but ventral to the thal. (H,I) In an adjacent sagittal section to A-G, *Gbx2*--derived axons traversed the rostral-caudal axis as long axonal bundles

that were oriented parallel to the ventral surface. In somatosensory cortex, the axons coalesced in a fingerprint pattern, consistent with the early formation of barrel cortex.

References

Adams, N.C., and Baker, G.E. 1995. Cells of the perireticular nucleus project to the developing neocortex of the rat. J Comp Neurol *359*, 613-626.

Bayer, and Altman 1991. Neocortical Development (New York, NY: Raven Press).

Brown, A., Brown, S., Ellisor, D., Hagan, N., Normand, E., and Zervas, M. (2009). A practical approach to genetic inducible fate mapping: a visual guide to mark and track cells in vivo. J Vis Exp , pii: 1687.

Brown, A., Machan, J.T., Hayes, L., and Zervas, M. 2011. Molecular organization and timing of Wnt1 expression define cohorts of midbrain dopamine neuron progenitors in vivo. J Comp Neurol *519*, 2978-3000.

Chen, L., Chatterjee, M., and Li, J.Y. 2010. The mouse homeobox gene Gbx2 is required for the development of cholinergic interneurons in the striatum. J Neurosci *30*, 14824-14834.

Chen, L., Guo, Q., and Li, J.Y. 2009. Transcription factor Gbx2 acts cell-nonautonomously to regulate the formation of lineage-restriction boundaries of the thalamus. Development *136*, 1317-1326.

Dymecki, S.M., and Kim, J.C. 2007. Molecular neuroanatomy's "Three Gs": a primer. Neuron *54*, 17-34.

Ellisor, D., and Zervas, M. 2010. Tamoxifen dose response and conditional cell marking: Is there control? Mol Cell Neurosci 45, 132-138.

Ellisor, D., Koveal, D., Hagan, N., Brown, A., and Zervas, M. 2009. Comparative analysis of conditional reporter alleles in the developing embryo and embryonic nervous system. Gene Expr Patterns *9*, 475-489.

Hagan, N., and Zervas, M. 2011. Wnt1 expression temporally allocates upper rhombic lip progenitors and defines their terminal cell fate in the cerebellum. Mol Cell Neurosci 49, 217-229.

Hevner, R.F., Miyashita-Lin, E., and Rubenstein, J.L. 2002. Cortical and thalamic axon pathfinding defects in Tbr1, Gbx2, and Pax6 mutant mice: evidence that cortical and thalamic axons interact and guide each other. J Comp Neurol *447*, 8-17.

Inan, M., and Crair, M.C. 2007. Development of cortical maps: perspectives from the barrel cortex. Neuroscientist *13*, 49-61.

Jones, E. 2007. The thalamus, Jones, eds. (Cambridge ; New York: Cambridge University Press).

Joyner, A.L., and Zervas, M. 2006. Genetic inducible fate mapping in mouse: Establishing genetic lineages and defining genetic neuroanatomy in the nervous system. Dev Dyn *235*, 2376-2385.

Li, J.Y., and Joyner, A.L. 2001. Otx2 and Gbx2 are required for refinement and not induction of mid- hindbrain gene expression. Development *128*, 4979-491.

Li, J.Y., Lao, Z., and Joyner, A.L. 2002. Changing requirements for Gbx2 in development of the cerebellum and maintenance of the mid/hindbrain organizer. Neuron *36*, 31-43.

Lo, L., and Anderson, D.J. 2011. A cre-dependent, anterograde transsynaptic viral tracer for mapping output pathways of genetically marked neurons. Neuron *72*, 938-950.

Luo, L., Callaway, E.M., and Svoboda, K. 2008) Genetic dissection of neural circuits. Neuron *57*, 634-660.

Luu, B., Ellisor, D., and Zervas, M. 2011. The lineage contribution and role of Gbx2 in spinal cord development. PLoS One *6*, e20940.

Madisen, L., Zwingman, T.A., Sunkin, S.M., Oh, S.W., Zariwala, H.A., Gu, H., Ng, L.L., Palmiter, R.D., Hawrylycz, M.J., Jones, A.R., Lein, E.S., and Zeng, H. 2010. A robust and high-throughput Cre reporting and characterization system for the whole mouse brain. Nat Neurosci *13*, 133-140.

Martinez-Barbera, J.P., Signore, M., Boyl, P.P., Puelles, E., Acampora, D., Gogoi, R., Schubert, F., Lumsden, A., and Simeone, A. 2001. Regionalisation of anterior neuroectoderm and its competence in responding to forebrain and midbrain inducing activities depend on mutual antagonism between OTX2 and GBX2. Development *128*, 4789-4800.

Miyashita-Lin, E.M., Hevner, R., Wassarman, K.M., Martinez, S., and Rubenstein, J.L. 1999. Early neocortical regionalization in the absence of thalamic innervation. Science *285*, 906-909.

Sunmonu, N.A., Li, K., Guo, Q., and Li, J.Y. 2011. Gbx2 and Fgf8 are sequentially required for formation of the midbrain-hindbrain compartment boundary. Development *138*, 725-734.

Vanderhaeghen, P., and Polleux, F. 2004. Developmental mechanisms patterning thalamocortical projections: intrinsic, extrinsic and in between. Trends Neurosci *27*, 384-391.

Vitalis, T., Cases, O., Engelkamp, D., Verney, C., and Price, D.J. 2000. Defect of tyrosine hydroxylase-immunoreactive neurons in the brains of mice lacking the transcription factor Pax6. J Neurosci *20*, 6501-6516.

Wassarman, K.M., Lewandoski, M., Campbell, K., Joyner, A.L., Rubenstein, J.L., Martinez, S., and Martin, G.R. 1997. Specification of the anterior hindbrain and establishment of a normal mid/hindbrain organizer is dependent on Gbx2 gene function. Development *124*, 2923-234.

Figure 1

Click here to download high resolution image

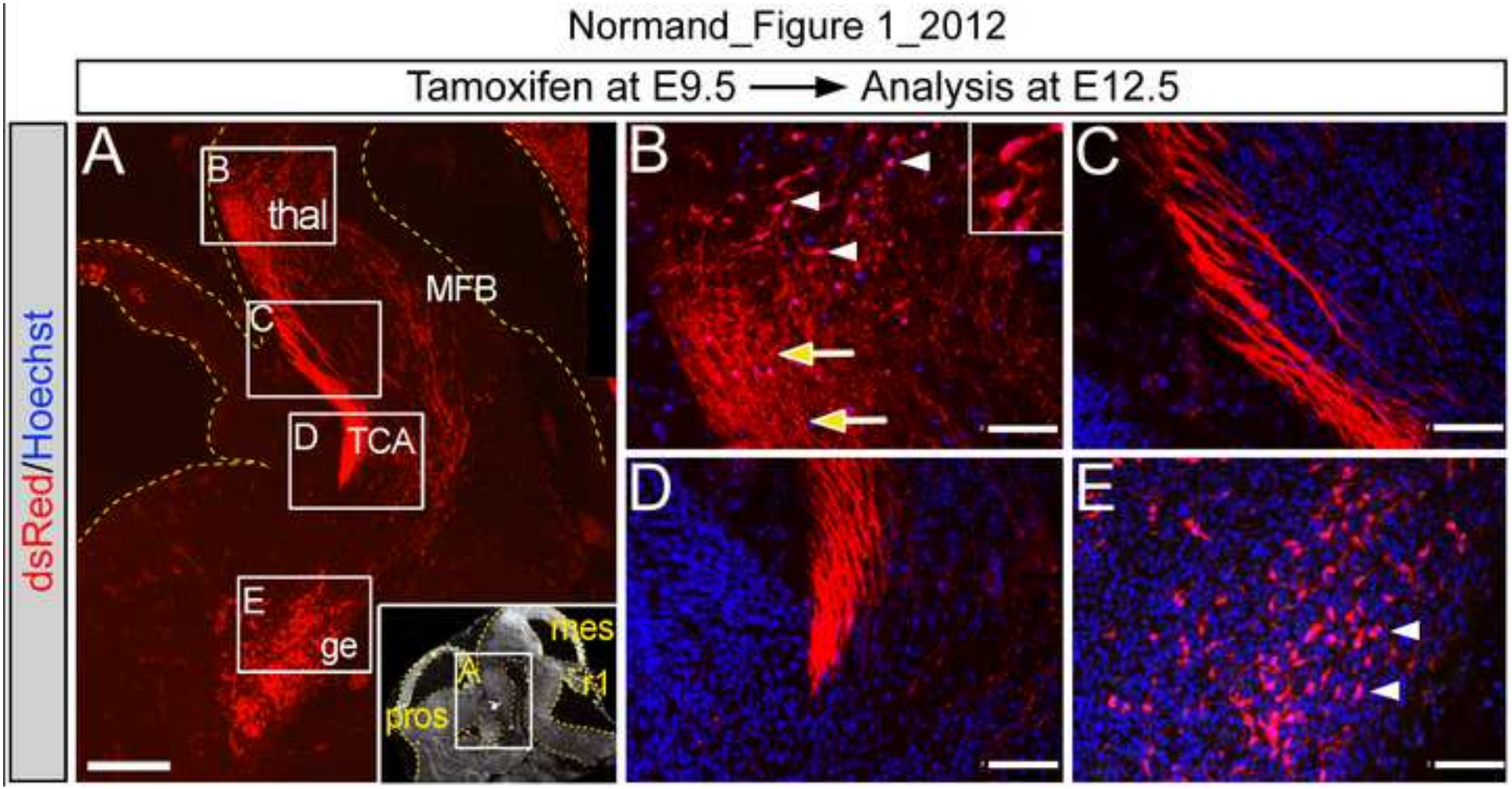

Figure 2

Click here to download high resolution image

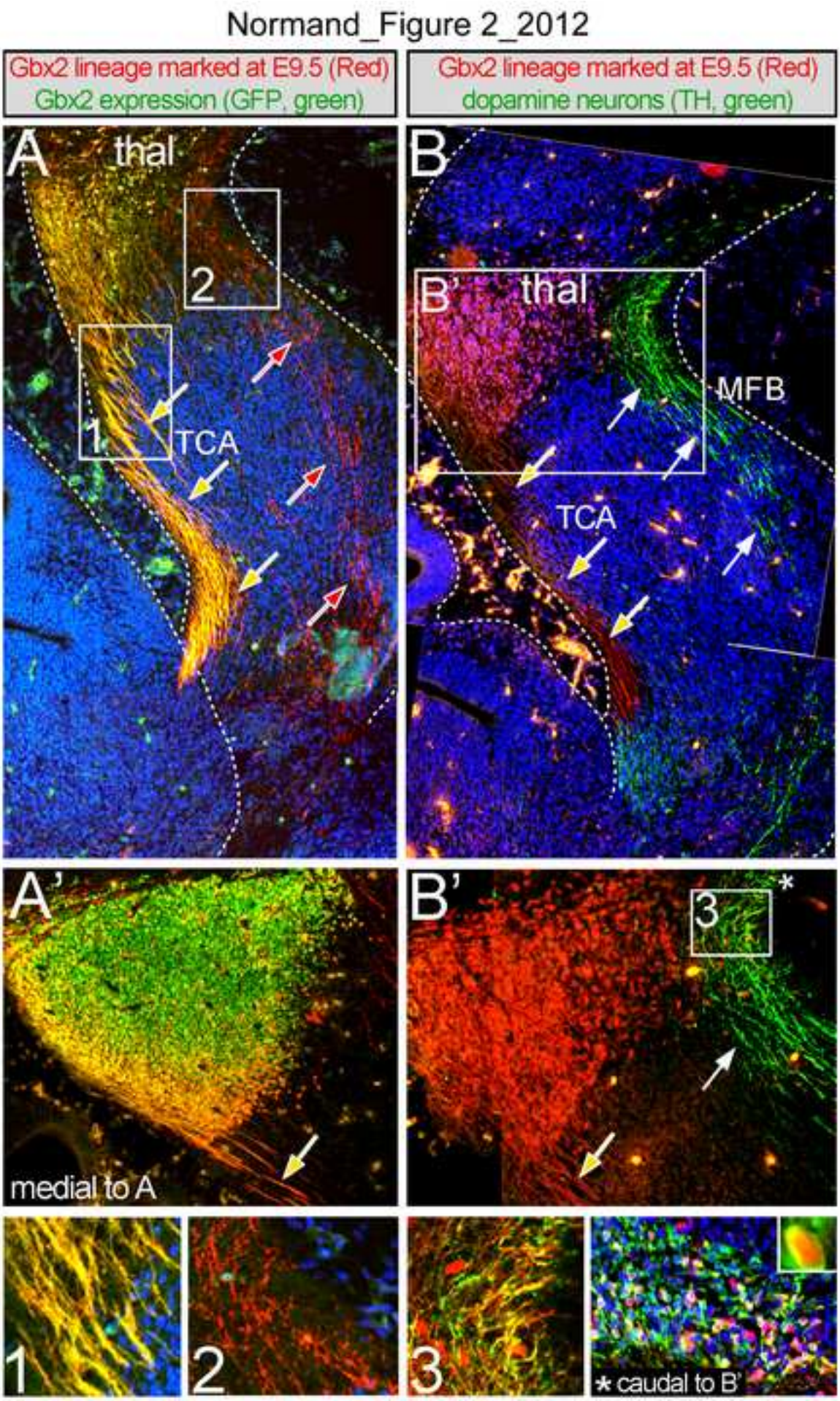

Figure 3

Click here to download high resolution image

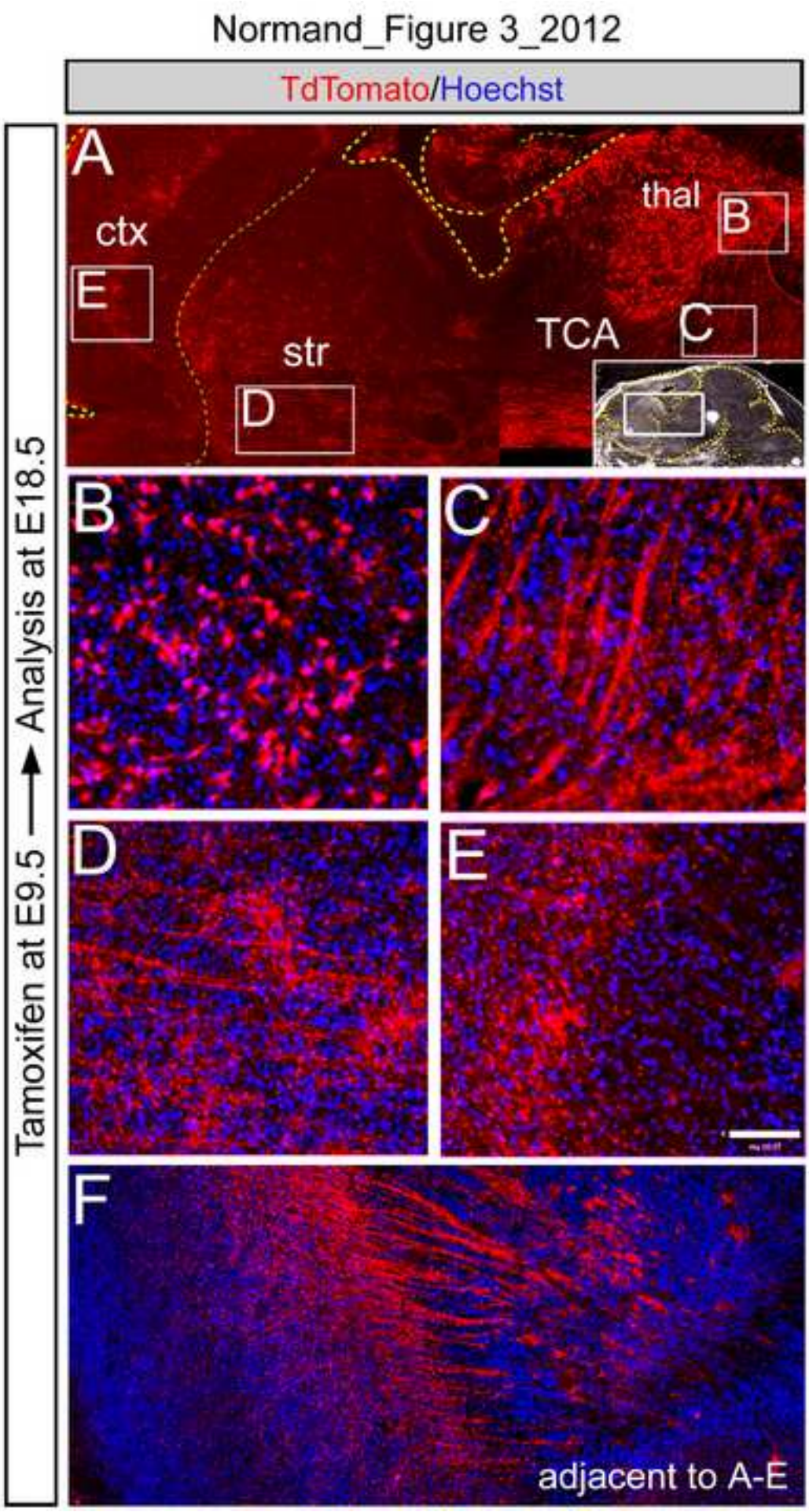

Figure 4

Click here to download high resolution image